THE IMPACT OF GRAVITY SEGREGATION ON MULTIPHASE NON-DARCY FLOW IN HYDRAULICALLY FRACTURED GAS WELLS

A Thesis

by

MARK DICKINS

Submitted to the Office of Graduate Studies of
Texas A&M University
in partial fulfillment of the requirements for the degree of

MASTER OF SCIENCE

August 2008

Major Subject: Petroleum Engineering

THE IMPACT OF GRAVITY SEGREGATION ON MULTIPHASE NON-DARCY FLOW IN HYDRAULICALLY FRACTURED GAS WELLS

A Thesis

by

MARK DICKINS

Submitted to the Office of Graduate Studies of
Texas A&M University
in partial fulfillment of the requirements for the degree of

MASTER OF SCIENCE

Approved by:

Chair of Committee,	Duane McVay
Committee Members,	Stephen Holditch
	Wayne Ahr
Head of Department,	Stephen Holditch

August 2008

Major Subject: Petroleum Engineering

ABSTRACT

The Impact of Gravity Segregation on Multiphase Non-Darcy Flow in Hydraulically Fractured Gas Wells. (August 2008)

Mark Dickins, B.S., The University of Texas at Austin

Chair of Advisory Committee: Dr. Duane McVay

Multiphase and non-Darcy flow effects in hydraulically fractured gas wells reduce effective fracture conductivity. Typical proppant pack laboratory experiments are oriented in such a way such that phase segregation is not possible, which results in mixed flow. Tidwell and Parker (1996), however, showed that in proppant packs, gravity segregation occurs for simultaneous gas and liquid injection at laboratory scale (1500 cm^2). Although the impact of gravity on flow in natural fractures has been described, previous work has not fully described the effect of gravity on multiphase non-Darcy flow in hydraulic fractures. In this work, reservoir simulation modeling was used to determine the extent and impact of gravity segregation in a hydraulic fracture at field scale. I found that by ignoring segregation, effective fracture conductivity can be underestimated by up to a factor of two.

An analytical solution was developed for uniform flux of water and gas into the fracture. The solution for pressures and saturations in the fracture agrees well with reservoir simulation. Gravity segregation occurs in moderate-to-high conductivity fractures.

Gravity segregation impacts effective fracture conductivity when gas and liquid are being produced at all water-gas ratios modeled above 2 Bbls per MMscf. More realistic, non-uniform-flux models were also run with the hydraulic fracture connected to a gas reservoir producing water. For constant-gas-rate production, differences in pressure drop between segregated cases and mixed flow cases range up to a factor of two. As the pressure gradient in the fracture increases above 1 to 2 psi/ft, the amount of segregation decreases. Segregation is also less for fracture half-length-to-height ratios less than or close to two. When there is less segregation, the difference in effective conductivity between the segregated and mixed flow cases is reduced. I also modeled the water injection and cleanup phases for a typical slickwater fracture treatment both with and without gravity effects and found that for cases with segregation, effective fracture conductivity is significantly higher than the conductivity when mixed flow occurs.

Gravity segregation is commonly ignored in design and analysis of hydraulically fractured gas wells. This work shows that segregation is an important physical process and it affects effective fracture conductivity significantly. Hydraulic fracture treatments can be designed more effectively if effective fracture conductivity is known more accurately.

ACKNOWLEDGEMENTS

I would like to express my sincere appreciation to Dr. Duane McVay for guiding this work and spending his valuable time throughout the course of this work. I would also like to thank Steven K. Schubarth, of Schubarth Inc., for sponsoring this work. Without his sponsorship this work would not have been possible. I also would like to thank Dr. S. Holditch and Dr. W. Ahr for serving as members on my advisory committee, and would additionally like to thank Dr. Holditch for his valuable suggestions about the content of this work.

TABLE OF CONTENTS

Page

LIST OF FIGURES

FIGURE Page

FIGURE Page

FIGURE Page

FIGURE Page

LIST OF TABLES

1. INTRODUCTION

1.1 STATEMENT OF THE PROBLEM

Hydraulic fracturing in gas reservoirs is a common practice to increase production rates. Multiphase and non-Darcy flow effects in hydraulically fractured gas wells reduce effective fracture conductivity, by reducing the effective permeability of the proppant. Using a higher permeability proppant in the design can compensate for the permeability reduction caused by non-Darcy multiphase flow. Accounting for non-Darcy multiphase flow in the design allows for the fracture treatment to be optimized. Optimizing fracture conductivity is required to achieve the most economical productivity possible (Economides et al., 2002).

Laboratory experiments on proppant packs are commonly done in the design phase in order to estimate the effective conductivity of the fracture. Typical proppant pack laboratory experiments are oriented in a way such that phase segregation is not possible, which results in mixed flow along the entire fracture length (i.e., two-phase flow where both phases flowing towards the wellbore occurs at all locations in the fracture). When the fracture is oriented vertically, as it is in the reservoir, gravity causes gas-water phase segregation within the fracture (Tidwell and Parker, 1996). When segregated flow occurs, there are areas in the fracture with single-phase gas flow separate and above that of single-phase water flow. Using conventional laboratory proppant pack experimental results may cause inaccurate conductivity estimation, since segregation will not occur.

This thesis follows the style of *SPE Journal.*

If segregation occurs in the field, taking into account segregation in laboratory conductivity tests may result in more representative effective conductivity measurements.

Reservoir simulation models are commonly run with one layer. This forces mixed flow as it is not possible for phase segregation to occur within a single layer with a standard reservoir simulation model. Using several layers in a model is the easiest and most accurate way of taking into account gravity segregation. Doing this in models with two flowing phases could improve the accuracy of the modeled hydraulic fracture, which should in turn lead to better design of hydraulic fracture treatments.

1.2 LITERATURE REVIEW

It is commonly known that various factors such as multiphase and non-Darcy flow cause lower than expected fracture half-length (Lolon et al., 2003). Although Lolon et al. defined effective fracture length in several ways, I use here the definition that is most applicable to my work. That is, effective fracture length is the length under single-phase conditions which results in the productivity observed under multiphase conditions. I will use this same definition, but replacing the words fracture length with fracture conductivity, as my work investigates fracture conductivity more than fracture length. Lolon et al. also defined effective fracture length as the length of the fracture that is accessible to gas flow and that is cleaned up of water. According to Lolon et al., the

effective fracture length is measured from the wellbore to the distance along the fracture with a total of 90% of the gas flow rate into the fracture. This effective fracture length is low at early times for the low dimensionless conductivity cases and higher for the high conductivity cases. Lolon et al. found that with increasing fracture conductivity more water is cleaned up, which results in longer effective fracture lengths. They found that, for long fractures (L_f = 800 ft), the gas enters the nearest half of the fracture under relatively low dimensionless fracture conductivity cases (C_{fD} = 3), and also enters the far half under higher dimensionless conductivity cases (C_{fD} = 30), while high amounts of gas enter the tip of the fracture in all cases.

Non-Darcy flow is the deviation from Darcy's law, due to fluid flow through tortuous pore pathways. Forchheimer (1901) developed a formula to show the deviation from Darcy's law and the resulting pressure drop when this is taken into account. It is common knowledge that multiphase non-Darcy flow lowers effective fracture conductivity. Taking into account multiphase non-Darcy effects in the fracture leads to more accurate modeling of the flow in the fracture. Lolon et al. used Frederick and Graves (1992) correlation for multiphase non-Darcy flow which leads to less non-Darcy flow effects compared to Geertsma's (1974) correlation, when the permeability is high (as in a fracture). Previous work by Olson et al. (2004) found that laboratory data for multiphase non-Darcy flow can be fit to a Geertsma type equation with good accuracy provided that the water saturation is not too high. Olson et al. also found that at high water saturations, running experiments is more difficult, which means that there is a lack

of laboratory data to compare to Geertsma's correlation at higher water saturations. Results of Lolon et al. agree with that of Tannich (1975), who first analyzed the effect of invaded fracture fluid on the productivity of gas wells, and the effect on fracture length. Tannich found that when conductivity is low, gas enters only near the wellbore and production rates are lower than at higher conductivities. Schubarth et al. (1998) examined the relationship between productivity and effective fracture length, in cases with varying fracture conductivity, closure pressure, and production rate for both single-phase and multiphase flow. Schubarth et al., as Tannich and Lolon et al. did, also found that the fracture has to be conductive enough to clean up the fracture. It is possible, that this conductivity required to clean up the fracture will be different if segregated flow is taken into account, as these authors did not account for segregation.

Montgomery (1990 a, 1990 b) used a 3D finite-difference simulator (SABRE) to simulate the injection phase using 1 injector at 10 BPM with a high fracture permeability of 10^6md. This results in a minimal pressure loss along the entire fracture length. In the bleed off phase (shut-in) the fracture permeability and length are reduced to the propped length. The production phase was modeled at constant gas production rate and converting to constant BHP when the minimum BHP is reached. This is one method of simulating fracture treatments, yet I did not follow this procedure in my work, as the simulator I used would not allow for varying permeability in time. Although this would be a preferred method as it is simpler and more logical, instead I used injectors along the fracture to create a zero pressure drop along the fracture during water injection.

Montgomery suggests that fracture conductivity is important in achieving the highest productivity possible, by minimizing the pressure drop in the fracture.

Barree et al. (2003) mentions that phase segregation negatively impacts effective fracture length, yet he does not explain any possible causes for this. He also lists other causes for low effective fracture length, such as multiphase non-Darcy flow, inefficient cleanup, and capillary phase trapping.

Penny and Jin (1995) quantified the impact of non-Darcy multiphase flow on effective fracture conductivity in the laboratory. They used 10-square-inch conductivity cells surrounded by sandstone cores, and applied a high closure pressure of 12,000 psi. As in most tests, the conductivity cell was oriented horizontally so that phase segregation was not present. Without taking into account damage, the conductivity of the proppant pack was reduced by a factor of 16 to 20, depending on the sand type, when taking into account multiphase and non-Darcy flow. Penny and Jin showed that for each MMscf/D of gas rate, a non-Darcy reduction factor of three can be applied to the conductivity, and another factor of three for each Bbl/MMscf of liquid produced. He suggests using these factors together, to determine the overall reduction in effective conductivity. However, these results were done in the lab and may not apply at the field scale.

Multiphase and non-Darcy flow effects in hydraulically fractured gas reservoirs also reduce fracture productivity in the field (Vincent et al., 1999; Schubarth et al., 1995).

Schubarth et al. observed in a study group of wells that production declined by as much as a factor of two when 20 Bbl of condensate per MMcf of gas was produced. Vincent et al. found that effective fracture conductivity is decreased by up to 98% from the single-phase values due to gel damage, proppant embedment, and non-Darcy multiphase flow. Flowers et al. (2003) found that gas reserves for each well could be increased with increased fracture conductivity.

Tidwell and Parker (1996) conducted laboratory experiments at two scales, meter scale in a 1500-cm^2 sand pack (equivalent to 1.27x1.27ft), and a core-scale 65-cm^2 linear cell with a surface area that is 4.3% of the larger sample. In the meter-scale experiment, viscous fingering and gravity segregation (**Fig. 1.1**) were observed to be the dominant processes for multiphase flow of gas and gel or water. He mentions that gravity can be accounted for by simply modeling the vertical dimension in a simulation study, or by a careful formulation of the pseudo relative permeability functions. He used an equation for relative permeability equal to saturations raised to a power exponent, using a power-law formulation,

$$k_{rg,w} = k_{r(Swir,Sgir)}\left(\frac{S_{g,w} - S_{(g,w)ir}}{1 - S_{gir} - S_{wir}}\right)^{N_{g,w}} \quad . \text{.....} \quad (1.1)$$

He found with increasing viscosity, the power exponent for the relative permeability functions increased. At early times, in the larger-scale sand pack, the pseudo relative permeabilities are linear. Tidwell and Parker showed that the core-scale samples do not

show segregation even when oriented vertically, as the sample is too small to show gravity effects.

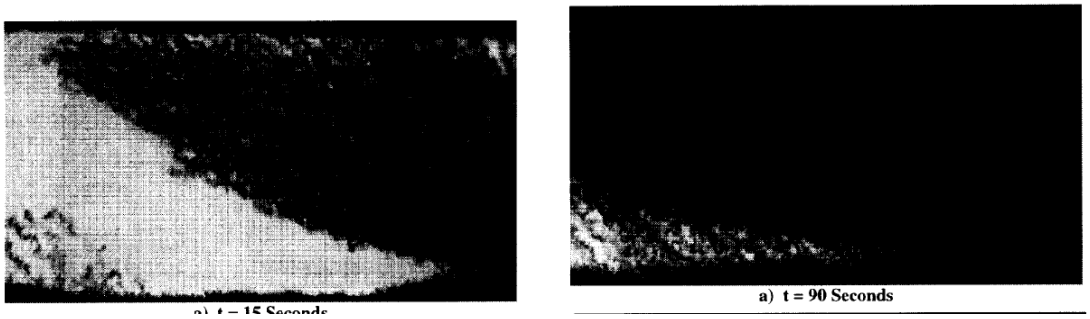

Fig. 1.1 Gas and water saturations (from Tidwell and Parker) in the fracture at t = 15 seconds (left), and t = 90 seconds (right). A strong gravity effect is observed causing phase segregation.

Linear relative permeabilities are commonly used in hydraulic fracture studies (Sullivan et al., 2006). Straight-line relative permeabilities have been historically used in natural fractures (De la Porte and Kossack, 2005) without considering the impact of using these unrealistic curves in engineering studies. They state that this rationale originated with Romm (1966). Romm's work was done in the lab on smooth parallel glass plates, so this experimental setup does not represent a fracture with roughness and asperities. Foulser et al. (1992) suggests using linear relative permeabilities for miscible flow in gas-oil systems with ultra-low interfacial tensions. Bidner and Savioli (2003) showed that if the dimensionless capillary number is larger than a certain value that depends on the type of rock (i.e. water-wet), residual phase saturation will be zero for both phases.

He shows (using Camilleri et al. (1987) functions for relative permeability) that the relative permeability functions approach linear form ($N = 1$), when fit to a power-law formulation (Eq. 1.1) if the residual phase saturation is 0. He showed that relative permeability functions are not a function of permeability, but rather a function of the interfacial fluid-fluid interactions and the wetting behavior of the rock.

Reservoir simulation models are commonly run with one layer in order to save computation time. This forces mixed flow as it is not possible to model phase segregation accurately within a single layer. One way of compensating for this is to assume linear relative permeabilities, which are only valid if complete segregation exists. Complete segregation would; however, require a very low pressure drop in the x-direction compared to the buoyancy forces in the vertical direction (Shi and Rossen, 1998). Buoyancy forces in the vertical direction are fixed, whereas the forces in the x-direction depend on the production rate. Complete segregation would also require no gas to be entering into the fracture the fracture at the highly water-saturated zone at the bottom, which is unlikely. Using several layers in a model is the easiest and most accurate way of taking into account gravity segregation.

Sullivan et al. (2006) showed relative permeability to gas and water in the fracture measured from laboratory proppant pack experiments as part of the Stim-Lab Proppant Consortium. His data show a residual water saturation of 17% and a non-linear shape for both gas and water curves with a Corey power exponent, $N_{w,g}$, of 2. Although the

Consortium includes all types of proppants, Sullivan et al. only show data for a typical resin-coated proppant. He recommends against using linear relative permeability curves, and demonstrates the impact of using the more accurate non-linear curves compared to the linear curves. He showed that using the linear curves in a simulation model results in significantly higher water cleanup.

Barree and Conway (2007) found the relative permeability in proppant pack experiments (for light-weight ceramic proppant) doing simultaneous gas-water displacement, and found a residual water saturation of 13-15%. He found gas and water relative permeability curves are more non-linear than data of Sullivan et al. show. Their data show a Corey exponent in the range of 3 to 4 for both gas and water curves.

Others have shown that using straight-line relative permeabilities is not accurate (Pruess and Tsang, 1990; Rossen and Kumar, 1992). Rossen and Kumar found that assuming straight-line relative permeability curves for a natural fracture is not accurate, unless gravity forces are dominating. They derived a percolation model within a natural fracture while quantifying the extent of segregation with a dimensionless parameter that includes density differences, fracture height, interfacial tension, and the average width of the fracture. For large values of the dimensionless parameter, the fracture relative permeabilities approach the straight-line form.

Rossen et al. (2006) used simulation and fractional flow theory to study water and gas injection in enhanced oil recovery processes in non-fractured porous media. They showed that if volumetric injection rates are fixed for water and gas and if injection is over the same interval for both, then the distance for segregation to be established is the same, whether or not the injection spans the entire vertical interval. Their work shows that segregation occurs after some distance, while the maximum distance until segregation occurs is when water injection is done above gas injection.

Several authors (Penny and Jin, 1995; Schubarth and Milton-Tayler, 2004) have showed the impact of closure stress on proppant permeability. Results from Penny and Jin are similar to results from the work of Schubarth and Milton-Tayler. These works use laboratory tests to show the relationship between effective permeability and closure stress.

The effect observed by Schubarth and Milton-Tayler is an increase in the non-Darcy coefficient (beta) with stress. The net effect on non-Darcy resistance involves both the beta coefficient and the permeability, and this effect is not documented in the works mentioned.

To summarize, Rossen and Kumar (1992, 1994) thoroughly investigated the problem of gravity segregation in a naturally-fractured system, but not for a hydraulic fracture. Tidwell and Parker (1996) found that gravity plays a key role in hydraulic fractures, but only in small-scale laboratory experiments. Others have documented phase segregation to be an important process that affects fracture conductivity.

However, previous works have not fully described the impact of gravity segregation on multiphase non-Darcy flow in hydraulically fractured gas wells.

1.3 OBJECTIVES

The overall objective of this research is to determine the impact of gravity segregation in the hydraulic fracture on the productivity of hydraulically fractured gas wells. Specific objectives are to:

- Determine controlling parameters on the amount and the impact of segregation effects.
- Determine the impact of gravity segregation on effective fracture conductivity.
- Relate effective fracture conductivity to well productivity under segregated and mixed (non-segregated) flow.
- Determine if perforations can be optimized to reduce water production when a hydraulic fracture connects multiple zones (both producing and aquifer zones).
- Determine the impact of closure stress on non-Darcy flow. If stress has a slight impact on non-Darcy flow, then it can be ignored in the modeling, which is useful to know when designing a fracture treatment.

2. METHODOLOGY

2.1 OVERVIEW

The impact of gravity segregation is investigated under three situations: simplified, uniform-influx flow conditions, cleanup of a gas well following hydraulic fracture stimulation, and long-term water production due to an initial mobile S_w in the reservoir.

First, data used in the study will be presented. Second, uniform influx will be considered as a first approach to modeling gas-water hydraulic fracture flow. An analytical solution will be shown for uniform influx of water and gas into the fracture. The solution for pressures and saturations in the fracture will be shown and compared to reservoir simulation in the mixed flow case. Third, more realistic, non-uniform-flux models will be analyzed with a hydraulically fractured well connecting to a gas reservoir producing water. Lastly, I will show the water injection and cleanup phases for a typical slickwater fracture treatment both with and without gravity effects.

I separately investigated the impact of stress on non-Darcy flow to determine if stress reduction in permeability causes an increase in non-Darcy flow effects.

2.2 DATA USED IN THE STUDY

Sullivan et al. (2006) showed relative permeability to gas and water in the fracture obtained from lab experiments. They used a typical resin-coated proppant in the measurements (**Fig. 2.1**).

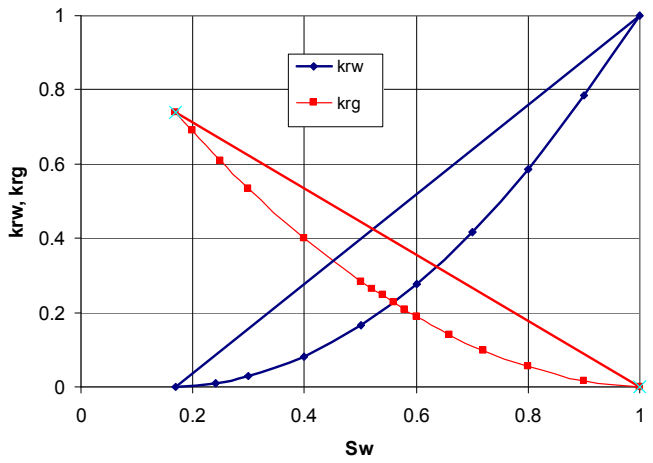

Fig. 2.1 Relative permeability for a resin coated proppant from Sullivan et al. (2006). Non-linear laboratory curves are shown along with the hypothetical linearized curves that connect the endpoints.

I fit their results for water/gas relative permeability to a Corey power-type equation,

$$k_{rg,w} = k_{r(Swir,Sgir)}\left(\frac{S_{g,w} - S_{(g,w)ir}}{1 - S_{gir} - S_{wir}}\right)^{N_{g,w}} \quad \text{.....(2.1)}$$

I found that the Corey power exponents for both the water and gas curves (N_w and N_g) are very close to 2, residual water saturation is 17%, and relative permeability to gas is 0.74 at the residual water saturation (**Table 2.1**).

Hydraulically fractured reservoir models use the fracture relative permeability curves shown in Fig. 2.1. Models with uniform influx use altered curves which simplified the analytical solution. The altered curves will be introduced in the section on uniform flux methodology (Section 2.3).

TABLE 2.1 COREY PARAMETERS IN ANALYTICAL MODEL

Corey parameters	Non-linear values	Linearized values
N_w	2.0	1
N_g	2.0	1
$k_{r(Swir)}$	0.74	0.74
$k_{r(Sgir)}$	1.0	1.0
S_{wir}	0.17	0.17
S_{gir}	0	0

I also use the linearized versions of curves from Sullivan et al. (Fig. 2.1) that he used to investigate the impact of the curve shape on production volumes of gas and water. The parameters for the linear curves are shown in Table 2.1, and are identical to the non-linear curves except that the Corey exponent for both water and gas ($N_{w,g}$) is 1. This is a method of linearizing the curves that gives the desired linear curvature while retaining

the same residual water saturation as the non-linear curves. By retaining the same residual water saturation (as Sullivan et al. did), I can isolate the effect of the curvature of the curves, and not introduce a new effect caused by a different residual water saturation. If the curves were actually linear, implying completely miscible flow, the residual water would be zero (Bidner and Savioli, 2003).

I took fracture relative permeability data from Barree et al. (2007) for a Light-Weight Ceramic proppant, and also fit his data to a Corey type equation. I then compared these to data of Sullivan et al. Barree et al. found that residual water saturation was 13-15%. I found that N_w and N_g both vary from 3 to 4 (3.5 is the best fit) (**Fig. 2.2**). I also found that maximum gas permeability (at residual water saturation) is 0.7. I chose to use the values of Sullivan et al. (N_w, N_g = 2.0), which have curvature between the Barree et al. highly non-linear data (N_w, N_g = 3.5) and linear curves (N_w, N_g = 1).

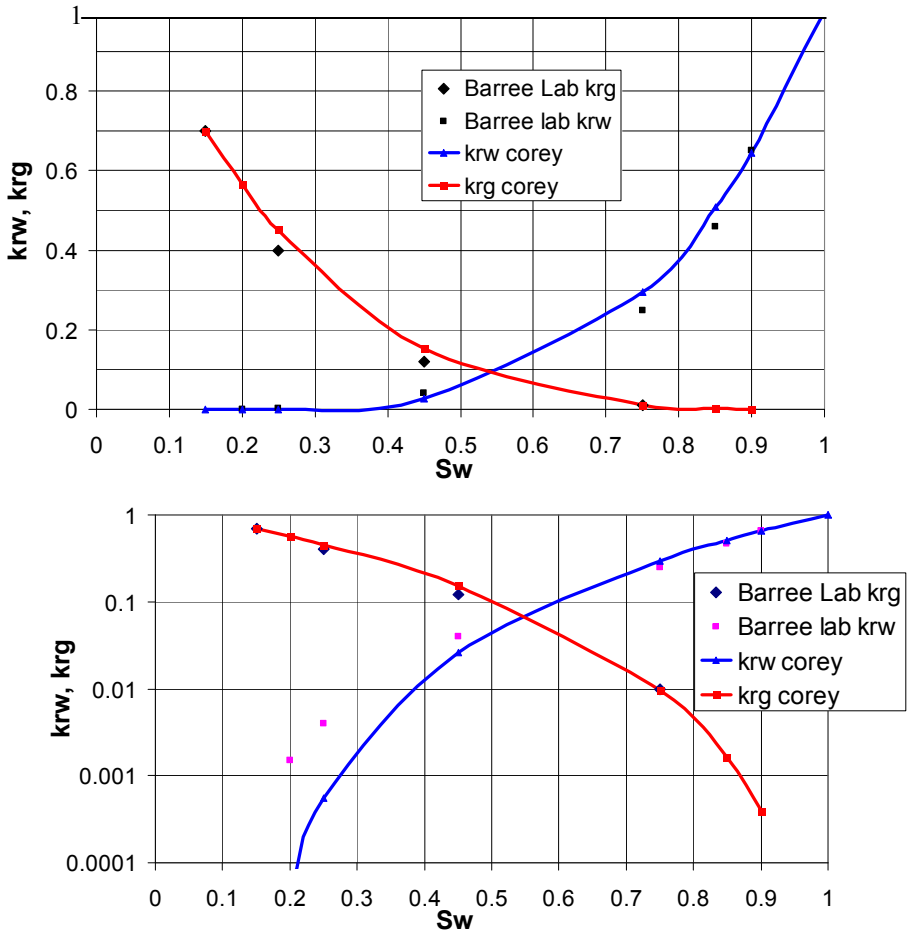

Fig. 2.2 Barree et al. (2006) relative permeability data for a light weight ceramic proppant fit to a Corey type equation. The top graph is on a linear scale while the bottom graph is on a semi-log scale. I found that N_w and N_g both vary from 3 to 4 (3.5 is the best fit). I also found that maximum gas permeability (at residual water saturation) is 0.7.

Forchheimer's equation (1901) as solved for the reduction factor in permeability (known as gas resistance factor in CMG and referred to as GRF in my work),

$$GRF = 1 + \beta(k \cdot k_{rg}) \frac{\rho}{\mu}\left(\frac{\vec{U}}{\phi}\right) \quad . \quad \text{.....(2.2)}$$

For non-Darcy flow, laboratory results for beta factors, β, in sand packs were researched. I found that most commonly accepted is Geertsma's (1974) correlation for non-Darcy flow,

$$\beta = \frac{48{,}511}{(k \cdot k_{rg})^{0.5}(\phi \cdot S_g)^{5.5}} \quad . \quad \text{..... (2.3)}$$

In Geertsma's original equation (not shown) the permeability has units of md, so beta has units of $1/[md]^{0.5}$. The units for beta in Eq. 2.3 are 1/ft, as the coefficient used (48,511) converts from the original units of Geertsma's equation in $1/[md]^{0.5}$ to units of 1/ft. In CMG it is possible to use Geertsma's correlation as well as Frederick and Graves (1994) 1st correlation (Eq. 2.4) and 2nd correlation (not shown).

$$\beta = \frac{7.89 \times 10^{10}}{(k \cdot k_{rg})^{1.6}(\phi \cdot S_g)^{0.404}} \cdot \quad \text{..... (2.4)}$$

Geertsma's correlation is more appropriate for proppant packs than Frederick and Graves 1st correlation. Geertsma's equation was developed using data from unconsolidated materials (sands, stainless steel powders) and data from consolidated sandstones. Frederick and Graves correlation (FG1), on the other hand, was developed for sandstones and carbonates with permeabilities in the range of 0.002 to 1,320 md, and is therefore not appropriate for high permeability proppant packs.

In addition to reduction in permeability due to non-Darcy multiphase flow, there is reduction in permeability due to stress (which I call $\left(k/k_{ref}\right)_{stress}$). Combining all three factors ($\left(k/k_{ref}\right)_{stress}$, k_{rg}, and GRF) gives the effective permeability to gas (Eq. 2.5, where k_{abs} is the absolute permeability). Stress-varying permeability is only included in a later section, while non-Darcy multiphase permeability reduction is included throughout my work.

$$k_{eff} = k_{abs}\left(\frac{k}{k_{ref}}\right)_{stress}\frac{k_{rg}}{GRF}. \quad \text{..... (2.5)}$$

Reservoir gas-water relative permeability curves (**Fig. 2.3**) were modified from Lolon et al. (2003) so that irreducible water saturation is 20% as compared to 40% in their work. This is done because I am modeling reservoir permeability up to 1 md whereas their work was specifically for tight gas (up to 0.1 md). The endpoint gas relative permeability (at S_{wirr}) remains unchanged at 0.44.

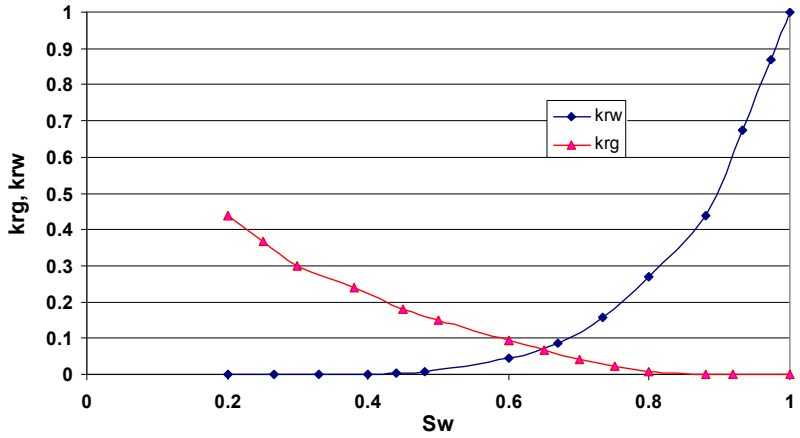

Fig. 2.3 Reservoir gas-water relative permeabilities in models that use a reservoir modified from Lolon et al. (2003) so that residual water saturation is 20% instead of 40%.

Gas-water capillary pressure in the reservoir is modeled as shown in **Fig. 2.4**. Capillary pressure in the fracture is assumed to be zero. Again, I modified the curve from Lolon et al. so that the residual water saturation is 20%, without changing the capillary pressure at the residual water saturation (93 psi).

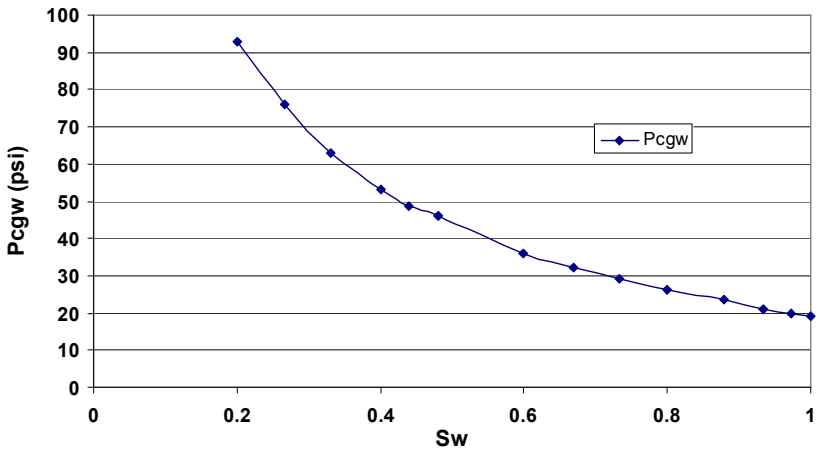

Fig. 2.4 Gas-water capillary pressure in the reservoir (modified from Lolon et al., 2003).

Gas fluid properties were taken from Wang (2006) for a gas with gravity of 0.6 and reservoir temperature of 250° F, and were calculated up to 10,000 psi. Initial reservoir pressure is 6,000 psi, but since injection of stimulation-water is at 12,000 psi the gas properties were linearly extrapolated to 12,500 psi following the trend at the last calculated point (10,000 psi). The gas expansion factor, E_g, and gas viscosity are shown in **Fig. 2.5.**

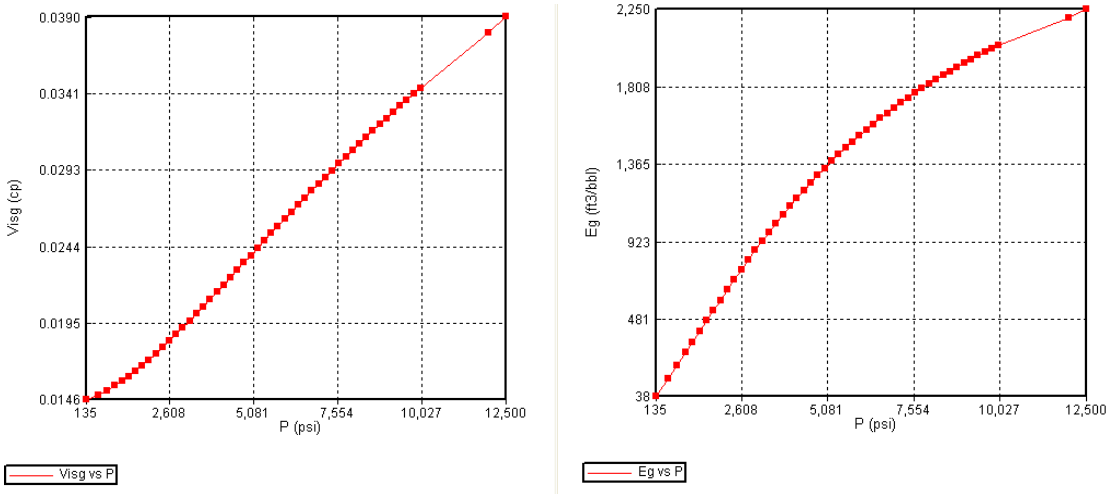

Fig. 2.5 Gas viscosity, μ_g, (left) and gas expansion factor, E_g, (right) for all models used.

In all models, the bottomhole pressure is set to 5,000 psi or 6,000 psi. For pressures above 5,000 psi, the $1/B\mu$ factor (same as E_g/μ) is relatively constant (varies less than 6% going from 5,000 to 10,000 psi, and varies less than 2% going from 6,000 to 10,000 psi) (**Fig. 2.6**). Since the $1/B\mu$ factor is approximately constant, Darcy's law can be used to

calculate productivity index without first transforming the equation to a pseudopressure formulation.

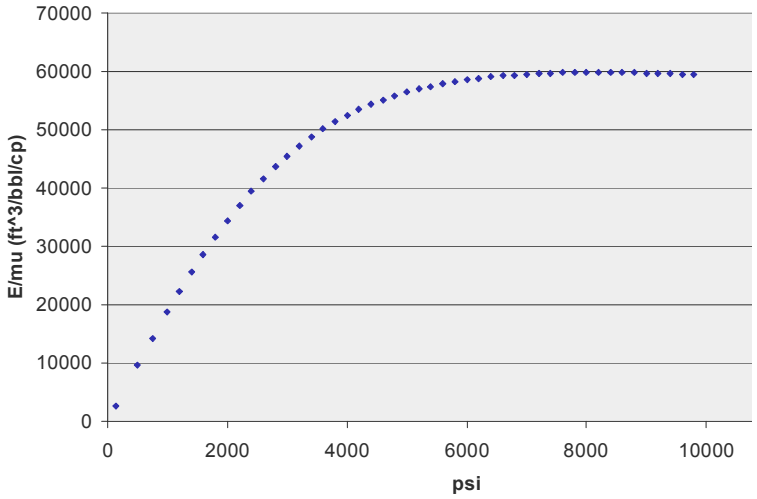

Fig. 2.6 Gas expansion factor divided by gas viscosity $E_g/\mu_g = 1/(B\mu)$, which is roughly constant at or above pressures of 6,000 psi.

Other fluid properties:

- $\rho_w =$ 64.05 lbm/ft^3
- $B_w =$ 1.04 stb/rb
- $c_w =$ 3.26x10^{-6} 1/psi
- $\mu_w =$ 1 cp
- $P_{ref,w}$(reference pressure for water properties) = 6000 psi

2.3 FRACTURE FLOW WITH UNIFORM INFLUX

I derive the uniform influx solution for mixed flow in order to verify the simulation results, and to better understand and describe the processes of multiphase non-Darcy flow in hydraulic fractures. Even though uniform flux never exists in an actual fracture, it is a useful mathematical construct as it allowed me to derive an analytical solution by assuming a time-invariant influx function that depends only on position in the fracture and gas density.

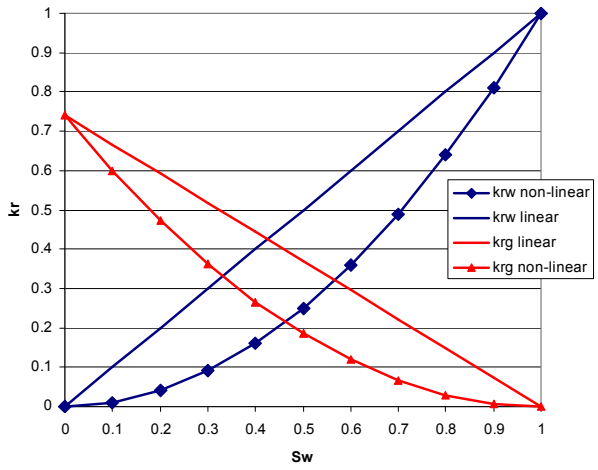

Fig. 2.7 Relative permeability functions from Table 2.1 normalized to S_{wir}=0.

For the simulation and analytical models done using uniform influx, the relative permeability functions were altered slightly to simplify the analytical solution (which is described in Section 2.4). I normalized the saturations such that the residual water saturation is zero. The Corey parameters remain the same (**Table 2.1**), with the

exception of the S_{wir}, which I reduced from 18% to 0%. Respective linear curves that have the same endpoints as the non-linear curves are also used (**Fig. 2.7**). In most simulation studies where normalized relative permeabilities are used, the Corey parameters remain the same from gridblock to gridblock, with the exception of residual water saturation. In the uniform flux modeling, the residual saturation in the fracture is not as important. This is because, in the analytical flow equations, saturation only appears in the non-Darcy flow terms (shown later in Section 2.4). The appropriateness of the resulting non-Darcy effects in the uniform flux case is described next.

Beta Factors in Uniform Flux Models:

The beta factor is a function of the product of proppant pack porosity with gas saturation ($\phi \cdot S_g$) as well as the effective permeability due to multiphase flow ($k_{eff} = k_{abs} \cdot k_{rg}$). Laboratory experiments on beta factors in proppant packs are commonly done at single-phase gas flow with no presence of residual water, or are done for two-phase flow of gas and water. However, they are not done for single-phase gas flow at the residual water saturation, so they are not useful in determining the appropriateness of the beta at the residual water saturation.

In addition to porosity and permeability, the beta factor (Eq. 2.3) also depends on the $\phi \cdot S_g$ product and the effective permeability $k_{abs} \cdot k_{rg}$ (due to multiphase flow). In both uniform flux and fractured reservoir models the relative permeability is the same at the

residual water saturation, so the $k_{abs} \cdot k_{rg}$ is the same in both models for a given proppant. Also, both uniform flux models and fractured reservoir models use porosity of 30% (or 35%). Uniform flux models use 0 residual water saturation; whereas hydraulically fractured reservoir models use the realistic 17% irreducible water saturation. This results in a higher $\phi \cdot S_g$ product ($\phi \cdot S_g$ = 0.3 at the residual water saturation) for the uniform flux models than the product for the fractured reservoir models with 0.3 porosity ($\phi \cdot S_g$ = 0.249 at the residual water saturation). This means that the beta factor (Eq. 2.3) is lower by a factor of $(0.3/0.249)^{5.5} = 2.79$ at the residual water saturation in the uniform flux models. Therefore, the uniform flux models $\phi \cdot S_g$ product (0.3) is equivalent to the $\phi \cdot S_g$ product for a realistic proppant pack residual water saturation of 17% (Sullivan et al.) and 36% porosity, which is reasonable.

For uniform flux models, I generated results for three general categories of proppants: high conductivity (Light Weight Ceramic Proppant with conductivity of 4,000-6,000 md•ft), medium conductivity (Resin Coated Sand with conductivity of 1,000-3,000 md•ft), and low conductivity (Jordan sand with conductivity of 200-1,000 md•ft). Thus, a range of proppant conductivities is covered with proppant pack permeabilities from 10 to 300 Darcies. I have plotted Geertsma's correlation (Eq. 2.3) for beta factor vs. proppant permeability in **Fig. 2.8**.

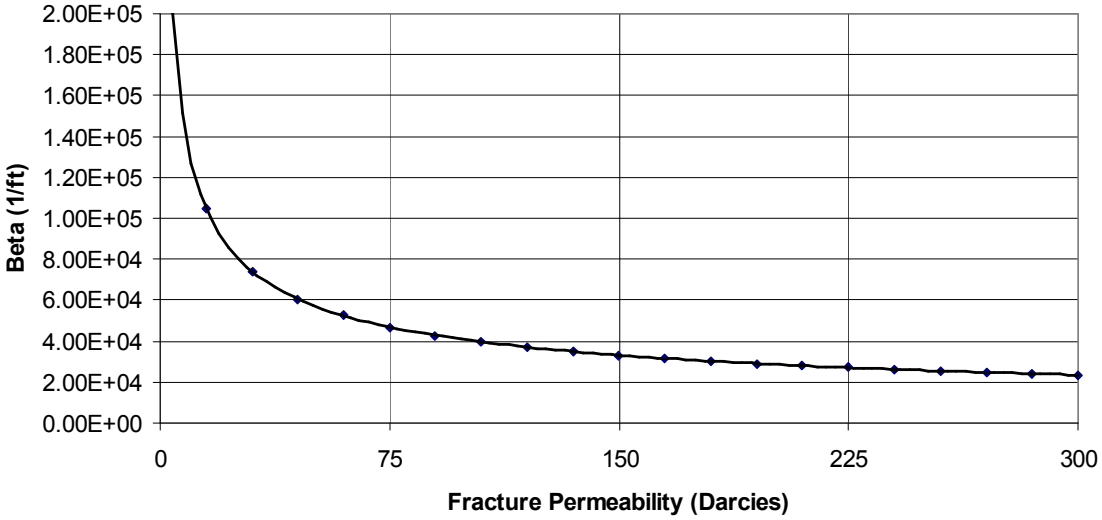

Figure 2.8 Beta factors for various proppant permeabilities using Geertsma's correlation.

I have also compared Frederick and Graves 1st correlation (FG1; Eq. 2.4) to Geertsma's correlation (Eq. 2.3) for a proppant permeability of 15 Darcies at a gas velocity of 850 ft/D. As explained earlier the FG1 correlation was developed for permeabilities in the range of 0.002 to 1,230 md. I have plotted both correlations (**Fig. 2.9**) and have shown that using Frederick and Graves 1st correlation in proppant packs severely underestimates the gas resistance factor (GRF, Eq. 2.2). This weak effect of non-Darcy flow when using the FG1 correlation is partially explained by the 5.5 power dependence of Geertsma's correlation (Eq. 2.3) on the $\phi \cdot S_g$ product, while Frederick and Graves correlation (Eq. 2.4) contains only a 0.4 power dependence on the $\phi \cdot S_g$ product. More importantly, the 1.6 power dependence on permeability in FG1 correlation (as compared to the 0.5 power dependence of Geertsma's correlation) causes a very small beta at high

permeabilities (as the FG1 correlation was not developed for high permeabilities). Thus, when the Frederick and Graves correlation is used in the models, I will consider the results to essentially be with Darcy flow.

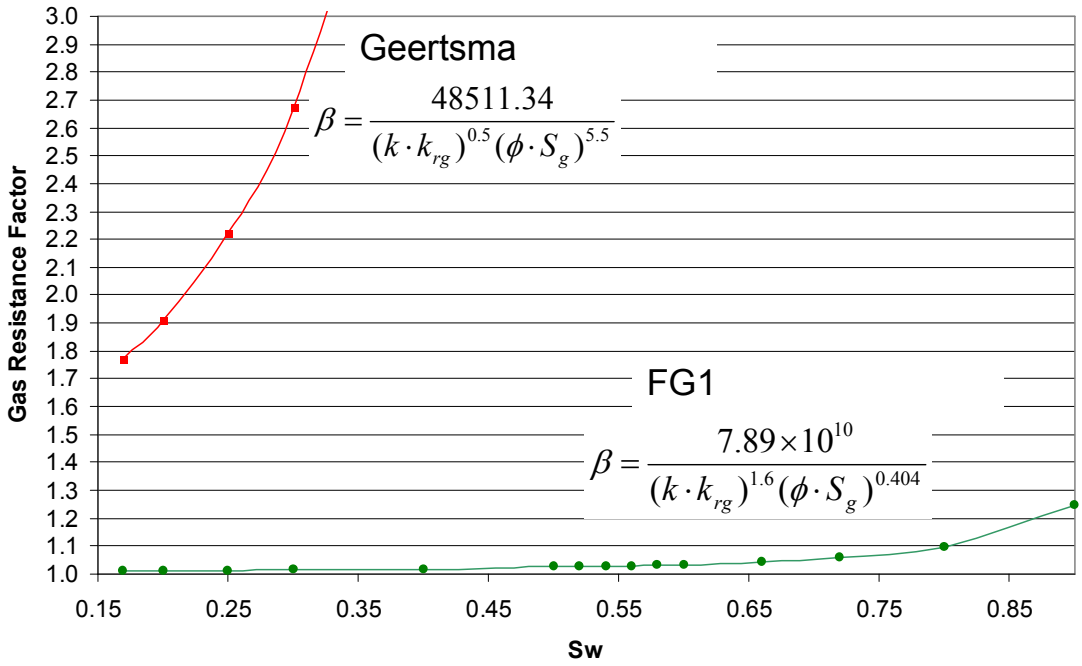

Fig. 2.9 Gas resistance factor versus water saturation for Geertsma's correlation and Frederick and Graves' 1st correlation. Values are at a gas velocity of 850 ft/D and proppant permeability of 15,000 md.

2.4 ANALYTICAL AND SIMULATION SOLUTION FOR UNIFORM INFLUX

Here I solve the mixed-flow problem analytically, for multiphase non-Darcy flow assuming an imposed uniform-influx function of both gas and water. I also outline the methods in simulation that result in uniform influx. The analytical solution method applies for any influx function (not only uniform influx), provided that the influx function is known and fixed.

In simulation models that allow for gravity-segregated flow, the fracture grid is an evenly spaced orthogonal grid, with 103 grid cells in the *i*-direction (fracture length) and 35 cells in the *k*-direction (vertical). The height is 100 ft, and the length is varied from 200 to 1000 ft. Models were also run that use only one cell in the vertical direction, resulting in mixed flow (i.e., no phase segregation).

Uniform influx is approximated in the simulations by placing a gas and water injector every 3 cells in the *i*-direction, for the mixed flow case. For the gravity segregated case, injectors are placed every 3 cells in both the *i*- and *k*-directions. Both cases are shown in **Fig. 2.10**. This results in having 34 injectors each for gas and water in the fracture in the mixed flow case, and 34 x 11 = 374 injectors in the segregated case. By constraining the injectors to inject at a constant rate of water or gas, and using equal injection for each injector, the flux is very close to uniform. The gas and water fluxes, as a function of distance along the fracture, are required in the derivation of the analytical solution.

TABLE 2.2 CASE PARAMETERS FOR UNIFORM FLUX SOLUTION

$(wk)_f$	200-6000 md•ft
x_f / h_f	2-10
q_g (Influx and production)	1-5 MMscf / D / wing
Y	5-30 Bbl/MMscf
p_{wf}	6,000 psi

To quantify the effects of segregation, I simulated cases with various gas rates (per fracture wing, or ½ of the hypothetical drainage area), water/gas ratios (Y), and fracture properties and geometries (**Table 2.2**). I isolated the affect of fracture aspect ratio from that of gas rate, conductivity and water/gas ratio. As the bottomhole pressure in the producer well is held constant, and injection (to simulate influx into the fracture) is done at a constant rate (Table 2.2), the simulations are run until steady-state is achieved whereby the pressure in the fracture is time-invariant and the injection rate into the fracture equals the production rate. In simulation, I quantify the impact of gravity segregation by comparing the pressure drop along the fracture in steady-state in the gravity segregated case to that of the mixed flow case.

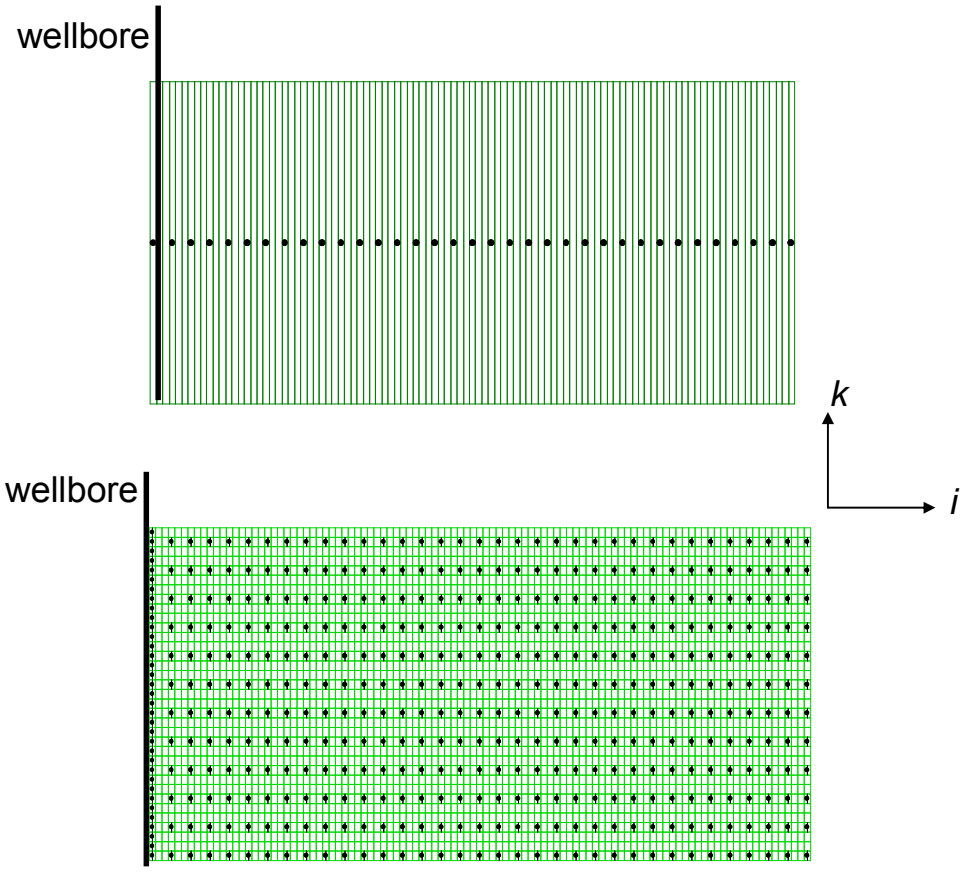

Fig. 2.10 Injection pattern for mixed-flow case (top) and segregated-flow case (bottom). To create uniform influx, injectors (dots) are spaced apart by 3 *i*-cells (both cases) and 3 *k*-cells (segregated case).

To derive an analytical solution for mixed flow with uniform influx, I start with the definition of gas flux, u_x^g (gas volume per unit time per unit area, also known as the Darcy velocity or superficial velocity), and convert to reservoir conditions for a gas rate q_g at surface conditions by using the gas expansion factor. Expressing this as a function, I arrive at

$$u_x^g(6{,}000\,psi) = \frac{q_g}{h_f w_f \cdot E_g(6{,}000\,psi)} \quad . \quad \text{.....(2.6)}$$

The gas x-velocity in the fracture at the producing wellbore (x = 0 ft) is given in Eq. 2.7 for a total influx (per half wing) q_g [MMscf/D], w_f = 0.02 ft, h_f = 100 ft, and gas expansion factor (Fig. 2.4) at 6000 psi.

$$u_x^g(p = 6400\,psi) = \frac{q_g[\text{MMscf/D}] \cdot 1{,}000{,}000\,ft^3/MMscf}{100\,ft \cdot 0.02\,ft \cdot (1530\,ft^3/bbl)(bbl/5.615\,ft^3)} = 1{,}834\,ft/D \quad \text{...(2.7)}$$

Since the gas and water rates are fixed for uniform flux, the flux function can be derived straightforwardly. Gas velocity u_x^g is shown as constant in Eq. 2.7, but there are two additional factors that I add for u_x^g. The gas flux at a position in the fracture represents the cumulative influx that has occurred up to that position (as the flow in the fracture is towards the wellbore), so should be a maximum at the wellbore (x = 0 ft) and zero at the fracture tip (x = 1,000 ft). Because this cumulative influx should show a linear form with respect to distance a linear behavior (as the injectors are distributed evenly), I introduce a factor of (1000 – x) / 1000 into Eq. 2.7. Also I add a factor of $12.46 / \rho_g(p)$ that takes into account a density that varies with pressure (Eq. 2.7 was for the density at 6,400 psi which is 12.46 lb_m/ft^3). The gas velocity function in Eq. 2.7 written as a function of position in the fracture, gas density, and total gas rate is

$$u_x^g(x,p,q_g) = q_g \cdot 1{,}834 \cdot \frac{1000-x}{1000} \cdot \frac{12.46}{\rho_g(p)} \quad . \quad \text{.....(2.8)}$$

This is graphed in **Fig 2.11** for a constant at $\rho_g(p)$ = 13 lb_m/ft^3 (p = 6,400 psi) and gas rate of 1 MMscf/D. The flux in the simulator agrees very closely with the analytical function shown above (**Fig. 2.12**). The slight difference in the curves is due to assuming constant density in Eq. 2.8 (pressure varies in simulation from 6,000 to 7,500 psi). Also the simulator used a discrete injection pattern (which causes stair-stepping), while the analytical function uses a smooth influx function (Eq. 2.8). The curves intersect (agree with each other) at x = 200 ft where the pressure in the simulation is 6,400 psi resulting in a density of 13 lb_m/ft^3.

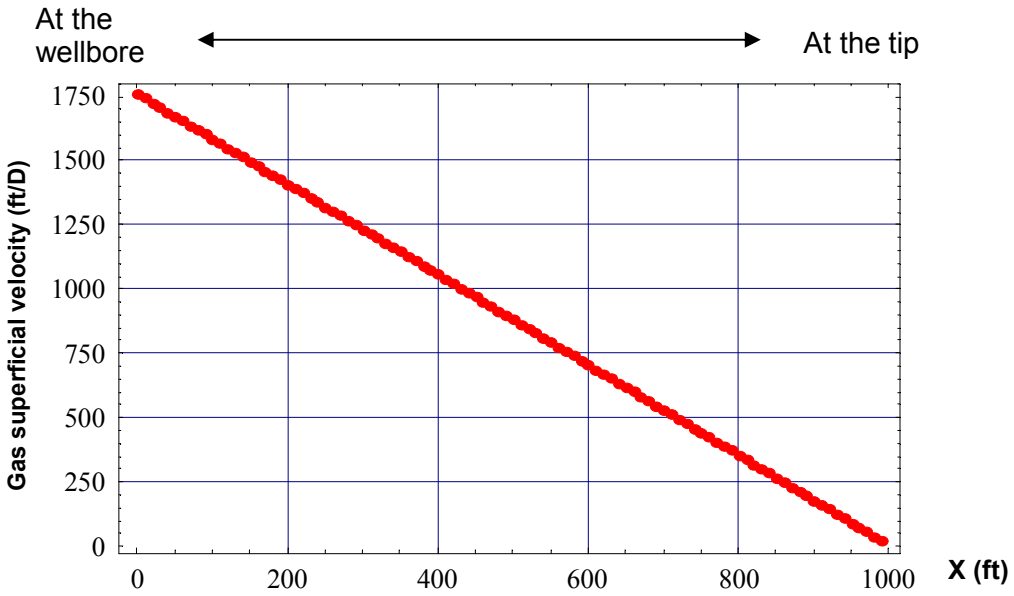

Fig. 2.11 Gas flux (i.e. Darcy velocity or superficial velocity) in the fracture in the $-x$ direction assuming uniform influx and no gas expansion effects.

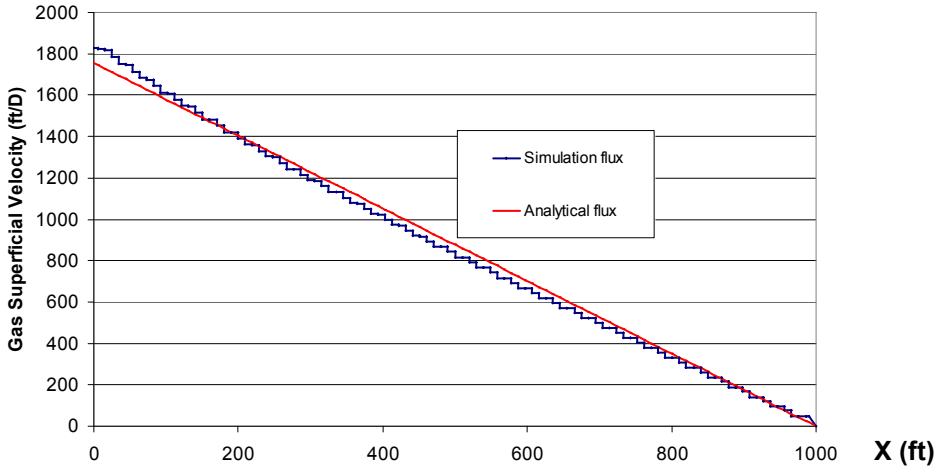

Fig. 2.12 Gas superficial velocity in the $-x$ direction vs. distance for the analytical function (assuming constant density) compared to simulation gas flux (density varies).

In a similar fashion to that done by Stone (1982), I solved for the water saturation along the fracture, given the constraint of water/gas ratio (Y) constant everywhere in the fracture. Stone showed that he could write the water/gas ratio as the ratio of Darcy's law for water to that of gas. I use his method, but extend it to use Forchheimer's equation, which I have rewritten to include multiphase non-Darcy flow as factored into the effective permeability (k_{eff}^{g} ; Eq. 2.5). There are no non-Darcy effects present for the water phase. YAfter doing this, I have

$$Y = 178{,}108 \frac{(B\mu)_g}{(B\mu)_w} \frac{k_{eff}^{w}}{k_{eff}^{g}} \quad , \qquad \text{.....(2.9)}$$

where the constant 178,108 converts from 1 MMscf to 1 Bbl so that the water/gas ratio is in units of Bbl/MMscf. Eq. 2.9 is comparable to Stone's Eq. 1. Next, assuming constant fluid properties shown in **Table 2.3**, the equation reduces to

$$Y = 16.40 \frac{k_{eff}^{w}}{k_{eff}^{g}} \quad . \quad \text{.....(2.10)}$$

TABLE 2.3 FLUID PROPERTIES AT 6,000 PSI:

Fluid type	B_g, B_w(stb/rb)	μ (cp)
Gas	0.0037	0.026
Water	1.04	1

Eq. 2.10 is valid for any vertical region in the fracture, as in steady-state the water/gas ratio for influx into the fracture, equals the water/gas ratio within the fracture at any gridblock, which equals the water/gas ratio at the producer. For the case with mixed flow, I straightforwardly solved this equation along the fracture using a constrained water/gas ratio along the fracture. For the segregated case, the gravity forces need to be modeled, in order to solve for the saturations as a function of vertical position.

For the mixed-flow case, I have shown our flux function earlier. To solve Eq. 2.10 I insert effective permeability to gas (Eq. 2.5) as a result of non-Darcy and multiphase flow, while ignoring stress effects.

$$Y = 16.40 \left[1 + \beta \cdot (k \cdot k_{rg}) \frac{\rho}{\mu} \cdot \left(\overrightarrow{U_x^g} \right) \right] \frac{k_{rw}}{k_{rg}} \quad \text{.....(2.11)}$$

After inserting relative permeability functions (Eq. 2.1), flux function (Eq. 2.8), and Geertsma's correlation for the beta factor (Eq. 2.3), I have

$$\frac{Y}{16.4} = \left[1+\left(\frac{48{,}511}{(\phi\cdot S_g)^{5.5}(k\cdot 0.74(1-S_w)^{N_g})^{0.5}}\right)(k\cdot 0.74(1-S_w)^{N_g})\left(\frac{\rho_g}{\mu}\right)_g \cdot q_g\left(1{,}758\cdot\frac{1{,}000-x}{x}\cdot\frac{13}{\rho_g}\right)\right]\cdot \frac{S_w{}^{N_w}}{0.74(1-Sw)^{N_g}} \quad \text{.....(2.12)}$$

It is clear now that gas density cancels (as mentioned in the derivation of the flux function, Eq. 2.8); however, I have to assume constant gas viscosity to remove the dependence on pressure. This is a good assumption if the pressure drop along the fracture is not too large, as the gas viscosity varies only 7% for pressures going from 6,000 to 7,000 psi.

TABLE 2.4 FRACTURE PARAMETERS USED IN CMG/ANALYTICAL COMPARISON

x_f	1,000 ft
h_f	100 ft
w_f	0.02 ft
q_g	1 MMscf / D / wing
water/gas ratio	20 Bbl/MMscf
k_f	50,000 md
$N_{w,g}$	1.0, 2.0
P_{wf}	6,000 psi

S_g and k_{rg} are functions of S_w, while ϕ, k, μ, Y, N, and q_g are constants. The only unknowns are x and S_w. This equation is easily solved by using the solve function within Mathematica, which finds the roots of the equation very quickly. By discretizing x from the wellbore (x = 0 ft) to the fracture tip (x = 1,000 ft), over 50 intervals, the solution for S_w is found at each x-value chosen. Only 50 intervals are needed as accuracy improves very slightly by going to 100 intervals. This was done for the case described in **Table 2.4**.

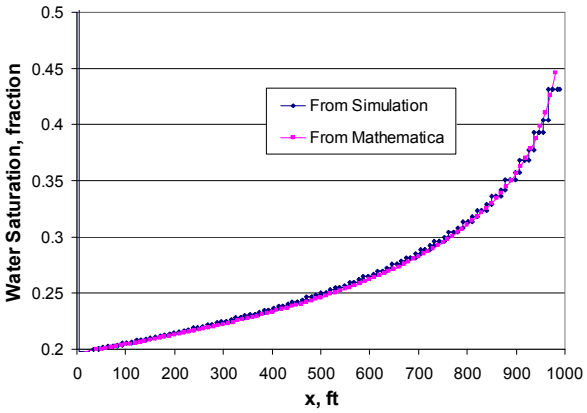

Fig. 2.13 Water saturation solution in simulation and analytical calculations.

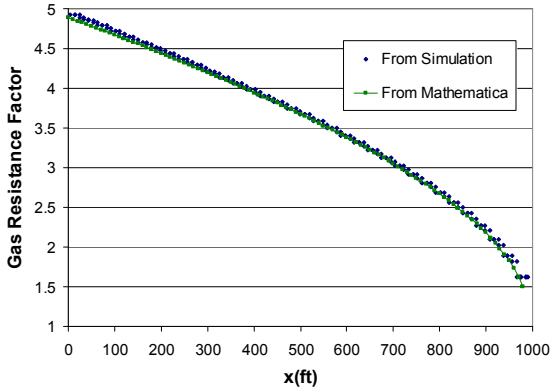

Fig. 2.14 Gas resistance factor solution in CMG and analytical calculations.

The results for saturations in the fracture agree very closely (within 1% tolerance) with the simulator in steady-state (**Fig. 2.13**) for the case described in Table 2.4 using linear relative permeabilities. The results for gas resistance factor (Eq. 2.2) for the same case are shown in **Fig. 2.14**, and show a very close agreement between simulation and analytical. This gives me confidence in the simulation model.

In steady-state the simulator achieves a water/gas ratio that is constrained, by varying the saturations until the product of $k_{rg}/[k_{rw}\cdot\text{GRF}]$ = constant (as in Eq. 2.10). I have plotted GRF and k_{rw}/k_{rg} vs. position in the fracture for the case described in Table 2.4 (linear relative permeabilities) in **Fig. 2.15** to show that where the gas resistance factor is high (near the wellbore where the velocity is high), the ratio of k_{rw}/k_{rg} decreases so that their product is constant.

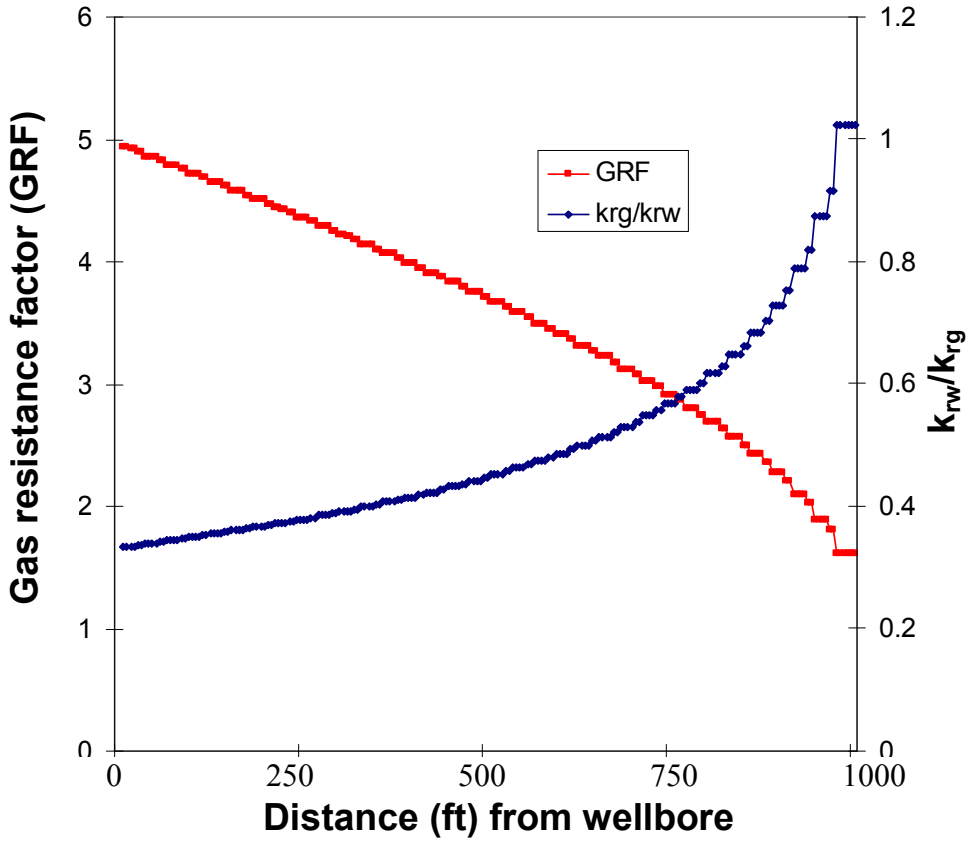

Fig. 2.15 Gas resistance factor and k_{rw}/k_{rg} vs. position in the fracture. As the gas resistance factor increases (near the wellbore where the velocity is high), the ratio of k_{rw}/k_{rg} decreases so that their product is constant.

Since I was not able to find the analytical solution for saturation and pressure in the gravity segregated case, I use the simulator for gravity segregated flow. In steady-state in the segregated model, there is segregation present depending on a number of factors, which are discussed in Section 3.1.

For mixed flow I found the solution for pressure drop by numerically integrating Forchheimer's equation (which is rewritten to look like Darcy's law, with k_{eff} including the non-Darcy and multiphase terms) along the fracture, where k_{eff} is the gas permeability (Eq. 2.5) and u_x is the gas velocity in the fracture (Eq. 2.8).

$$\frac{dp}{dx} = \frac{\overrightarrow{u_x^g}(x)}{0.00633 \cdot k_{eff} \cdot \frac{1}{\mu}} \quad . \quad \text{.....(2.13)}$$

$$\Delta p = \int_0^{xf} \left(\frac{dp}{dx} \right) dx \quad . \quad \text{.....(2.14)}$$

This is done straightforwardly in Mathematica. The comparison of pressure drop (Δp) between Mathematica and CMG is shown (**Table 2.5**) for the mixed flow case using linear fracture relative permeabilities and the data in Table 2.4. Also shown in Table 2.6 is the pressure drop comparison for the same case (Table 2.4) but using non-linear relative permeabilities ($N_{g,w} = 2$). Pressure drop in simulation and the analytical calculation agree to within 6% in all cases.

TABLE 2.5 PRESSURE DROP (PSI) ALONG THE FRACTURE BY RELATIVE PERMEABILITY TYPE

Relative permeability curves		**linear**	**non-linear**
no gravity	Analytical	393	982
	Simulation	408	984

2.5 EFFECT OF STRESS ON NON-DARCY FLOW WITH UNIFORM INFLUX

The methodology for determining the effect of closure stress on fracture permeability and non-Darcy flow is outlined in this section.

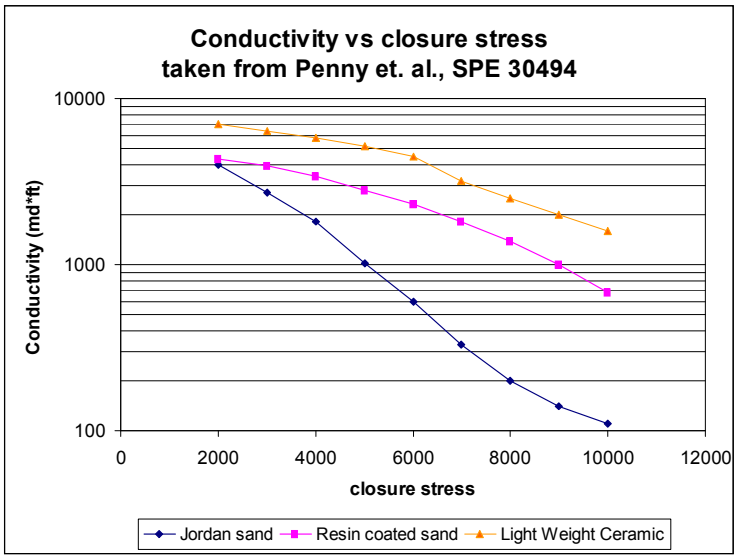

Fig. 2.16 Conductivity vs. closure stress from Penny et al. (1995).

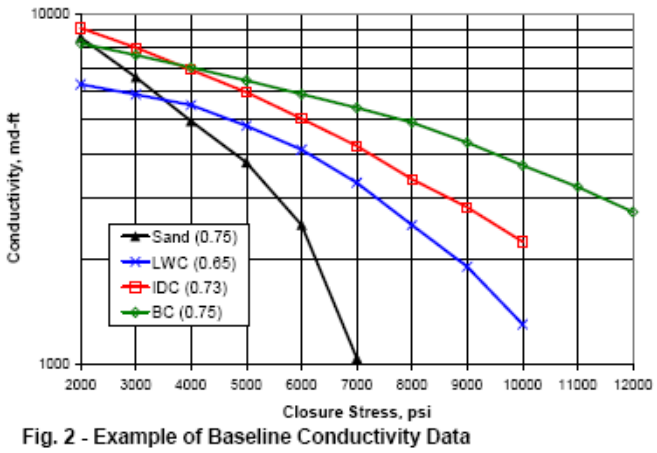

Fig. 2.17 Conductivity vs. closure stress from Schubarth and Milton-Tayler (2004).

Several authors (Penny and Jin, 1995; Schubarth and Milton-Tayler, 2004) have showed the impact of closure stress on proppant permeability. Empirical tests done by Penny and Jin and Schubarth and Milton-Tayler yield relationships between proppant conductivity and stress. Results from Penny and Jin (1995), are shown in **Fig. 2.16**, and work of Schubarth and Milton-Tayler (2004) is shown in **Fig. 2.17**.

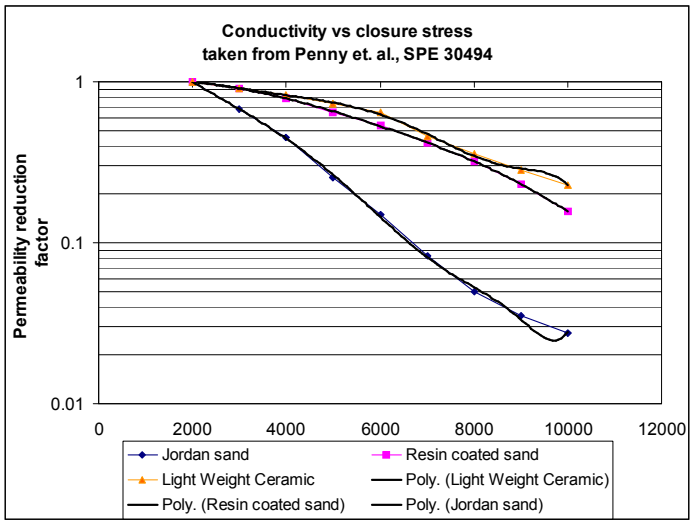

Fig. 2.18 Conductivity vs. closure stress taken from Penny and Jin (1995) and normalized.

After I normalized the permeability values in Fig. 2.16, I describe the relationship between $\left(k/k_{ref}\right)_{stress}$ and closure stress (**Fig. 2.18**). Values are normalized such that the permeability reduction factor ($\left(k/k_{ref}\right)_{stress}$) is 1 at 2,000 psi stress for each proppant type. These data were then fit to a 6th order polynomial, in order to determine a functional relationship for use in further analytical calculations. Even though non-Darcy

resistance changes with closure stress (as non-Darcy resistance depends on permeability), as a first approach I will ignore changes in non-Darcy resistance as a function of stress. Later, I will include this change in non-Darcy resistance, since Schubarth and Milton-Tayler observed an increase in beta with stress (**Fig. 2.19**).

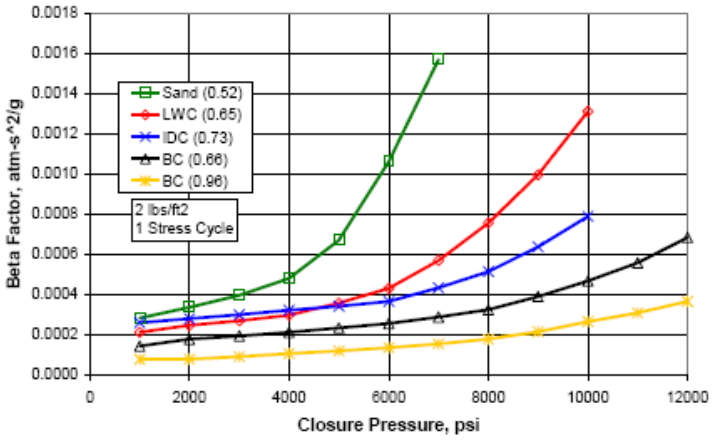

Fig. 2.19 Increase in beta factors due to closure stress from Schubarth and Milton-Tayler (2004).

The net effect of lowering permeability on non-Darcy resistance (Eq. 2.2) involves both beta and the permeability. The stress reduction in permeability is a function of closure stress, which in turn is a function of fluid pressure. The polynomial fit equation in Fig. 2.14 for the Resin coated sand yields the relationship between stress reduction and closure pressure as $\left(k/k_{ref}\right)_{stress}$ = 8.183E-24 σ_c^6 - 2.692E-19 σ_c^5 + 3.261E-15 σ_c^4 - 1.625E-11 σ_c^3 + 1.787E-08 σ_c^2 - 3.284E-05 σ_c + 1.080. I first modeled a case where overburden σ =12,000 psi. The closure stress, σ_c acting on the proppant grains is then the total stress minus fluid pressure or σ_c = 12,000 – p from the fundamentals of

poroelasticity. To model a situation with higher closure stress, the overburden is chosen to be 15,000 psi which causes the closure stress to become 15,000 - p. I used the different overburden cases to ensure that closure stress is 2,000 psi at the wellbore. I use Berg's (1970) formula (Eq. 2.15) to quantify the relationship between permeability and the following variables: porosity (ϕ), mean particle diameter (Md) and ΔPD (the difference between mean and 90th percentile particle diameters).

$$k = 5.1x10^{-6}\phi^{5}(Md)^{2}e^{-1.385(\Delta PD)} \quad \text{..... (2.15)}$$

The above equation shows that permeability is expected to reduce when porosity reduces and other variables remain constant. This proportionality dependence of permeability with porosity is

$$k \propto \phi^{5} \quad \text{.....(2.16)}$$

Schubarth and Milton-Tayler (2004) shows results agree well with Berg's for the various parameters in the relation. As I have lab values for reduction in permeability, and not for reduction in porosity, I use Eq. 2.16 to determine the reduction in porosity for a given reduction in permeability. I have inserted Eq. 2.16 into Geertsma's equation (Eq. 2.3), to replace the porosity term with permeability. Then I divide beta at 2,000 psi closure stress ($k = k_1$) and beta at some higher closure stress (with $k = k_2$). The result of this division is

$$\frac{\beta(\sigma_c = 2{,}000\,psi)}{\beta(\sigma_c > 2{,}000\,psi)} = \frac{1}{\left(\frac{k_2}{k_1}\right)^{0.5}\left(\frac{k_2}{k_1}\right)^{0.2\cdot 5.5}} = \frac{1}{\left(\frac{k_2}{k_1}\right)^{1.6}} \quad \text{.} \quad \text{.....(2.17)}$$

Now, I have found a method to determine the net affect on beta for a case where closure stress is higher than 2,000 psi as compared to a case with closure stress = 2,000 psi. The net affect on non-Darcy resistance (Eq. 2.2) depends on beta as well as the permeability.

2.6 HYDRAULICALLY FRACTURED RESERVOIR WITH TWO-PHASE FLOW

Models in previous sections only considered the fracture and did not model the reservoir. Here I model the fracture and reservoir, for a quarter symmetry system. Flow occurs from the reservoir, through the fracture, and to the wellbore. Stress effects are ignored in reservoir models, and are only considered for the uniform flux models.

A fine grid is used near the wellbore and near the fracture tip. The difference between mixed-flow and segregated-flow models is the discretization in the vertical direction. In the model with one layer (**Fig. 2.20**), mixed flow occurs, as there is no vertical discretization. In the model with vertical discretization, (**Fig. 2.21**), gravity phase segregation is allowed. During production, the phase segregation of water and gas in the fracture is apparent, as illustrated in Fig. 2.21.

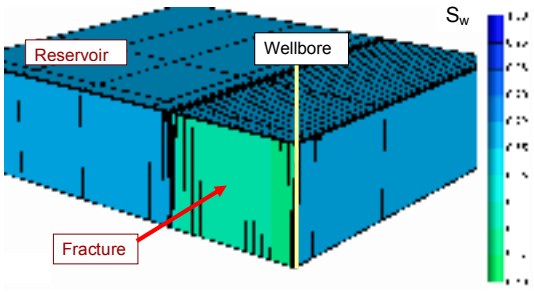

Fig. 2.20 Model is run with no vertical discretization to prevent gravity segregation from developing.

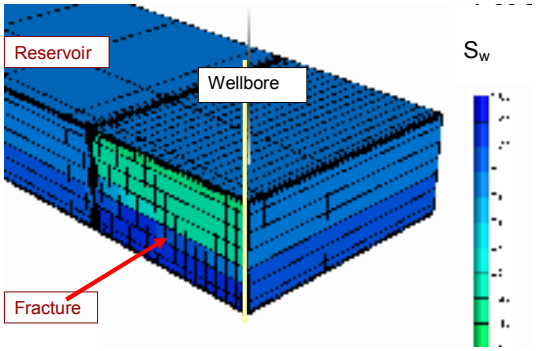

Fig. 2.21 Model is run with gravity-segregated flow by using vertical discretization.

One quarter of a square drainage area is modeled in the simulations. The reservoir is assumed to be homogenous, and at a uniform initial water saturation that gives rise to multiphase flow in the reservoir and fracture. Also, single phase flow models are run to isolate the effect of multiphase flow in the fracture. As mentioned earlier, for all fractured reservoir models I use relative permeability for a typical resin coated proppant pack derived from lab tests by Sullivan et al. (Fig. 2.1). Non-Darcy flow is modeled using Geertsma's correlation (Eq. 2.3) as described earlier.

Fracture, reservoir, and production parameters are given below:

- k_f = 1,500-30,000 md
- x_f = 640 ft, h_f, h = 25 ft
- S_{wi} = 0.68 (for multiphase flow models)
- q_g (calculated) = 0.44 MMscf/D (2 wings; i.e. the quarter system rate multiplied by 4)
- Grid: only a quarter of fracture and reservoir system is modeled; See **Table 2.6**.
    - i x j x k = 42 x 8 x 29

  - The grid is finer at the tip and wellbore (to model areas with high flux accurately) and also at the top and bottom of the fracture (to capture segregation effects accurately)

- Drawdown (calculated) = $\bar{p} - p_{wf}$
- Well index is very high in the perforated cell block ($i = 1, j = 1$), so that the calculated bottomhole pressure will be very close to the gridblock pressure in the simulation.

TABLE 2.6 GRID DIMENSIONS USED IN RESERVOIR/FRACTURE MODEL (FT)

Δx = 0.02 0.1 0.2 0.4 0.75 2.0 5.0 10.0 20.0 14*40 20 10 5 2 0.75 0.4 0.2 0.1 0.1 0.3 1.0 2.0 5.0 10.0 20.0 80.0 400 400 400
Δy = 0.02 0.05 0.3 1.0 5.0 50.0 250 500.0
Δz = 0.05 0.15 0.45 1.5 4.5 7*10 4.5 1.5 0.45 0.15 0.05

Dimensionless productivity, J_D, can be calculated (Eq. 2.16) once the gas rates and drawdown are both calculated from the simulation. Also, fluid properties are assumed constant as the $1/B\mu$ product is relatively constant at pressures above 5,000 psi (Fig. 2.5). Non-Darcy effects are present in the reservoir; however, they are neglected as explained below. Effective permeability k_{eff} is measured in the reservoir as defined in Eq. 2.5 using the relative permeability at the initial water saturation of the reservoir. Doing this removes the unwanted effect of multiphase flow in the reservoir on the productivity, so that only multiphase flow in the fracture impacts the productivity.

$$J_D = \frac{q[MMscf/D]\cdot 4\cdot 1\times 10^6 \mu_g}{2\pi\cdot 0.00633h\cdot k_{eff}\left(\overline{p}-p_{wf}\right)\left(\frac{E_g}{5.615}\right)} \quad \text{.} \quad \text{.....(2.16)}$$

Dimensionless conductivity (Eq. 2.17) and the difference in effective conductivity from segregated to mixed flow will be investigated along with changes in dimensionless productivity. The original dimensionless fracture conductivity (the single-phase fracture conductivity) is shown below where the reservoir is at the effective permeability, $k_{res,eff}$.

$$C_{f_D} = \frac{wk_f}{x_f k_{res,eff}} \quad \text{.} \quad \text{.....(2.17)}$$

Effective dimensionless fracture conductivity (due to multiphase non-Darcy flow in the fracture) is calculated in Eq. 2.18, where both the reservoir and fracture are at the effective permeability ($k_{res,eff}$ and $k_{f,eff}$ respectively).

$$C_{fD,eff} = \frac{wk_{f,eff}}{x_f k_{res,eff}} \quad \text{.} \quad \text{.....(2.18)}$$

Non-Darcy forces are neglected in the reservoir in calculation of both conductivity (Eqs. 2.17-2.18) and productivity (Eq. 2.16), as these equations use constant reservoir permeability. However, this being said, productivity calculations according to Eq. 2.16

are accurate to within 1%. I determined this by using fracture-face permeability damage as a proxy for determining the effect of gas resistance factor on the reservoir permeability. It is observed in a model producing two phases from the reservoir that the gas resistance factor in the reservoir is no more than 1.66 (permeability loss of 40%) in the j-plane that extends from the fracture plane to a distance of 0.06 ft perpendicularly away from the fracture plane. After that distance and until a distance of 0.3 ft away from the fracture face, the gas resistance factor is no more than 1.06 (permeability loss of 6%). Having run productivity calculations (not shown) for damage in the reservoir adjacent to the fracture, I have determined the following: for a permeability loss of 75% (higher than the permeability loss described above), and for a damage distance of 1.4 ft (more than the damage distance described above), the resulting reduction to productivity index is no more than 1.2% for dimensionless conductivity in the range of 0.5 to 25. Therefore I can safely assume that ignoring gas resistance in the reservoir will result in no more than a 1.2% error in calculation of dimensionless productivity (Eq. 2.16).

2.7 FRACTURED RESERVOIR UNDER CLEANUP

In cases where cleanup of injected stimulation water is modeled, the only mobile water in the reservoir is injected water. As in the previous section, segregated flow models will be compared to mixed flow models (**Fig. 2.22**).

Case 1 uses Frederick and Graves 1st correlation for non-Darcy flow (Eq. 2.4) (which is essentially Darcy flow for high permeabilities, as in the fracture) and the linear relative permeabilities (Fig. 2.1). Case 2 is more realistic in that it uses Geertsma's correlation and non-linear relative permeabilities. By comparing Case 1 with Case 2 I will determine if the impact of gravity effects depends on the degree of non-Darcy flow and relative permeabilities used. In Case 3 there are two reservoirs (one a gas reservoir, the other an aquifer) connected only by a hydraulic fracture. Mobile water is being produced from the aquifer, while the well is being cleaned up. In Case 4, there are 4 zones connected by a hydraulic fracture. Case 4 is similar to Case 3 in that there is mobile water coming from a reservoir zone; however, Case 4 does not use the injected-water stage.

Water is injected over longer times (19 hours) than a typical fracture treatment (several hours) in order to achieve a similar amount of total injected water in the simulation as in a typical treatment. In Case 1 and 2 (**Fig. 2.23**), all injectors have a maximum 2,500 Bbl/D rate constraint with a maximum P_{wf} constraint of 12,000 psi, and inject sequentially such that the injectors near the wellbore are open for the longest time to

simulate the injection of water while the fracture is propagating (Fig 2.23, **Table 2.7**). The injector at the wellbore is on for the entire duration of the simulated treatment (0.80 days). Case 3 (**Fig. 2.24**) uses a slightly different injection scheme (**Table 2.8**), whereas the injection is for 0.8 days at 12,000 psi but no restriction is in place on injection rates.

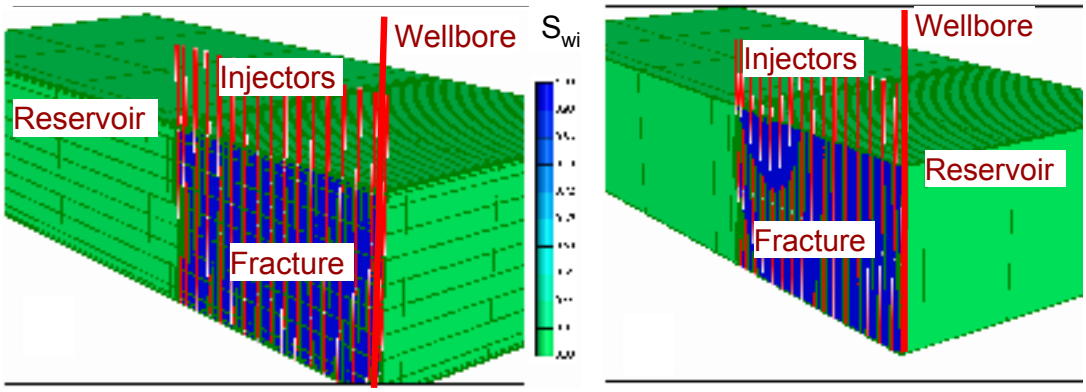

Fig. 2.22 Model with segregated-flow (left) will be compared to mixed-flow model (right).

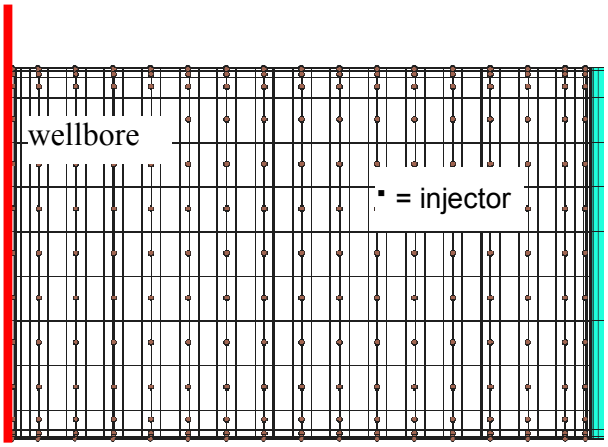

Fig. 2.23 Injectors used in the study, to provide injection of stimulation water over the course of the hydraulic fracture treatment.

TABLE 2.7 INJECTOR TIMINGS (CASES 1 & 2)

Distance from wellbore (ft)	*i* (cell number)	Time injection begins (days)
0	1	0
30	12	0.1
72	14	0.15
114	16	0.2
156	18	0.225
198	20	0.25
240	22	0.275
282	24	0.3
324	26	0.35
366	28	0.4
408	30	0.45
450	32	0.5
492	34	0.55
534	36	0.6
576	38	0.65
618	40	0.7
660	42	0.75

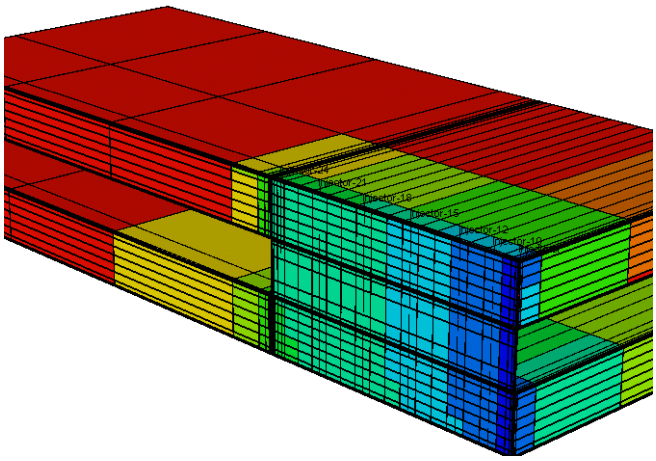

Fig. 2.24 Case 3: Two reservoirs connected by a fracture, with an impermeable zone separating the reservoirs so that the only communication is through the fracture.

TABLE 2.8 INJECTOR TIMINGS (CASE 3)

Distance from wellbore (ft)	*i* (cell number)	Time injection begins (days)
0	1	0
60	10	0.15
140	12	0.22
260	15	0.3
380	18	0.45
500	21	0.6
600	24	0.7

Fracture and reservoir parameters for Cases 1-3 are given below.

- w_f = 0.04 ft
- L_f = 650 ft

Fracture and reservoir parameters for Case 1 are given below.

- Frederick and Graves 1st correlation for non-Darcy flow and linear fracture relative permeabilities (Fig. 2.1)
- k_{res} = 1 md
- k_f = 15,000 md
- ϕ = 0.3
- C_{fD} = 3.1 (for k_{res} = 1 md)

Fracture and reservoir parameters for Case 2 are given below.

- Geertsma's correlation for non-Darcy flow and non-linear fracture relative permeabilities (Fig. 2.1)
- k_{res} = 0.1, 1 md
- ϕ = 0.35
- k_f = 50,000 md
- C_{fD} = 10 (for k_{res} = 0.1 md)
- C_{fD} = 100 (for k_{res} = 1 md)

Fracture and reservoir parameters for both Case 1 and Case 2 are given below.

- S_{wi} = 30% (slightly above the irreducible water saturation of 20%)

    - k_{rg} = 0.3, k_{rw} = 0.0001 @ S_g=0.7
- h = 83 ft
- Grid spacing:
    - Δx = 0.02 0.03 0.04 0.05 0.1 0.2 0.4 0.75 2.0 5.0 10.0 20.0 27•21.1 20 10 5 2 0.75 0.4 0.2 0.1 0.1 0.3 1.0 2.0 5.0 10.0 20.0 80.0 400 400 400
    - Δy = 0.02 0.03 0.06 0.12 0.3 1.0 5.0 50.0 250 500.0
    - Δz = 0.05 0.15 0.45 1.5 4.5 7•10 4.5 1.5 0.45 0.15 0.05

Fracture and reservoir parameters for Case 3 are given below.

- Top reservoir: S_{wi} = 95%
    - h = 25 ft
- Lower reservoir: S_{wi} = 30% (slightly above the irreducible water saturation of 20%)
    - k_{rg} = 0.3 @ S_g = 0.7
    - h = 25 ft
- Grid spacing
    - Δx = 0.02 0.1 0.2 0.4 0.75 2.0 5.0 10.0 20.0 14*40 20 10 5 2 0.75 0.4 0.2 0.1 0.1 0.3 1.0 2.0 5.0 10.0 20.0 80.0 400 400 400
    - Δy = 0.02 0.05 0.3 1.0 5.0 50.0 250 500.0
    - Δz = 0.25 0.5 2.0 5*4.0 2.0 0.5 0.25 0.5 1.5 5 10 5 1.5 0.5 0.25 0.5 2.0 5*4.0 2.0 0.5 0.25

Case 4 resembles a situation where stimulation-water injection phase is not included, so is a longer term water production case. Water/gas ratio is such that the amount of water is reasonable for a cleanup situation. There are 4 reservoir-quality zones with slightly mobile water connected by a hydraulic fracture, such that they provide gas and water flow into the fracture (**Fig. 2.25**). The zones communicate with each other via the hydraulic fracture only, as there are impermeable zones separating each of the 4 gas zones.

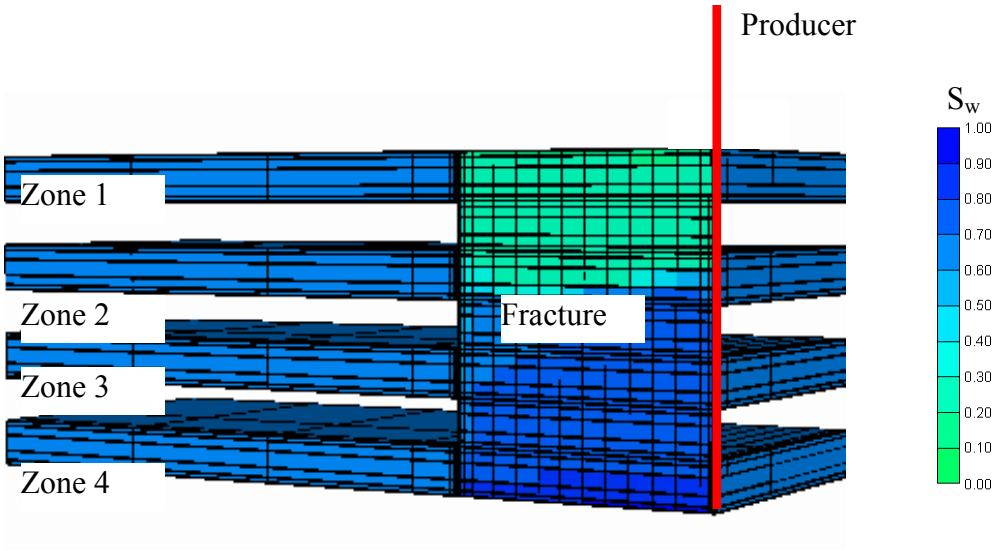

Fig. 2.25 Steady-state water saturation during production for the Case 4 fractured reservoir with 4 homogenous and isotropic zones with equal height.

Fracture and reservoir parameters for Case 4 are given below.

- h_f = 100, 400 ft
- In each of the 4 reservoir zones:
    i. $h = h_f / 7$

ii. S_{wi} = 66%

iii. k_{rg} = 0.05, k_{rw} = 0.08 (@ S_{wi} = 66%)

- k_f = 300, 3000 md
- w_f = 0.04 ft
- k_{res} = 0.3md
- $k_{res,eff}$ = 0.015 md
- L_f = 640 ft
- Original C_{fD} = 1.2, 12, 120

Conductivity is measured as in Cases 1-3, where the reservoir is taken at the effective permeability, and the fracture is at the original conductivity (assuming single-phase is present). The fracture is completed in two different cases. One case is where the top and 2nd from the top zones are completed (which I call Z1 + Z2). The other case is where the top and bottom zones are completed (which I call Z1 + Z4).

3. SIMULATION RESULTS AND DISCUSSION

3.1 SEGREGATION EFFECTS WITH UNIFORM INFLUX

I quantified the impact of gravity segregation by comparing the pressure drop in the gravity-segregated case to that of the mixed-flow case. The pressure drop is measured from the wellbore to the point that is located halfway vertically at the fracture tip to the point that is halfway vertically at the wellbore. Average pressure gradient is calculated by dividing the pressure drop by the fracture length. Pressure gradient (*dp/dx*) is inversely proportional to the effective permeability (Eq. 2.13). The amount of segregation is determined relatively between cases and visually. When one case shows a more distinguishable zone with high gas saturation separate from and above a zone with high water saturation, then I claim that there is more segregation apparent in that case. I found that the amount of segregation (determined visually) increases over time, as the simulation approaches steady state (**Fig. 3.1)**. In Fig. 3.1 the wellbore occupies the left side of the fracture and is produced at a constant bottomhole pressure of 6,000 psi (at the lowest perforation in the wellbore). When looking at the figure, it is apparent that more segregation occurs at the later times, and the fracture is most segregated at steady-state.

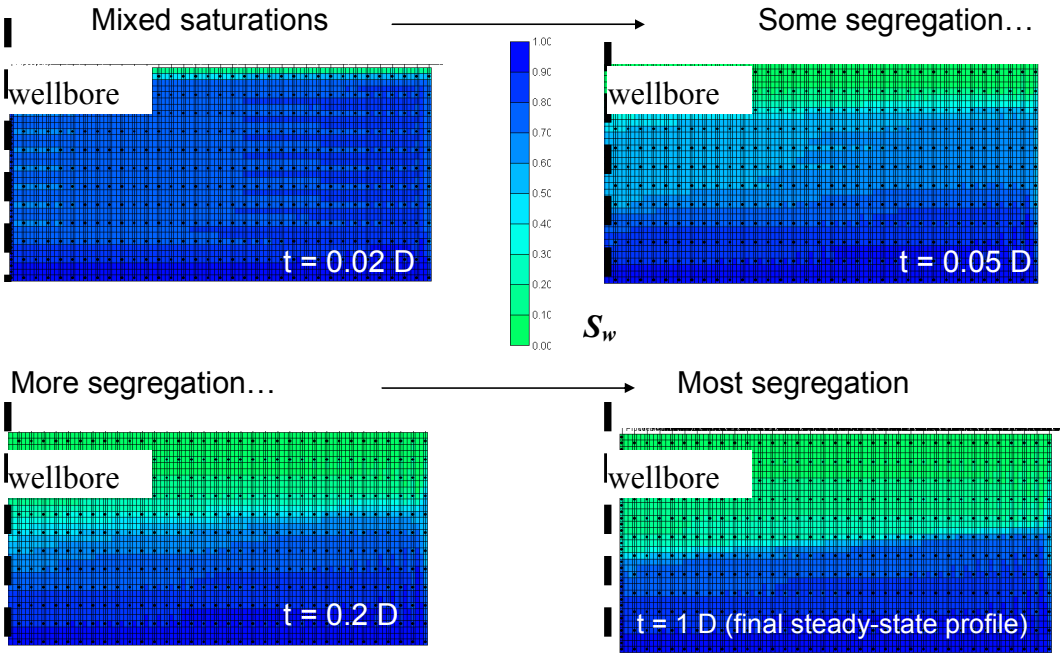

Fig. 3.1 Water saturation maps in the fracture at various times. In the simulation, the amount of segregation increases over time. The amount of segregation is determined visually, and is highest at steady-state.

Gas rate, water/gas ratio, and fracture permeability together determine the resulting pressure gradient and amount of segregation in the fracture. First I compared the amount of segregation in models with varying fracture conductivity at a fixed aspect ratio (10), gas rate (1 MMscf/D per fracture wing, or half of the hypothetical drainage area), and water/gas ratio (20 Bbl/MMscf). Second I varied the aspect ratio and compared cases with the same conductivity, gas rate, and water/gas ratio. Lastly I compared cases with varying gas rate and at the same conductivity, aspect ratio, and water/gas ratio. In all cases in this section fracture height is 100 ft.

Steady-state water saturation plots are shown in **Fig. 3.2** for fractures with an aspect ratio of 10 and conductivities of 400 and 600 md•ft. **Fig. 3.3** is for fracture aspect ratios of 4 and conductivities of 600-1,500 md•ft. **Fig. 3.4** is for fracture aspect ratios of 2 and conductivities of 1500-6,000 md•ft. The amount of segregation is determined visually, by comparing the saturations in the fracture for different cases. Higher conductivities show more segregation; however, aspect ratio and conductivity are also important. By comparing aspect ratios of 2 and 4 at a constant conductivity and gas rate (**Fig. 3.5**), it is apparent that larger fracture length-to-height ratios will show more segregation for the uniform-influx case. This also occurs as shown later for the non-uniform-flux models. By keeping conductivity and aspect ratio constant, and varying the gas rate, I see that at lower gas rates (and corresponding pressure gradients) more segregation occurs (**Fig. 3.6**). The resulting average pressure gradient (total pressure drop divided by fracture length) is 0.32 psi/ft (q_g = 1.5 MMscf/D), 0.53 psi/ft (q_g = 2 MMscf/D) and 1.07 psi/ft (q_g = 3 MMscf/D). If gas rate is lower, the amount of segregation decreases similarly as it does when the conductivity increases or the fracture length to height ratio decreases. The first two effects (lower gas rate and higher conductivity) result in more segregation because a lower pressure gradient in the horizontal direction relative to the pressure gradient in the vertical direction results. When the horizontal and vertical pressure gradients are closer to equal in magnitude, or the vertical pressure gradient is higher than the horizontal, then more segregation occurs. When the fracture length to height ratio is higher (the third effect that causes more segregation), and gas rate is fixed, the flux in the vertical direction is less. Because the pressure gradient in the vertical direction is

fixed (0.44 psi/ft in the water zone), the required permeability to gas to cause buoyancy to the gas zone is less when the flux is less. When the required permeability is less, then the water saturation is higher in the water zone, which means that more segregation occurs. Therefore, for longer fractures at a fixed gas rate, the more segregation occurs (for uniform flux). This is because segregation is caused by having a sufficient vertical pressure gradient relative to the horizontal pressure gradient.

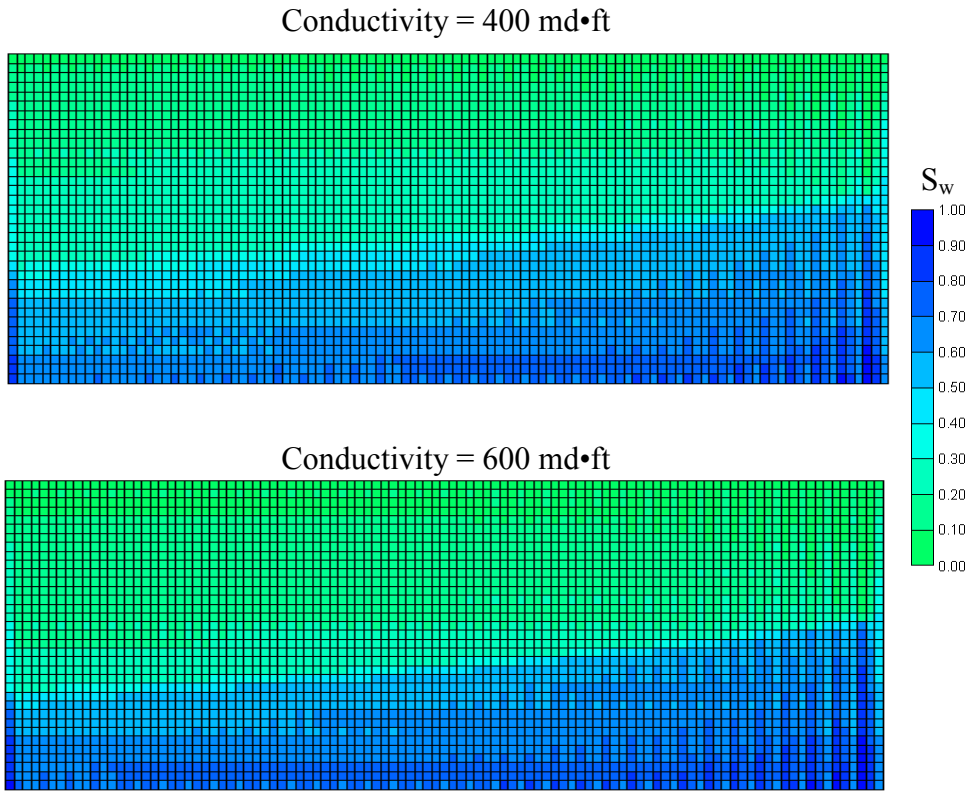

Figure 3.2 Steady-state saturation maps in the fracture for conductivity of 400 (top) and 600 md•ft (bottom). Long fracture, with aspect ratio (x_f / h_f) of 10.

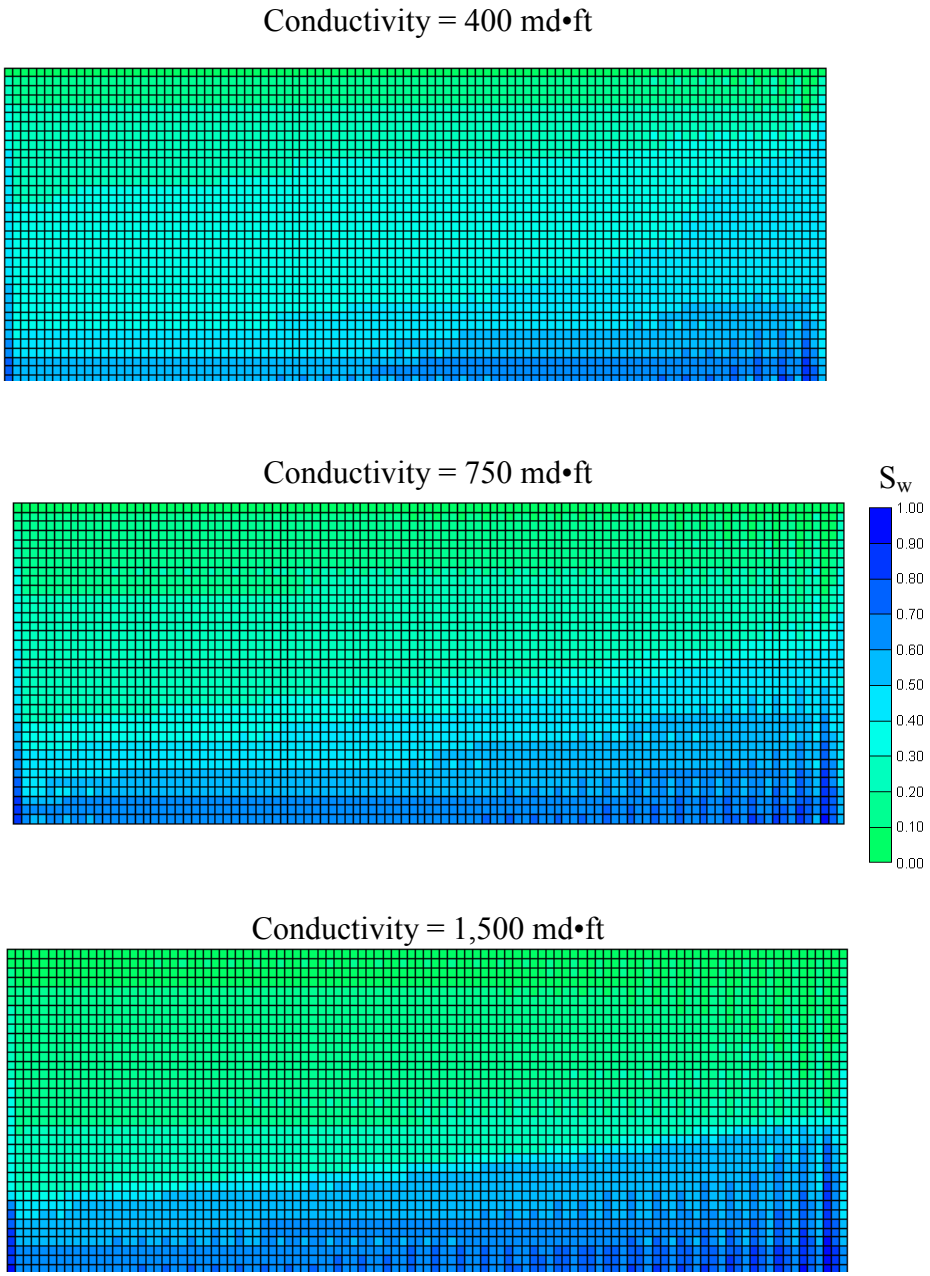

Figure 3.3 Steady-state saturation maps in the fracture for conductivity of 400 (top), 750 (middle) and 1,500 md•ft (bottom). Fracture, with aspect ratio (x_f / h_f) of 4.

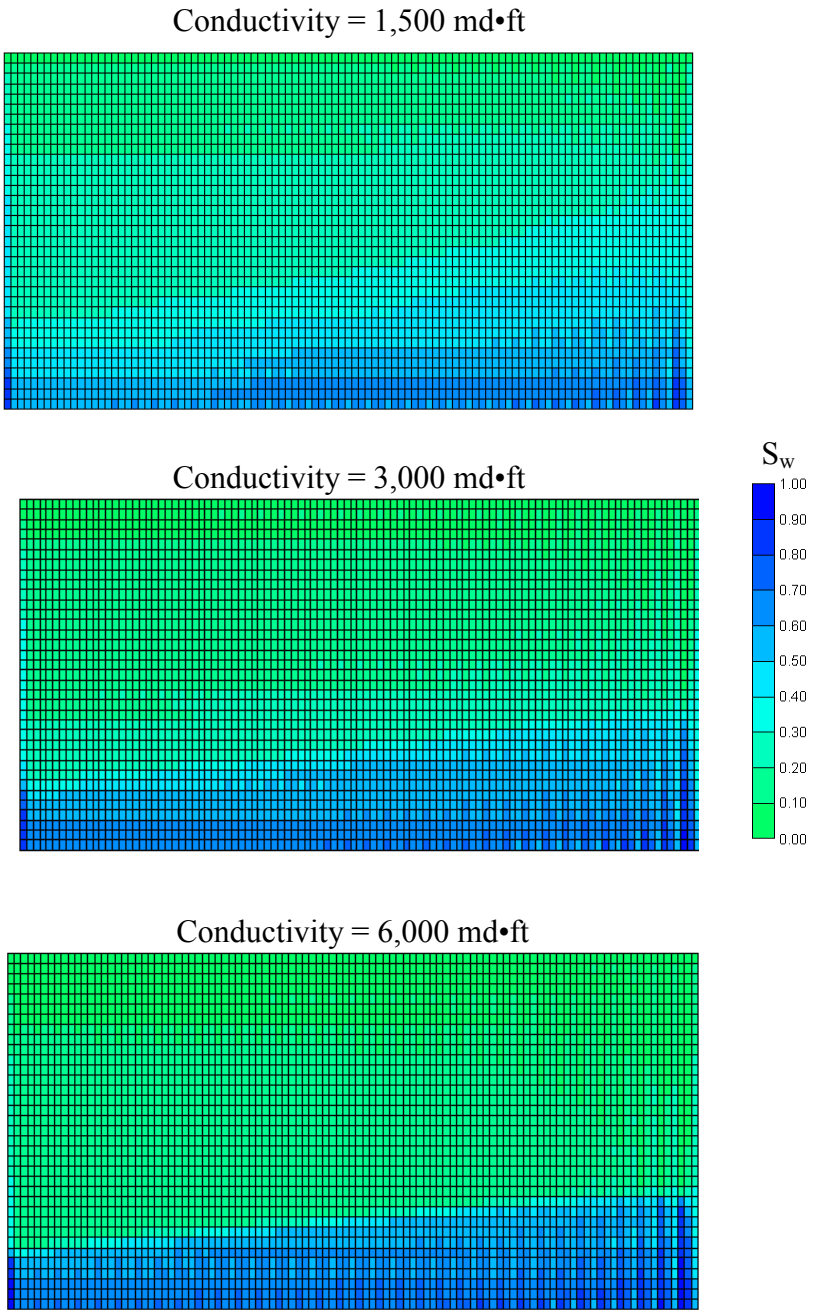

Figure 3.4 Steady-state saturation maps in the fracture for conductivity of 1,500 (top), 3,000 (middle) and 6,000 md•ft (bottom). Fracture, with aspect ratio (x_f / h_f) of 2.

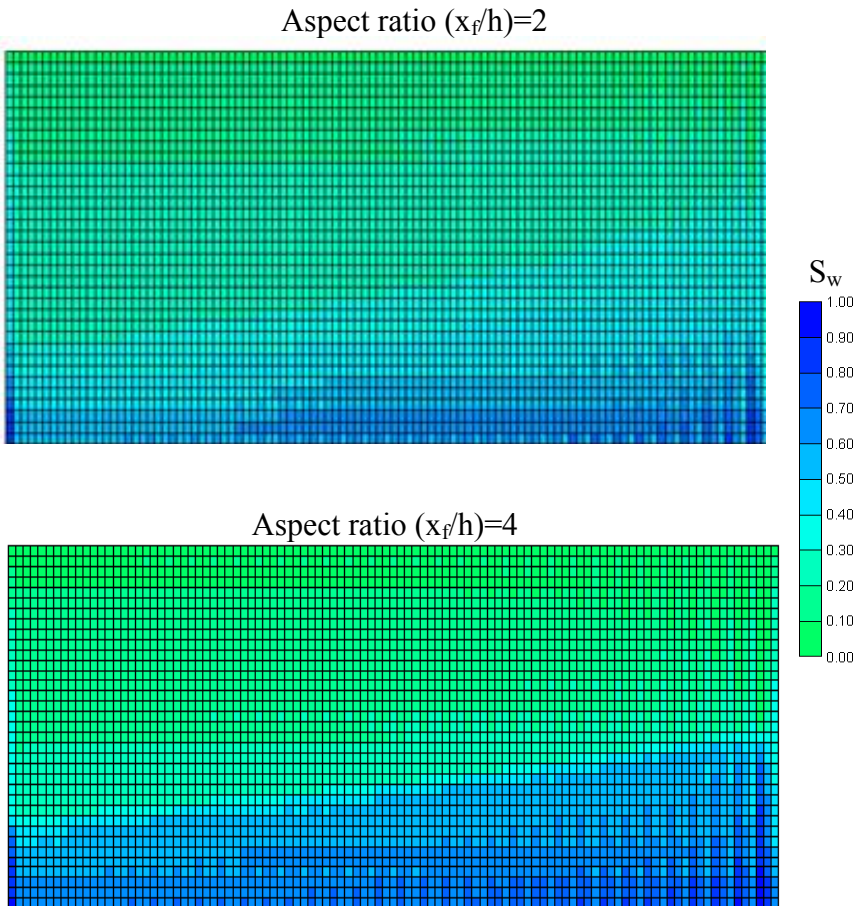

Figure 3.5 Steady-state saturation maps in the fracture for varying aspect ratio (x_f / h_f) of 2 (top) and aspect ratio of 4 (bottom). Both are for conductivity of 1,500 md•ft and gas rate of 1 MMscf/D (per fracture wing).

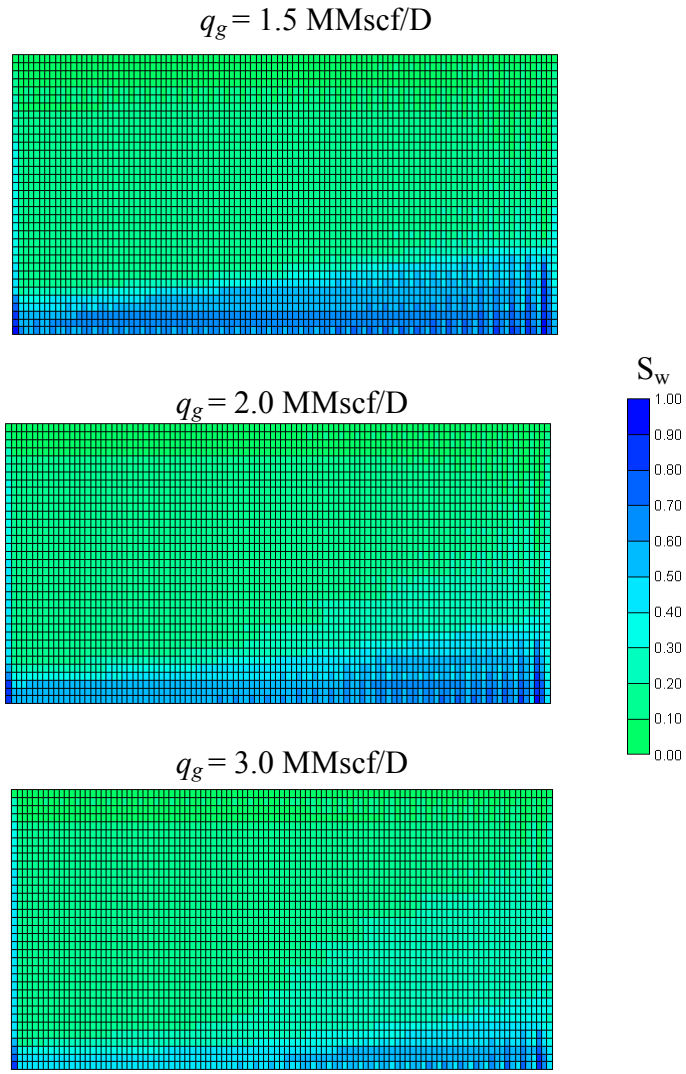

Figure 3.6 Steady-state saturation maps in the fracture for varying gas rate of 1.5 (top), 2.0 (middle), and 3.0 MMscf/D (bottom). All are for aspect ratio (x_f / h_f) of 2 and conductivity of 6,000 md•ft.

I also analyzed cases that are the same as the segregated flow cases shown in the previous pages, but in mixed flow. I compared the resulting pressure drop to segregated

flow cases. I found that the pressure drop is always higher for mixed flow, and the segregated-flow model is used as a base to determine the increase in pressure drop for the mixed flow models. This is a quantitative observation and not visual. I define the increase in pressure drop to be the percentage that the pressure drop is higher by in mixed flow when compared to segregated flow. I found that segregation impacts pressure drop, and effective conductivity. Because of the impact on effective conductivity, well productivity is also affected. An increase in pressure drop corresponds directly to a decrease in effective fracture permeability, as I have shown earlier that the two are related (Eq. 2.13). I found that segregation impacts pressure drop or effective conductivity when the degree of phase segregation is higher and depends further on:

1. the relative permeabilities used in the model
2. the degree of non-Darcy flow and the non-linearity of non-Darcy flow with respect to saturation

The latter two effects, relative permeabilities and non-Darcy flow, are important because of their non-linear natures. In mixed flow, the non-linear relationship of the gas resistance factor and relative permeability becomes pronounced as the water saturation is higher in mixed flow. Conductivity and gas rate both ultimately affect the pressure gradient in the x-direction along the fracture, which in turn affects the amount of segregation in the fracture, as the y-direction pressure gradient does not change. By having a x-direction pressure gradient that is more comparable to the y-direction gradient, segregation effects are stronger. The fracture length to height ratio also affects

the amount of segregation in the fracture. **Fig. 3.7** shows that the increase in pressure drop due to mixed flow ultimately depends on the average pressure gradient in the fracture (total pressure drop along the fracture length divided by fracture half-length). This is because, at lower resulting pressure gradients in the x-direction, the amount of segregation is higher, which corresponds to an increased impact of segregation effects (larger difference between mixed-flow and segregated-flow pressure drops). I also observe that the impact of mixed flow on pressure drop due to varying gas rate (with fixed conductivity) and varying conductivity (with fixed gas rate) follow a very similar trend.

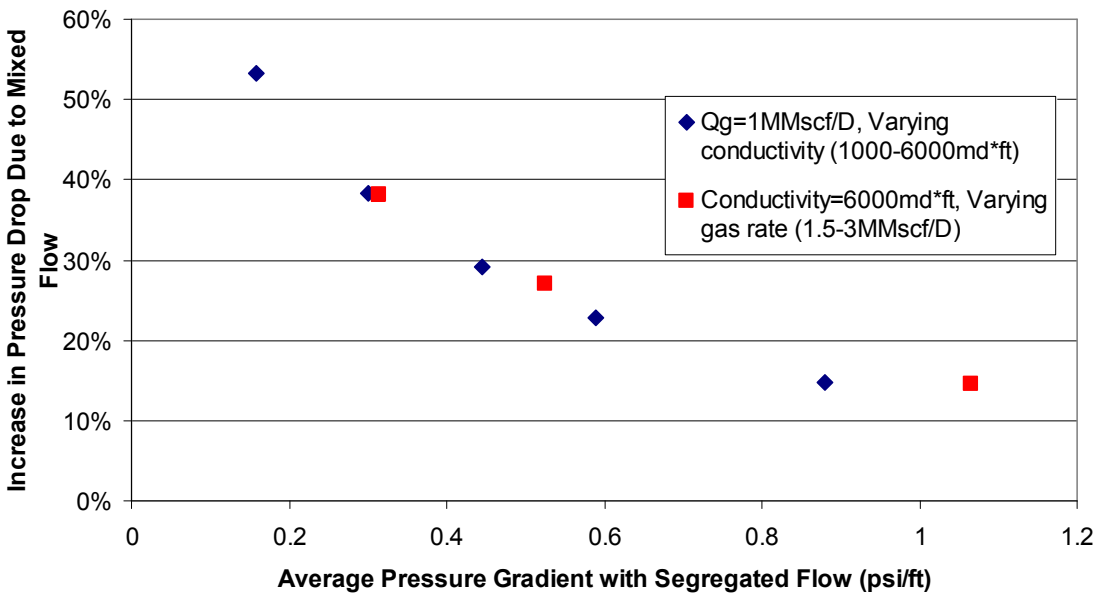

Figure 3.7 Increase in pressure drop due to mixed flow versus average pressure gradient in the fracture. Aspect ratio (x_f/h) = 2 and water/gas ratio of 20 Bbl/MMscf.

For uniform flux models, I observed from saturation plots that the water/gas ratio affects the pressure gradient without affecting the degree of segregation in the fracture. Using increase in pressure drop due to mixed flow as a proxy for determining the amount of segregation, I show support for the above conclusion. The curve for increase in pressure drop due to mixed flow versus pressure gradient is shifted horizontally when the water/gas ratio changes from 10 to 20 Bbl/MMscf (**Fig. 3.8**). As it is shifted horizontally, there is no difference on pressure drop due to mixed flow going from 10 to 20 Bbl/MMscf. This can also be seen when the gas rate is plotted rather than pressure gradient on the independent axis (**Fig. 3.9**) at a fixed conductivity of 6,000 md•ft. The curves are at water/gas ratios of 10 and 20 Bbl/MMscf, yet overlay; this verifies the above conclusion. Finally, as I vary the water/gas ratio from 5-30 Bbl/MMscf, the increase in pressure drop due to mixed flow (while using non-linear relative permeabilities) varies very little (varies from 60-70%) (**Fig. 3.10**). I conclude from Fig. 3.9 that using the non-linear relative permeabilities with Geertsma's correlation causes a difference between segregated and mixed-flow models and that using linear relative permeabilities with Geertsma's correlation shows very little difference between segregated and mixed-flow models. I also conclude that for cases with noticeable segregation effects (at least 20% difference between mixed flow and segregated flow pressure drops) changes in pressure drop depend more on percent changes in the gas rate and conductivity than percent changes in the water/gas ratio.

I mentioned previously that the impact of segregation effects is caused partly by relative permeabilities and non-Darcy flow. Non-Darcy flow is responsible for the impact on pressure drop in the linear relative permeability case (Fig. 3.10) as it obviously cannot be due to non-linearities in the relative permeabilities. In **Fig. 3.11** I show that segregation effects are important when non-linear relative permeabilities and Frederick and Graves 1st correlation (FG1) for non-Darcy flow is used. Using the FG1 correlation shows negligible non-Darcy effects (as explained in Section 2.2), so is essentially Darcy flow. Segregation is important when non-linear relative permeabilities and Frederick and Graves 1st correlation is used because of the non-linear relative permeabilities, as it cannot be caused by non-Darcy flow, since non-Darcy effects are minimal. **Fig. 3.12** combines and summarizes the effect of pressure gradient and the effect of fracture length on the impact of segregation. As the fracture length to height ratio increases towards 10, or the pressure gradient decreases, gravity segregation effects increase. For the fracture-length to height ratio of 10, gravity segregation effects are important for average pressure gradients up to 2 psi/ft. For fracture length to height ratios equal to 4 or less, there is not a significant increase in pressure drop due to mixed flow for average pressure gradients above 1.2 psi/ft.

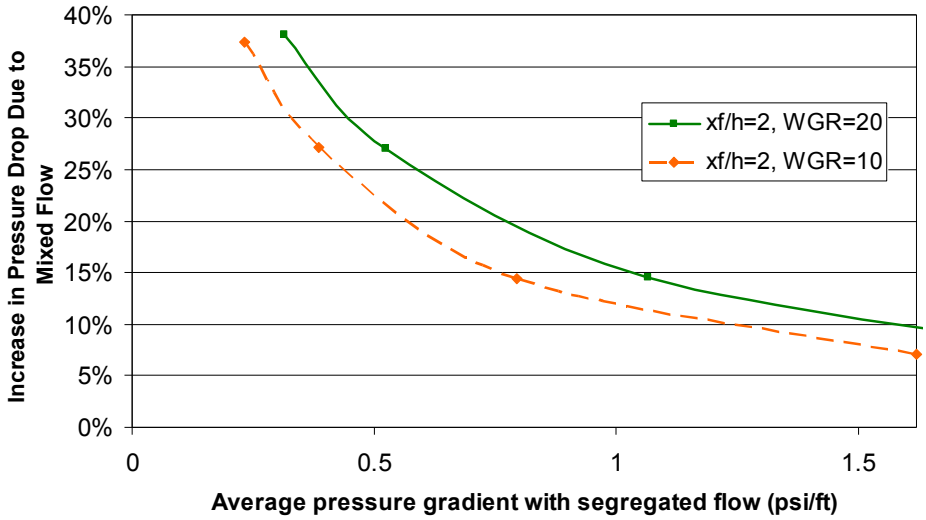

Figure 3.8 Increase in pressure drop due to mixed flow versus average pressure gradient in the fracture. The effect of varying water/gas ratio (while keeping conductivity and gas rate constant) is to change the pressure gradient in the fracture without changing the amount of gravity effects.

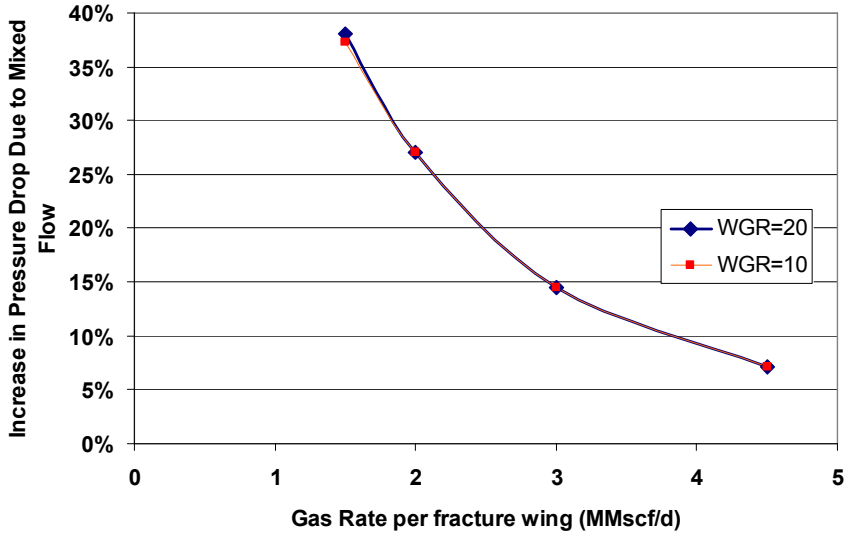

Figure 3.9 Increase in pressure drop due to mixed flow versus gas production rate. The curves of pressure drop vs. gas rate for water/gas ratio of 10 Bbl/MMscf and 20 Bbl/MMscf overlap. Results are at conductivity of 6000 md·ft and aspect ratio of 2.

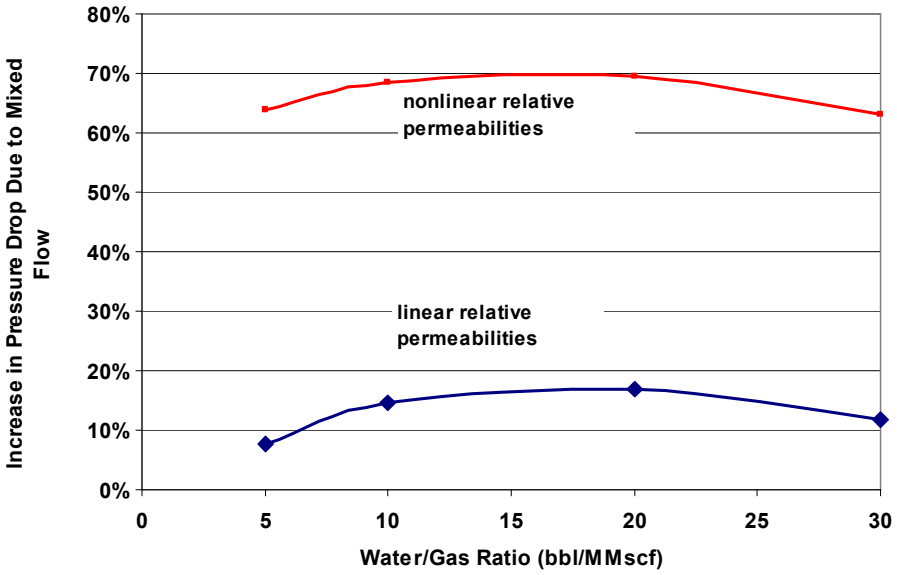

Figure 3.10 Increase in pressure drop due to mixed flow versus water/gas ratio (Y) in the fracture. The effect of water/gas ratio on the difference in total pressure drop between mixed-flow and segregated-flow models is very slight.

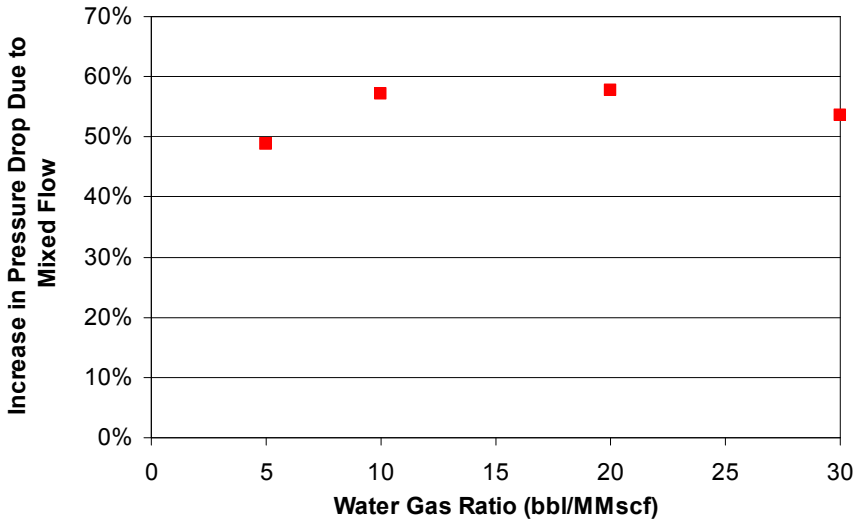

Figure 3.11 Increase in pressure drop due to mixed flow versus water/gas ratio. Using non-linear relative permeabilities with Frederick and Graves 1st correlation shows that the difference is primarily due to non-linear relative permeabilities, as Frederick and Graves correlation shows very small non-Darcy effects.

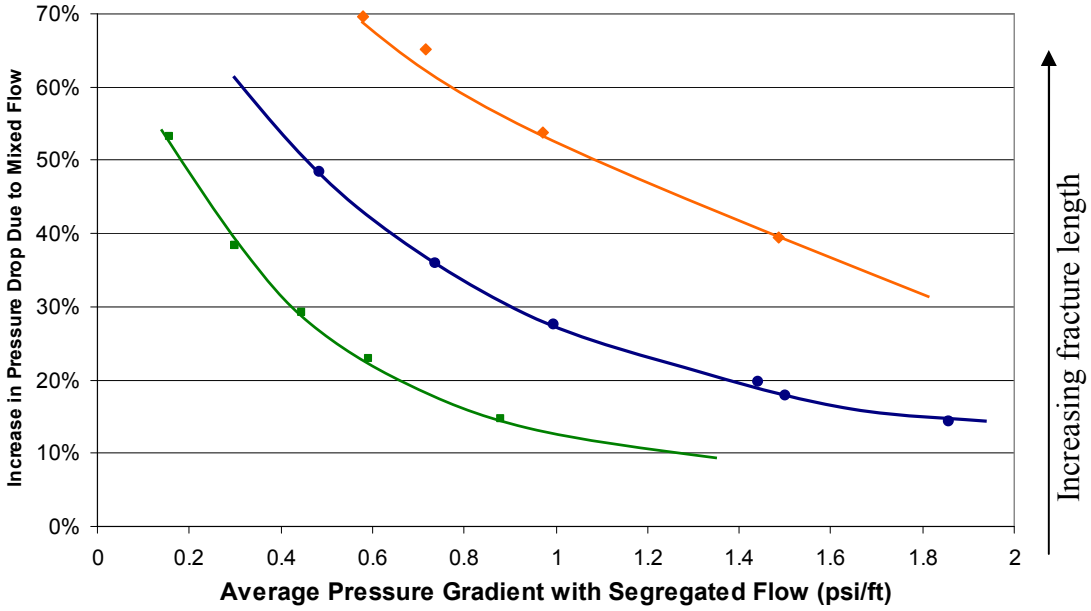

Figure 3.12 Increase in pressure drop due to mixed flow versus average pressure gradient in the fracture. Effect of fracture length and pressure gradient on segregation effects at a water gas ratio of 20.

3.2 EFFECT OF STRESS ON NON-DARCY FLOW WITH UNIFORM INFLUX

I used the fracture-only models with uniform influx and mixed flow and added in the additional effects of stress causing reduction in permeability and porosity. I used previously published results for the effect of stress on permeability, and used Berg's correlation to determine a reduction in porosity for a given reduction in permeability. I ran cases for a resin-coated proppant where the closure stress is not less than 2,000 psi at the fracture tip (as this is the minimum stress value in the normalized curves, Fig. 2.18). The closure stress increases to 6,000 psi at the wellbore (as the bottomhole pressure is constrained to 6,000 psi) for a flow rate of 3 MMscf/D and the lower overburden case (12,000 psi overburden).

For the simulated Jordan sand, even for a slightly lower flow rate, the pressure drop is very large so that I used the higher overburden case and flow rate of 2.5 MMscf/d case to achieve closure stress at the tip that is not less than 2,000 psi. The closure stresses increases to 9,000 psi at the wellbore, due to the increased pressure drop in this case. The wellbore pressure is fixed at 6,000 psi, which results in the 9,000 psi closure stress at the wellbore. To isolate the effect of stress for proppants with varying baseline conductivity, the base conductivity was normalized for all types of proppants (See Fig. 2.18). This was done such that, at a closure stress of 2,000 psi, the permeability is the same for all proppant types. Because of this, the pressure gradient (dp/dx; Eq. 2.13) and resulting pressure drop, Δp (Eq. 2.14), are identical for the different proppants at 2,000 psi closure stress. The base case is for no stress effects.

At the lowest gas flow rate simulated, 1.5 MMscf/D (per fracture wing, or ½ of the hypothetical drainage area), the effect due to stress is negligible (except for the Jordan sand case). However, at 2.5 MMscf/D (for the Jordan sand case; **Fig. 3.13**) and 3 MMscf/D (for the light weight ceramic and resin coated sand; **Fig. 3.14**), stress effects are important. The results given (calculated numerically using Mathematica with Eqs. 2.13 and 2.14) for Δp represent the total pressure drop along the fracture, which is inversely proportional to the effective permeability. For Jordan sand, the net effect of stress on permeability $\left(\frac{k}{k_{ref}}\right)_{stress}$ and porosity $\left(\frac{\phi}{\phi_{ref}}\right)_{stress}$ is to increase pressure drop by 200% for the 2.5 MMscf/D case (with 15,000 psi overburden and results in 9,000 psi stress in the near wellbore region, and 2,000 psi stress at the fracture tip). For the light weight ceramic and resin coated sand, the net effect of stress on permeability is to increase pressure drop by roughly 25% (for gas rates of 3.0 MMscf/D), when the overburden is 12,000 psi and stress is 6,000 psi in the near wellbore region, and drops off to 2,000 psi at the fracture tip.

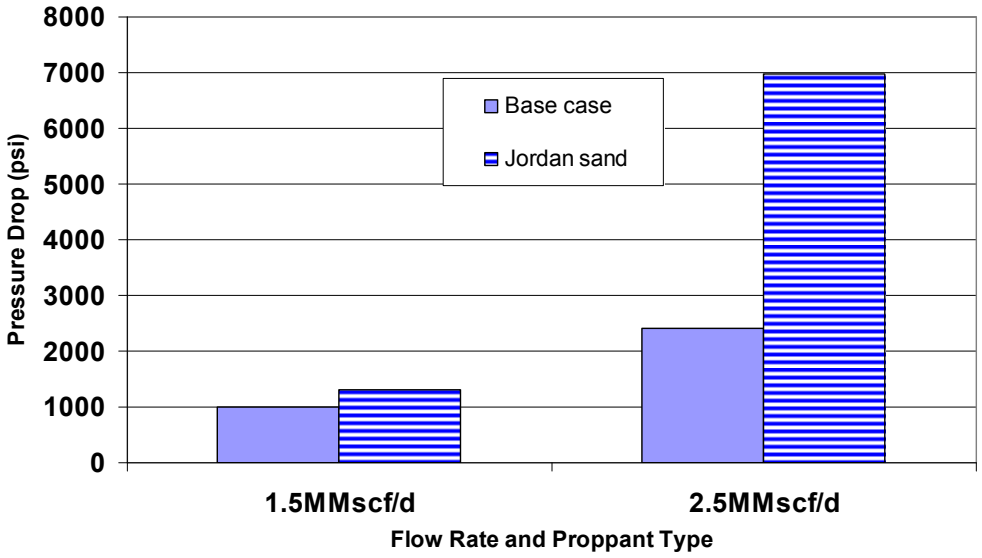

Fig. 3.13 Pressure drop with and without stress effect on permeability, for various flow rates and Jordan sand proppant. Water/gas ratio of 20 Bbl/MMscf and 10,000 md base permeability (at 2,000 psi closure), $w_f = 0.02$ ft.

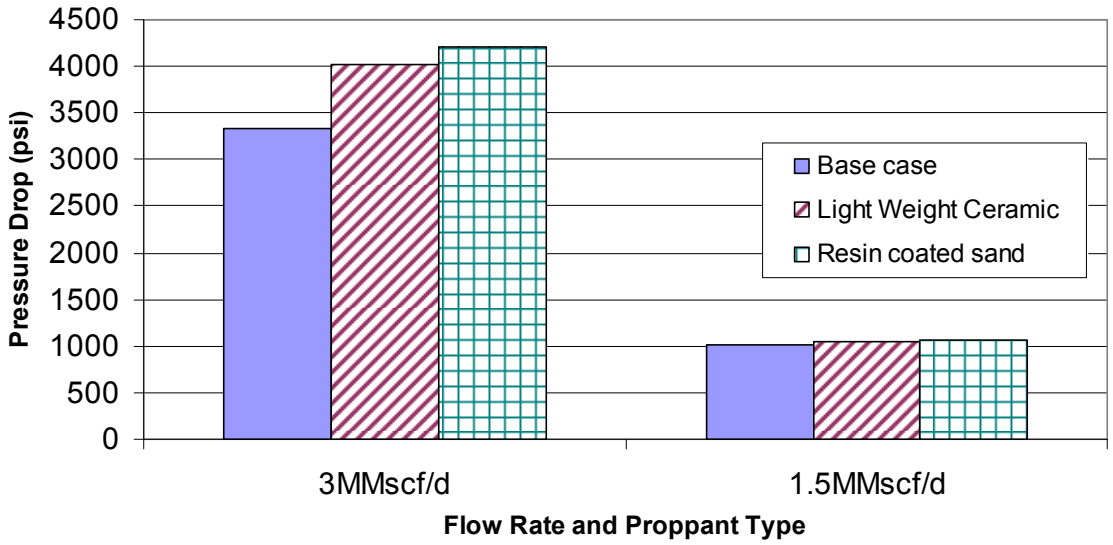

Fig. 3.14 Increase in pressure drop due to stress affecting permeability for light weight ceramic and resin coated sand proppants. Water/gas ratio of 20 Bbl/MMscf and 10,000 md base permeability (at 2,000 psi closure), $w_f = 0.02$ ft.

Now, I complicate the problem by considering the affect of stress on non-Darcy flow. From work of Schubarth and Milton-Tayler (Fig. 2.19) I found the effect of stress on non-Darcy resistance for a light weight ceramic proppant that shows a reduction in permeability by a factor of 0.63, when closure stress = 6,000 psi. To find the reduction in porosity, I use Berg's correlation (as outlined in Section 2.5). Using both reduction in porosity and reduction in permeability results in a higher beta factor. I predict beta increases by a factor of 2.1 due to both changes in porosity and permeability.

$$\frac{\beta(before)}{\beta(after)} = \frac{1}{\left(\frac{k_2}{k_1}\right)^{1.6}}$$

$$= 2.1, if: {}^{k_2}\!/_{k_1} = 0.63$$

The actual change in beta (in CMG simulation) is a factor of 1.90 (since the water saturation has decreased slightly.) Again from work of Schubarth and Milton-Tayler (Fig. 2.19), the change in beta seen in lab tests is a factor of 1.90 going from 2,000 to 6,000 psi closure stress. Our results show that using Berg and Geertsma's correlation in CMG agree well with lab tests from Schubarth and Milton-Tayler for beta. Therefore, if closures stress effects are present in the model, one can confidently use Berg's correlation to find reduction in porosity for a given reduction in permeability. I did not model closure stress except in this section. I also conclude that accounting for stress reduction in porosity and permeability while using Geertsma's correlation for the beta factor results in a realistic beta factor.

3.3 HYDRAULICALLY FRACTURED RESERVOIR WITH TWO-PHASE FLOW

Flow in the fracture for the hydraulically fractured reservoir model is similar to that of the uniform-flux modeling, except that the influx to the fracture is now caused by reservoir depletion rather than forced influx. One quarter of a square drainage area is modeled in the simulations. The reservoir is assumed to be homogenous and at uniform initial water saturation that gives rise to multiphase flow in the reservoir and fracture. Also, single-phase flow models are run to isolate the effect of multiphase flow in the fracture. As mentioned earlier, for all fractured reservoir models I use relative permeability for a typical resin-coated proppant pack derived from lab tests by Sullivan et al. (Fig. 2.1). Non-Darcy flow is modeled using Geertsma's correlation (Eq. 2.3) as described earlier, while cases are also with minimal non-Darcy effects by using Fredrick and Graves correlation (Eq. 2.4). Water flux in the reservoir is caused by initial water saturation of 68%. Models flowing single-phase gas were also run at an initial water saturation of 30%. Flow in models in this section is more representative of an actual hydraulically fractured reservoir as compared to the uniform flux models.

Effective gas permeability is reduced in mixed flow compared to segregated flow due to variations in saturations and gas resistance factor. The effective permeability is calculated using Eq. 3.1, where Δh is the thickness of each gridblock in the fracture.

$$k_{eff} = \frac{\sum_{\Delta h} k_{rg} \Delta h / (GRF)}{h} k_{abs} \quad \text{.....(3.1)}$$

Thus, permeability is averaged over the fracture height in the segregated case and then compared to the case with mixed flow. The effective permeability is determined for both cases at an x-position halfway along the fracture length and at an x-position near the wellbore. As in the uniform flux models, here I found that for mixed flow as the wellbore is approached, the gas velocity is higher which causes the water saturation to be lower. This is caused by higher gas resistance at higher gas velocities, and because of this, the resulting gas saturation is higher to compensate for the higher gas resistance, such that the k_g/k_w ratio stays the same.

Because there is segregation, the upper part of the fracture has lower water saturation, so that the part of the fracture conductive to gas has a lower gas resistance factor. The lower part of the fracture contributes very little to the conductivity of the fracture as the water saturation is high in the lower part of the fracture. Segregated-flow models gas *x*-velocities (**Fig. 3.15**) are roughly two to three times as high as in mixed flow at the top cell of the fracture ($y = 0$), where the gas *x*-velocity is highest. I also observed that *x*-velocities are also higher than the mixed flow velocities in the segregated model not just in the top cell ($y = 0$), but anywhere in the upper portion of the fracture (with gas saturation above 60%). This is caused by having less of the fracture height conductive to gas in the segregated case. When this happens, gas rises up out of the highly water saturated zone and into the highly gas saturated zone, and from there flows in the *x*-direction to the wellbore. The *x*-velocity in both the segregated and mixed flow cases

appears to differ from gas *x*-velocity profiles for uniform influx. A significant amount of the flux occurs in the last 40 ft of the fracture, near the tip, so that the slope of gas velocity vs. distance is much higher (this means more gas influx per fracture length has occurred in this region). This influx near the fracture tip is the main difference between the uniform flux models and models in this section.

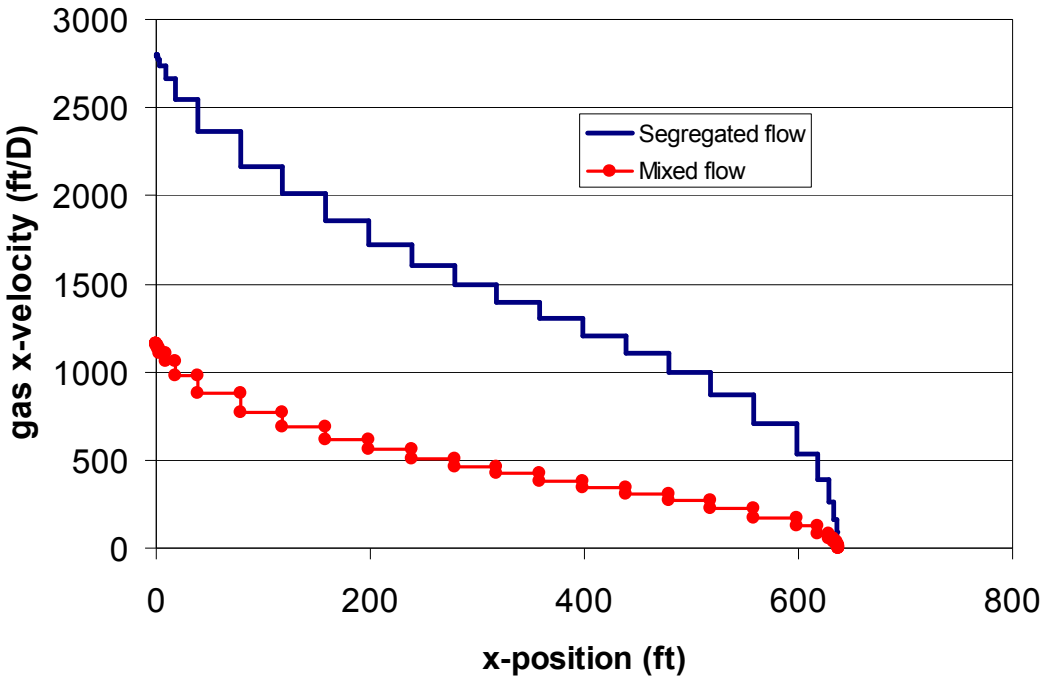

Fig 3.15 Gas *x*-velocity in the fracture versus *x*-position for mixed flow and segregated flow (at a y-position at the top of the fracture).

Gas resistance factor and water saturation (used in the calculation of k_{rg}) were taken from simulation and plotted as a function of vertical position. Gas resistance factor versus vertical position in the fracture is shown in **Fig. 3.16** for mixed flow and segregated flow at x-positions near the wellbore (x = 1 ft), and near the fracture x-center

(x = 330 ft). In mixed flow the gas resistance factor is constant for $0 \le y \le 25$ because there is only one vertical cell. As y increases from 0 ft (top of the fracture) to 25 ft (bottom of the fracture), gas resistance factor jumps from 3 to 9 at y = 15 ft. For $y \ge 15$ ft, the contribution to the gas effective permeability is much smaller than for $y < 15$ ft. Even though the gas velocity is higher in segregated flow, the resulting gas resistance factor is lower (in the upper part of the fracture), because of lower water saturations in this region and the non-linear nature of the non-Darcy coefficient (beta) with respect to water saturation (Eq. 2.3).

Having lower water saturation in the upper part of the fracture also results in higher gas relative permeability (averaged over vertical thickness). This occurs in spite of the fact that the lower part of the fracture is at high water saturation so that the relative permeability to gas is very low in this region. The vertical average of gas relative permeability is higher in segregated flow is because of the non-linear nature of the relative permeability curves with respect to water saturation. The water saturation is also plotted (**Fig. 3.17)** for the purpose of calculating the effective gas permeability (Eq..1) in both mixed flow and segregated flow.

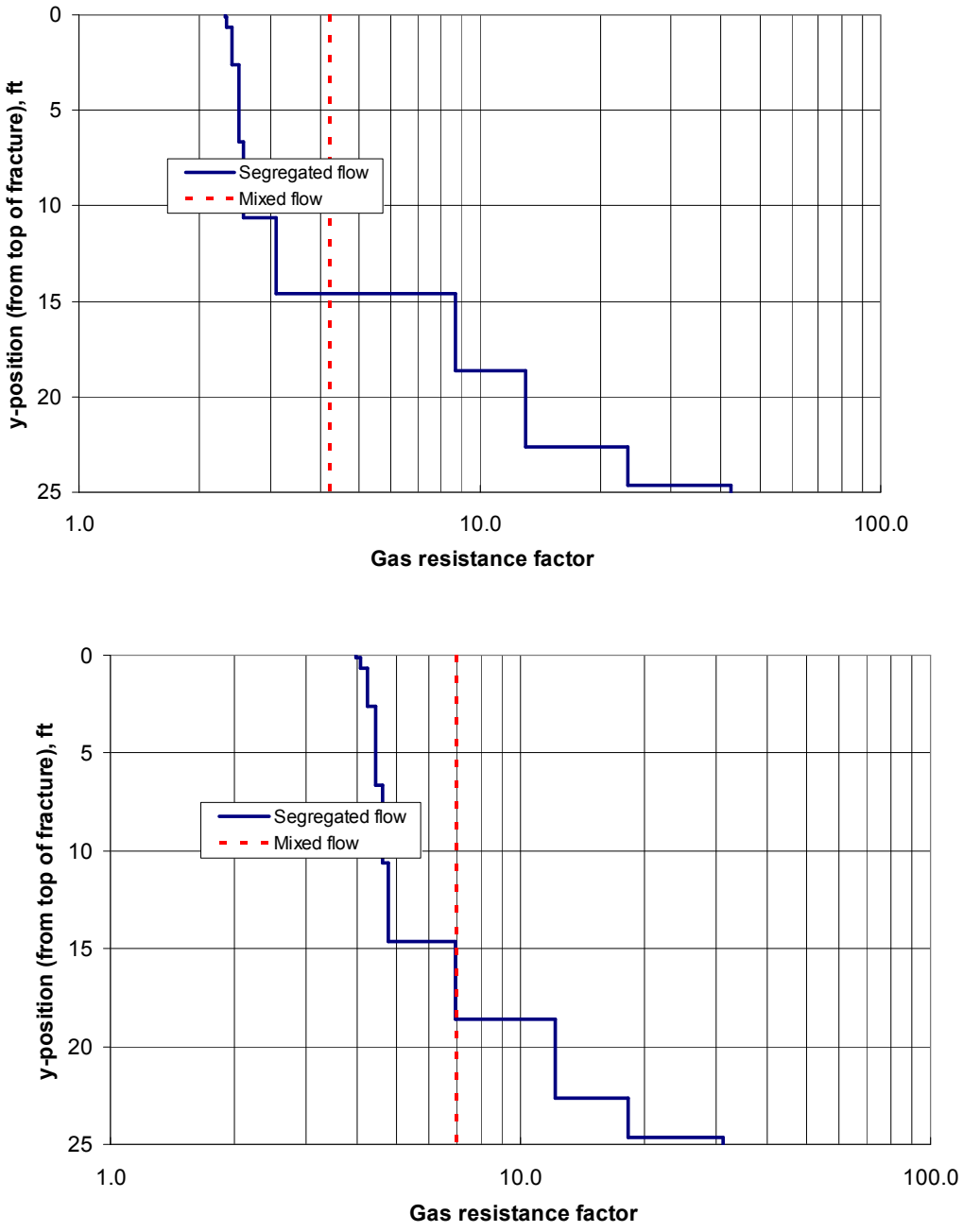

Fig. 3.16 Gas resistance factor vs. vertical distance is plotted at the x-center of the fracture (x = 330 ft) (top) and at the wellbore (x = 1 ft) (bottom) for both mixed flow and segregated flow.

Gas-water phase segregation exists in the fracture as evidenced by the vertical water saturation profile. I found only slight segregation in the reservoir.

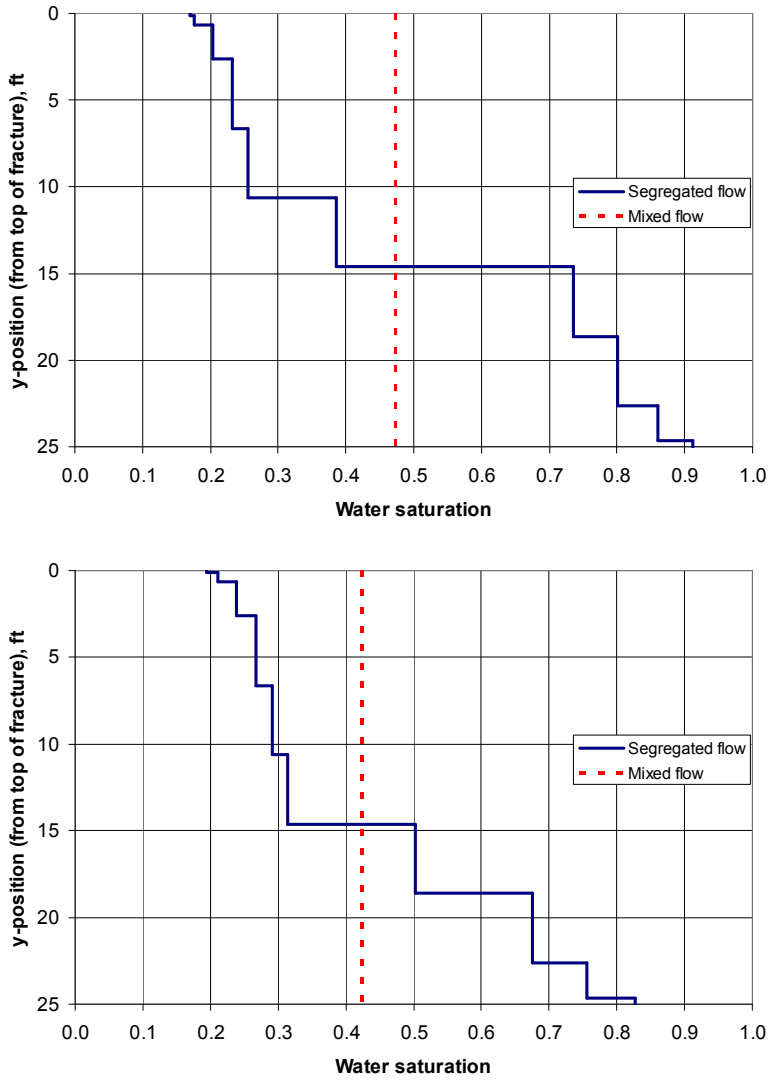

Fig. 3.17 Water saturation vs. vertical distance is plotted at the x-center of the fracture (x = 330 ft) (top) and at the wellbore (x = 5 ft) (bottom) for both mixed flow and segregated flow. In mixed flow the line is constant because there is only one vertical cell.

The effective permeability (Eq. 3.1) for segregated-flow and mixed-flow models is shown in **Table 3.1**. Due to relative permeability and gas resistance effects, between one third and one half of the effective permeability is lost because of mixed flow in the fracture (45% loss in effective permeability at the x-center of the fracture).

TABLE 3.1 EFFECTIVE PERMEABILITY FOR MIXED AND SEGREGATED FLOW USING NON-LINEAR RELATIVE PERMEABILITIES WITH GEERTSMA'S CORRELATION AT A WATER/GAS RATIO OF 31-34 BBL/MMSCF

$C_{fD} = 18.8$	**Mixed flow**	**Segregated flow**
At x-center of fracture (x= 320 ft)		
k_{eff}	1,061	1,942
% change in k_{eff}	**-45%**	--
Near wellbore (x = 5 ft)		
k_{eff}	768	1,194
% change in k_{eff}	**-36%**	--

So far I have illustrated cases using the laboratory non-linear fracture relative permeabilities and Geertsma's correlation for non-Darcy flow. Table 3.2 shows the change in effective permeability due to mixed flow at the wellbore and the x-center of the fracture, for all four permutations of the following: non-Darcy or Darcy flow and non-linear or linear fracture relative permeabilities.

TABLE 3.2 PERCENT LOSS IN EFFECTIVE PERMEABILITY DUE TO MIXED FLOW USING VARIOUS RELATIVE PERMEABILITIES AND DARCY OR NON-DARCY FLOW		
$C_{fD} = 18.8$	***x*-center of fracture (*x* = 320 ft)**	**Near wellbore (*x* = 1 ft)**
Non-linear k_r with Geertsma	**-45%**	**-36%**
Linear k_r with Geertsma	**-15%**	**-16%**
Non-linear k_r with Darcy flow	**-40%**	**-40%**
Linear k_r with Darcy flow	**-0.5%**	**-8%**

I conclude that if non-linear relative permeabilities are used (with an exponent of 2) or if non-Darcy effects are modeled (with Geertsma's correlation), mixed flow models will, if a significant amount of segregation exists in the segregated model, underestimate conductivity by 15-45%. If both Darcy and linear relative permeabilities are used, there is less than 0-8% loss in conductivity due to mixed flow as compared to segregated flow. However, in the cases modeled, I can see that non-linear relative permeabilities (with Darcy flow) have a larger effect on loss in effective conductivity due to mixed flow (-40%) than non-Darcy flow (using Geertsma's correlation with linear relative permeabilities, -15%). This agrees with results from the uniform-flux models, where the segregation effects on pressure drop were mostly due to the non-linear relative permeabilities, and to a somewhat lesser extent due to non-Darcy flow.

In this section I describe another method for determining effective conductivity. By comparing graphs of dimensionless productivity vs. dimensionless conductivity, the difference in productivity and conductivity between the mixed-flow and segregated-flow cases can be determined. Before calculating effective conductivity, dimensionless productivity is calculated as shown in Eq. 2.16, while original conductivity is calculated as shown in Eq. 2.17. In the previous method, effective conductivity was calculated according to Eq. 2.18. However, in this method, effective conductivity is calculated from the resulting reduction in productivity. The pressure drop term in the productivity calculation (Eq. 2.16) is calculated when the well is in pseudo steady state flow and is equal to the reservoir pressure minus the bottomhole pressure (constant at 5,000 psi). The parameters used in the calculation of the dimensionless productivity (for the same example as in Table 3.1) are given in Table 3.3. The gas rates for the entire drainage area (both fracture wings) are 0.44-0.48 MMscf/D for both cases. The slight difference in gas rate does not matter as the productivity is dimensionless and therefore accounts for variations in both pressure and gas rate. Fluid properties $E_{g,}$, μ_g , are measured at the bottomhole pressure of 6,000 psi as the $B\mu$ product does not vary more than 2% for pressures in the range of 6,000 psi to 12,000 psi. Reservoir permeability k_{eff} is at the initial water saturation and although non-Darcy effects are present in the reservoir, these are negligible as explained in Section 2.2.

TABLE 3.3 DIMENSIONLESS PRODUCTIVITY FOR MIXED FLOW AND SEGREGATED FLOW USING NON-LINEAR RELATIVE PERMEABILITIES WITH GEERTSMA'S CORRELATION		
	Mixed flow	**Segregated flow**
Original conductivity C_{fD}	**18.8**	**18.8**
q_g (for ¼ of the drainage area, MMscf/D)	**0.110**	**0.121**
q_g (entire drainage area, MMscf/D)	**0.440**	**0.484**
$\overline{p} - p_{wf}$	**1726**	**1592**
E_g (stb/rb)	**240**	**240**
μ_g **(cp),**	**0.024**	**0.024**
h **(reservoir thickness)**	**25**	**25**
$k_{eff,res}$	**0.05**	**0.05**
$J_D = \dfrac{q[MMscf/D]\cdot 4\cdot 1\times 10^6 \mu_g}{2\pi\cdot 0.00633h\cdot k_{eff}\left(\overline{p}-p_{wf}\right)\left(\dfrac{E_g}{5.615}\right)}$	**0.512**	**0.612**

The dimensionless productivity in segregated flow and mixed flow is shown in **Fig 3.18** for cases with original conductivity varying from 1.8 to 19. I see the dimensionless productivity is reduced because of mixed flow compared to segregated flow by 16% at an original C_{fD} of 19. At an original C_{fD} = 10, dimensionless productivity is reduced by 15%. At an original C_{fD} = 1.8, productivity is reduced by 12%.

To determine the effective dimensionless fracture conductivity, the dimensionless productivity is evaluated at the same original dimensionless fracture conductivity (18.8 in the example in Table 3.3) for both the mixed flow and segregated flow models (J_D =

0.512, and 0.612 respectively for the example in Table 3.3). The **conductivity that achieves this productivity in single-phase flow** is found and compared (this is the same as the effective conductivity). The original conductivity was 18.81 in both cases. The effective (single-phase flow) conductivity in the mixed flow and segregated flow cases is 0.944 and 1.712, respectively. This was determined by finding the appropriate conductivity on the single-phase line that achieves the observed multiphase productivity. In Fig 3.18, the arrows pointing from the single-phase curve towards the x-axis show the effective conductivity.

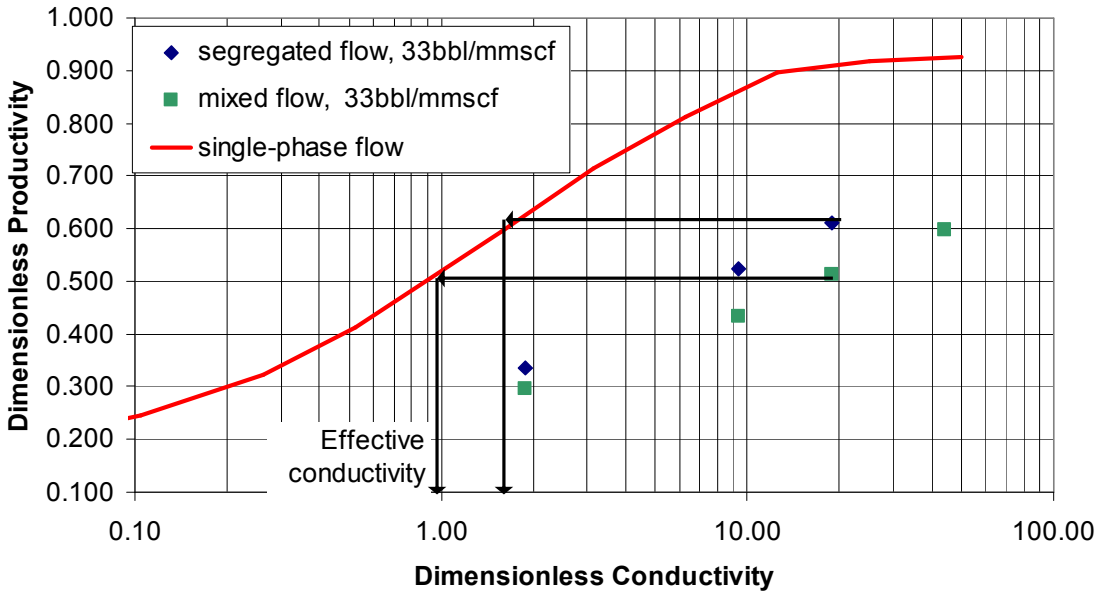

Fig 3.18 Dimensionless productivity vs. dimensionless conductivity is shown on a semi-log plot. I see that at a conductivity of 18.8, the dimensionless productivity is 0.61 in the segregated flow model compared to 0.51 in the mixed flow model.

This means that effective conductivity in mixed flow is 0.944 compared to the original conductivity of 18.8, while in segregated flow at the same original conductivity (18.8) the effective conductivity is 1.712. This is a reduction in conductivity of 44.9% due to mixed flow. In the direct method given earlier (quantifying the saturation and gas resistance maps in the fracture) I had determined a 36-45% reduction in effective conductivity (Table 3.1). Both methods of determining effective fracture conductivity give very agreeable similar results. Using the second method illustrates both the impact on dimensionless productivity and dimensionless conductivity (**Fig. 3.19**). Due to segregated multiphase-flow at 33 Bbl/MMscf at a gas rate per well of 0.44 MMscf/D, the productivity is reduced by 30-50% for original dimensionless conductivities in the range of 2-30. And on top of this multiphase reduction, productivity is reduced further due to mixed flow by 12-16% for original conductivities in the range of 1.8-30. Effective conductivity is reduced by 55-60% because of mixed flow for original conductivities in the range of 1.8-30. Thus, for the models shown above there is a significant loss in dimensionless productivity caused by mixed flow which should not be ignored, and this is caused by a large loss in effective conductivity.

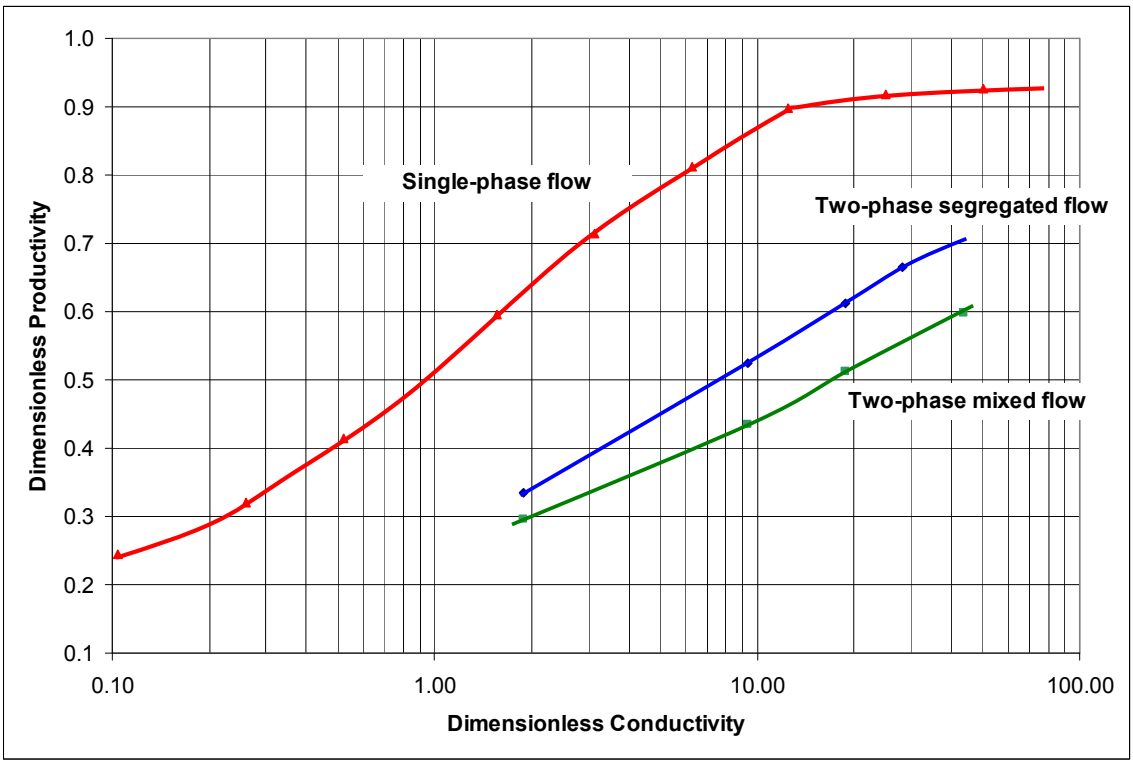

Fig 3.19 Dimensionless productivity vs. dimensionless conductivity for single-phase flow (top curve), multiphase flow with segregation, and multiphase flow with no segregation.

So far I have illustrated cases using the second method and using laboratory non-linear fracture relative permeabilities and Geertsma's correlation for non-Darcy flow. When I used Darcy flow and linear fracture relative permeabilities, I found less than 1% reduction in dimensionless productivity due to mixed flow. This is why segregation effects have not received much attention in the past.

3.4 FRACTURED RESERVOIR UNDER CLEANUP

The fractured reservoir under cleanup is similar to the fractured reservoir model shown earlier, except that the produced water in Case 1 and 2 is entirely due to injected stimulation water. Case 1 uses Frederick and Graves 1st correlation for non-Darcy flow (Eq. 2.4) (which is essentially Darcy flow for high permeabilities as in the fracture) and the linear relative permeabilities (Fig. 2.1) while Case 2 is more realistic in that it uses Geertsma's correlation and non-linear relative permeabilities. By comparing Case 1 with Case 2 I will determine if the impact of gravity effects depends on the degree of non-Darcy flow and relative permeabilities used. In Case 3 there are two reservoirs (one a gas reservoir, the other an aquifer) connected only by a hydraulic fracture. Mobile water is being produced from an aquifer, while the well is being cleaned up. In Case 4, there are 4 reservoir zones connected by a hydraulic fracture. Case 4 produces mobile formation water, with pseudo steady-state water production at water/gas ratios in the range of 15-17 Bbl/MMscf. Case 4 is similar to Case 3, with the exception that Case 4 does not include the injection stage.

Case 1:

Case 1 uses Frederick and Graves 1st correlation for non-Darcy flow (Eq. 2.4) (which is essentially Darcy flow for high permeabilities as in the fracture) and linear relative permeabilities. **Fig. 3.20** shows the injected and produced water volumes in the segregated case as well as the gas production rate for the 50 days of production. Cumulative water recovery reaches 28% (of 21,304 Bbl injected) by 50 days, and increases only to 30% by 110 days. The figure on page 101 shows gas production peaks at 6 MMscf/D for both half wings (entire drainage area) and declines with time and the producing bottomhole pressure is constant. Values for the mixed flow case are almost identical and are not shown here.

Parameters in Case 1 used to calculate dimensionless conductivity are given below.

- w_f = 0.04 ft
- L_f = 650 ft
- k_{res} = 1 md
- $k_{res,\ eff}$ = 0.3 md
- k_f = 15,000 md
- C_{fD} = 3.1

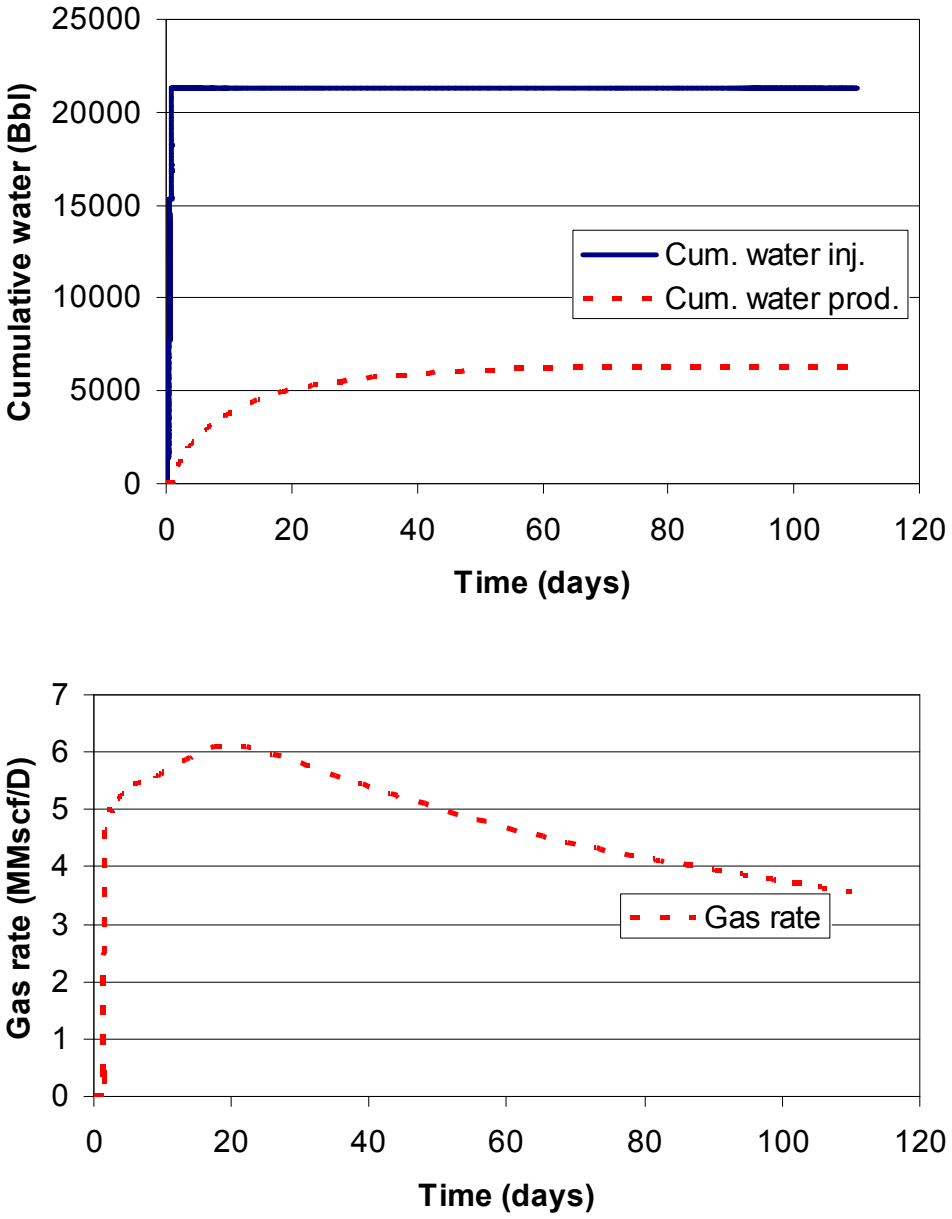

Fig. 3.20 Case 1: Injected water and produced water (top), gas rate (bottom) for t = 0-110 D, showing less than 30% recovery of the injected water.

I linearly extrapolated data from Lolon et al. (2003), for injected water vs. permeability to higher permeabilities (1 md) than he modeled (0.005 to 0.1 md). I found that injected

water is roughly 20,000 STB (for the drainage area) for a fracture length of 645 ft and fracture height of 100ft. The fracture height in Case 1 is only 75 ft, and injected water is 21,304 Bbl, so is comparable to values from Lolon et al. **Fig. 3.21** shows the time development of the water saturation profile in the fracture for the first 24 days of production. Water saturation in the fracture starts off high and declines, while at the same time phase segregation between gas and water occurs. **Fig. 3.22** shows the water saturation maps for days 35-90, while **Fig. 3.23** shows the final profiles at t = 110 days in both the fracture and in the reservoir adjacent to the fracture (j = 2). These maps show higher water saturation than initial saturation in the j-plane 2 adjacent to the fracture, after the fracture is completely cleaned up and the water/gas ratio is less than 1 Bbl/MMscf after 50 days. This acts similarly to fracture face damage, which lowers the productivity as mentioned in Section 2.2. Segregation in the reservoir in this and other j-layers is very minimal, even though the reservoir permeability is isotropic with vertical permeability equal to horizontal permeability.

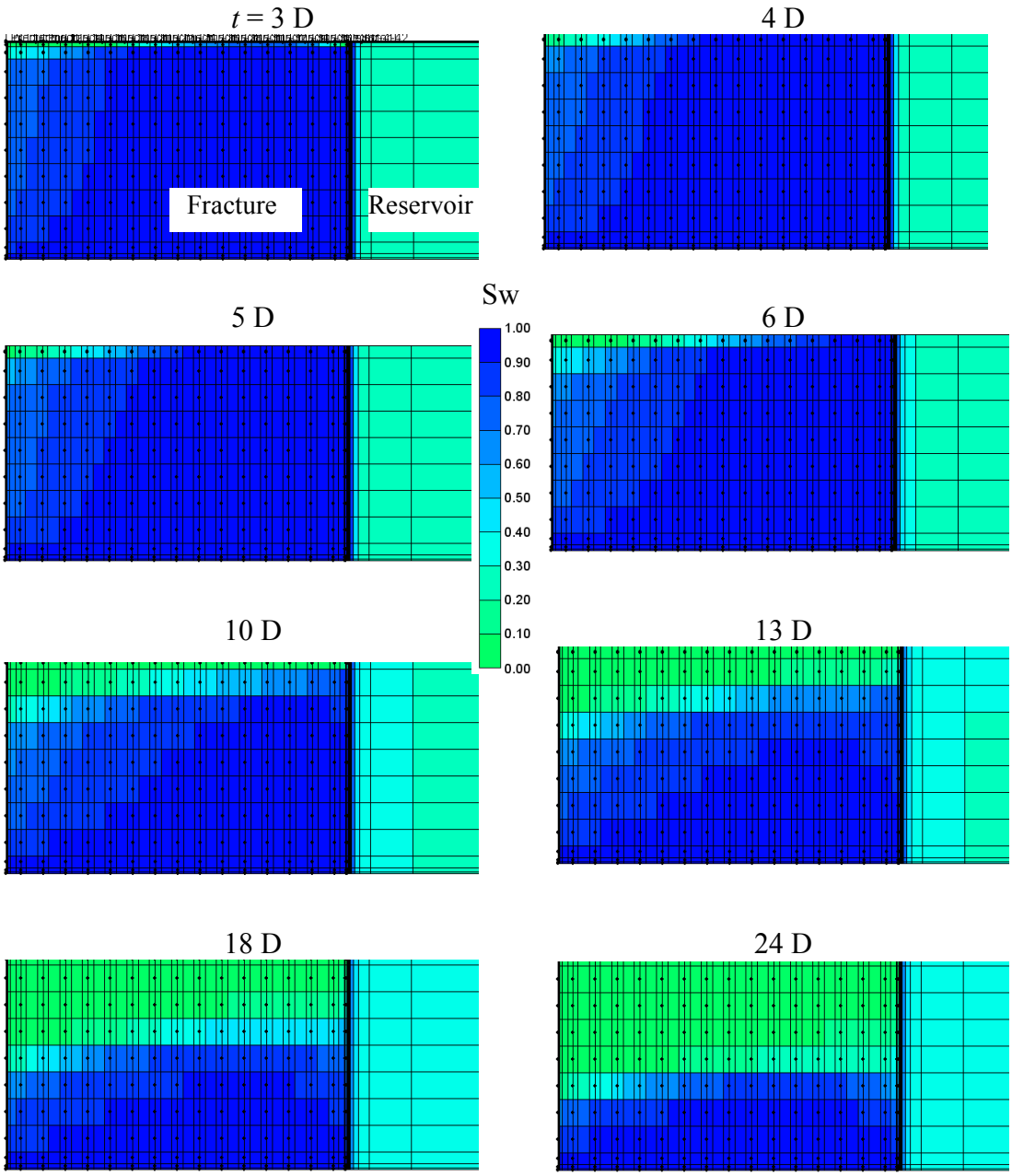

Fig. 3.21 Case 1: Water saturation maps for t = 3 – 24 D.

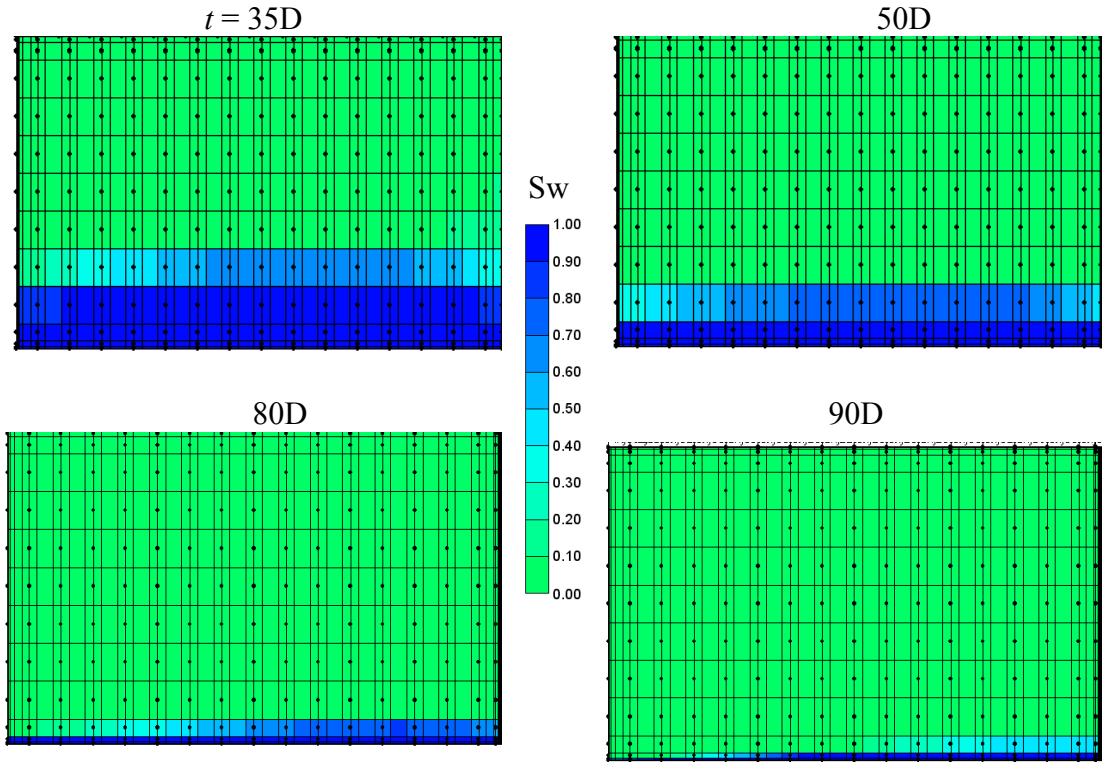

Fig. 3.22 Case 1: Water saturation maps for t = 35 – 90 D.

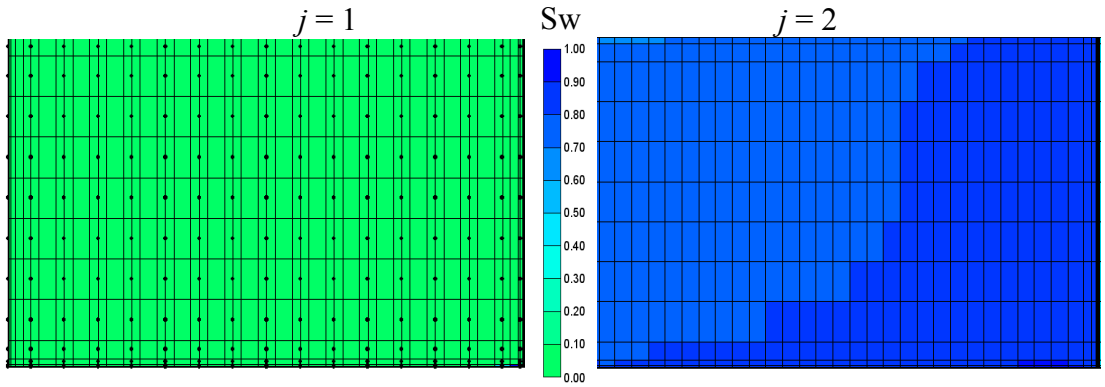

Fig. 3.23 Case 1: Water saturation maps for t = 110 D in the fracture (j = 1; left) and in the reservoir adjacent to the fracture (j = 2; right) showing a high water saturation in the reservoir adjacent to the fracture after the fracture is completely cleaned up. Segregation in the reservoir is minimal, even though the reservoir permeability is isotropic.

Comparing the results for mixed flow with that of segregated flow, I see in **Table 3.4** that injected volumes of water are almost identical (less than 1% difference). Injection in the mixed flow and segregated flow cases is done at a constant bottomhole pressure. For the segregated case, the entire vertical interval is perforated. This causes the pressure in the wellbore to vary very little vertically. Table 3.4 also shows that there is almost no difference in 50-day cumulative production between mixed-flow and segregated-flow models when perforations are in the entire vertical interval. I conclude that if Darcy flow is present in the fracture and linear relative permeabilities are used, then there will be negligible difference (less than 1%) in 50-day cumulative production volumes between segregated and mixed flow.

TABLE 3.4 CASE 1: PRODUCTION DATA FOR 1 MD CASE, C_{FD} = 3.1

***t* = 50 days**	**Average reservoir pressure (psi)**	**Cum. gas prod. (MMcf)**	**Cum. water prod. (STB)**	**Cum. water inj. (STB)**
Mixed flow	5795	274.2	6,112.	21,264.
Segregated flow	5797	271.6	6,128.	21,304.

Case 2:

In Case 1, I found that gravity effects are not important when Darcy flow and non-linear relative permeabilities are present in the fracture, and this agrees with results from the section 3.3. In Case 2 I use Geertsma's correlation for non-Darcy flow, and non-linear fracture relative permeabilities, and I show that gravity plays an important role. As in Case 1, the perforations are in the entire vertical interval of the fracture. Also, as in Case 1, the only mobile water in the reservoir is injected water. Parameters in Case 2 used to calculate dimensionless conductivity are given below.

- w_f = 0.04 ft
- L_f = 650 ft
- k_{res} = 0.1, 1 md
- $k_{res,\ eff}$ = 0.03, 0.3 md
- k_f = 50,000 md
- Original C_{fD} = 100 (0.1-md case), 10 (1-md case)

In the 0.1-md permeability case (**Fig. 3.24**), from 0-10 days, the gas rates are substantially different for mixed and segregated flow. Gravity effects play an important role for 0-50 days in the 1-md case (**Fig. 3.25**). In the 1-md case the water/gas ratio declines to 1.5 bbl/MMscf after 50 days (**Fig. 3.26**), and gravity effects are still important even at these low WGR's.

In the 0.1-md case the water/gas ratio is still fairly high (> 7 bbl/MMscf), even after 50 days of cleanup has occurred (Fig. 3.26). However, gas rates between mixed flow and segregated flow converge to within 10% after only 10 days (WGR = 16 bbl/MMscf), and converge to within 2% after 20 days (WGR = 12 bbl/MMscf). During this time (10 to

20 days) there is still a significant amount of water in the fracture, yet the mixed-flow and segregated-flow rates have converged.

The original dimensionless conductivity in the 0.1-md case is 100, but the effective conductivity is less than 100. It is in fact is much less than 100, when the water/gas ratio is very high. At t = 4.5 days, the water/gas ratio is 61 Bbl/MMscf and I calculated the effective conductivity (at the x-center of the fracture) to be 2.5 (which is lower than the original conductivity by a factor of 40). As water is cleaned up (**Fig. 3.27**), the effective conductivity increases, and in the mixed-flow case eventually becomes high enough so that extra conductivity due to segregated flow does not improve productivity (and the rates converge). At t = 10 days (recall that the mixed flow and segregated flow rates are within 20%), the effective mixed flow dimensionless conductivity is 7.81. After 20 days, the effective conductivity has become high enough ($C_{fD,\ eff}$ = 11.5) in mixed flow so that any extra conductivity due to segregated flow does not improve productivity (mixed flow and segregated flow rates are within 2%). For effective dimensionless conductivity greater than 10 (for t > 20 days), the curves converge as there is a smaller change in productivity for a given change in conductivity (Fig. 3.19). In Fig. 3.19 the effective dimensionless conductivity is the conductivity corresponding to a given productivity plotted on the single-phase flow curve. For the single-phase curve (Fig. 3.19), the productivity becomes limited after effective conductivity increases above 10. I conclude that the productivity has become limited in the mixed-flow, 0.1-md case (so any increase in conductivity does not improve productivity), between t = 10 and 20 days.

In the 1-md case, the gas rates for segregated and mixed flow take longer to converge than the 0.1-md case (Fig. 3.25), and still have not converged after 50 days. This is because the original dimensionless conductivity is now lower (10). This means that the effective conductivity is much less than 10 at early times when the water/gas ratio is high, and is less than 10 for all times. For an effective conductivity less than 10, there will be a difference between segregated flow and mixed flow productivity. This occurs in the 1-md case for times shown less than 50 days. I conclude that any water in the fracture (Fig. 3.27, at t = 50 days WGR is low at 1.5 bbl/MMscf) will cause a difference in production rates between mixed flow and segregated flow (20% difference at t = 50 days with WGR = 1.5; Fig. 3.25). This occurs provided that the effective conductivity (in mixed flow) is lower than 10.

Fig. 3.27 also shows that there is negligible segregation in the reservoir even though isotropic permeability is assumed. Since segregation in the reservoir is not present, it cannot be the reason for any differences between mixed-flow and segregated-flow productivity for the cases modeled.

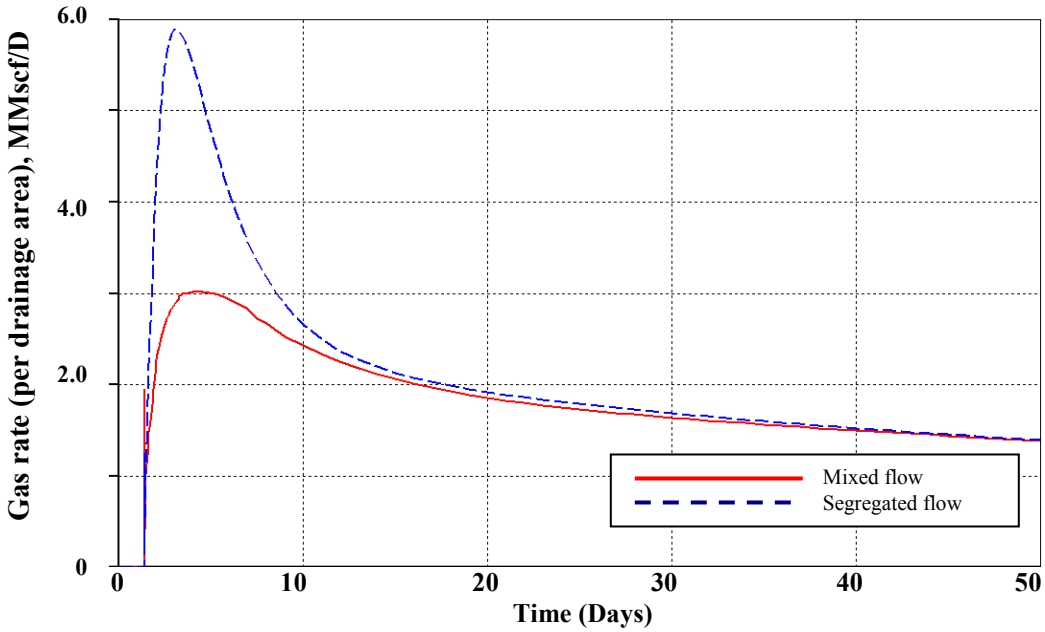

Fig. 3.24 Case 2: Gas production rate, 0.1-md case for mixed flow and segregated flow.

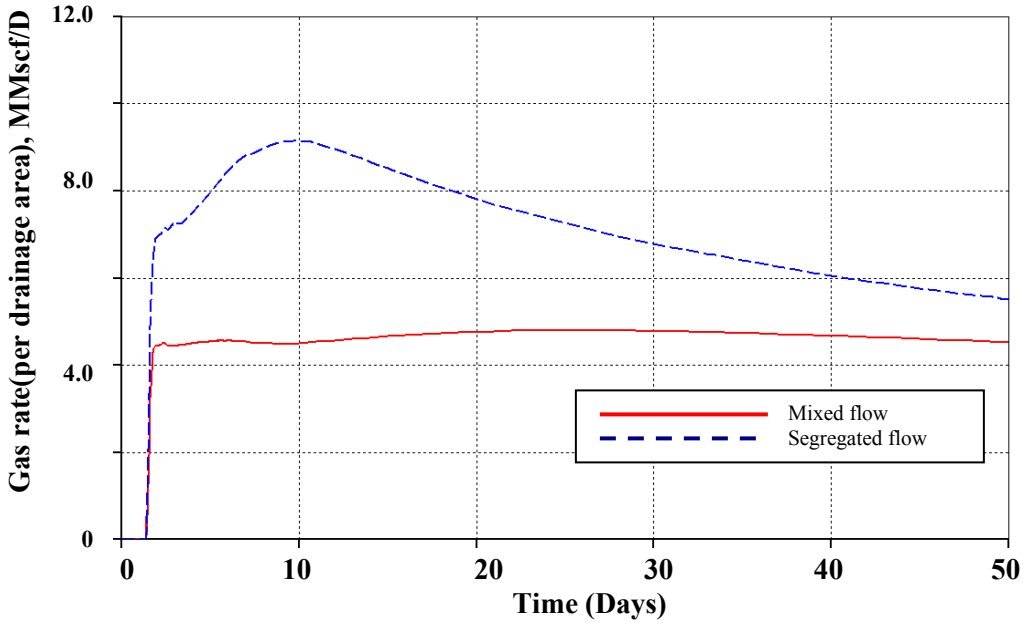

Fig. 3.25 Case 2: Gas production rate, 1-md case for mixed flow and segregated flow.

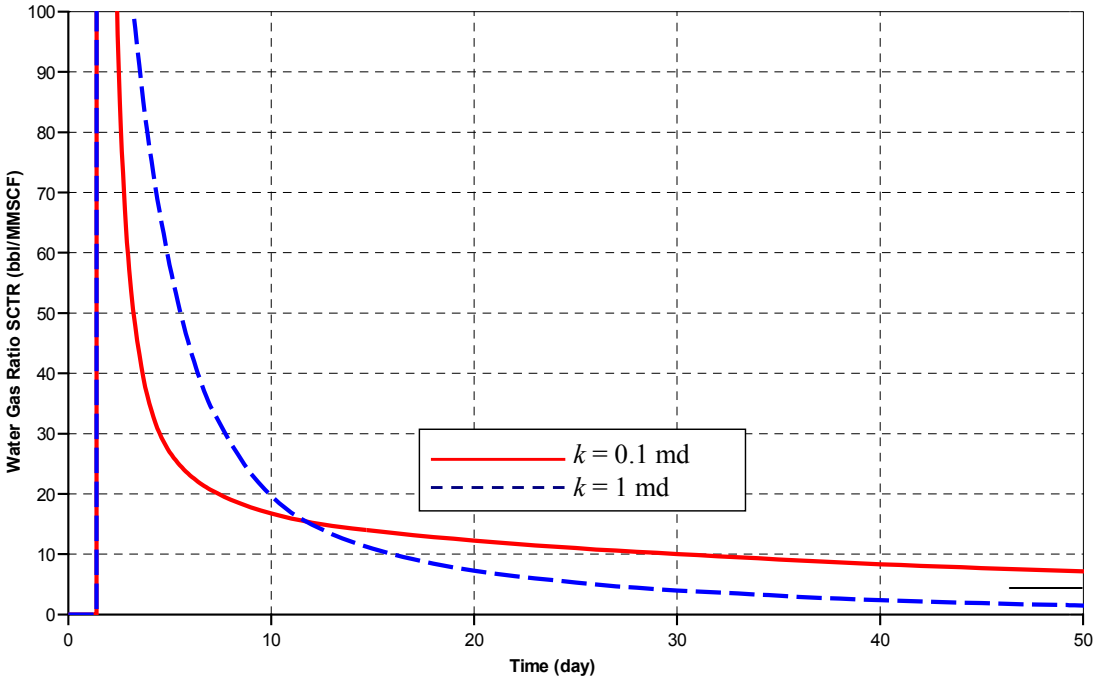

Fig. 3.26 Case 2: Water/gas ratio vs. time for the 0.1-md and 1-md cases. The water/gas ratio is above 7 for all times 0-50 days for the 0.1-md case. For the 1-md case, the water/gas ratio declines to 2-3 bbl/MMscf after 50 days.

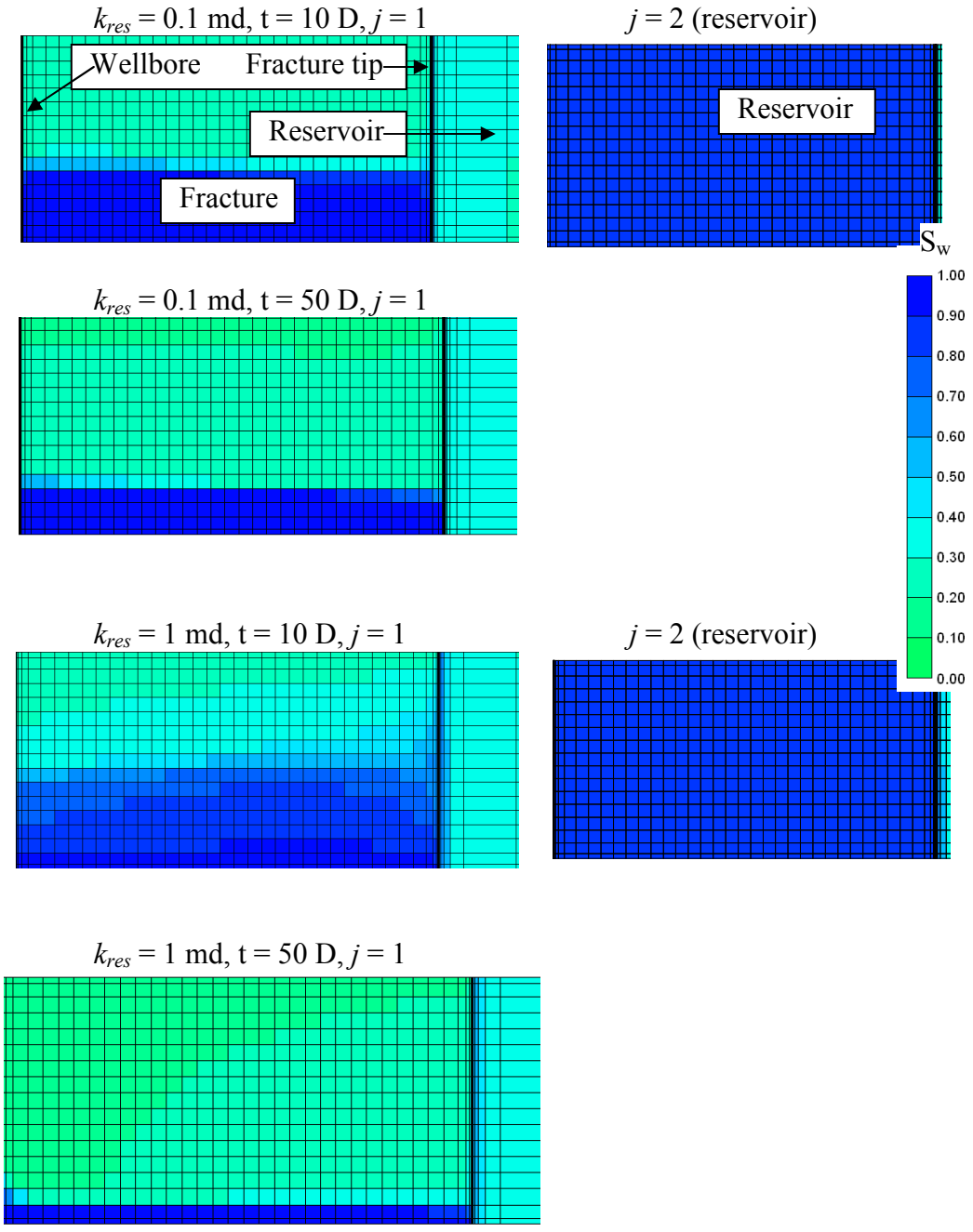

Fig. 3.27 Case 2: Water saturation maps in the fracture (left side plots) and in the reservoir (j=2) right side plots for 0.1-md case (upper plots), and 1-md case (lower plots).

I found a significant difference (35%) in 50-day cumulative gas production in the 1-md case and a smaller but still significant (13%) difference in production in the 0.1-md case (**Table 3.5**).

TABLE 3.5 CASE 2: PRODUCTION/INJECTION VOLUMES OF GAS AND WATER

t = 50 days		Cum. Gas prod. (MMcf), after 50 days	Injection STB water	Cum. Water prod (STB)
k = 0.1 md, C_{fD} = 100	Segregated flow	104.8	10256	2944
	Mixed flow	90.8	10080	2840
% difference in mixed flow		-13%	-2%	-4%
k = 1 md, C_{fD} = 10	Segregated flow	348	22100	6872
	Mixed flow	226	21840	5624
% difference in mixed flow		-35%	-1%	-19%

Fig. 3.28 shows injected versus cleanup volumes of water for the 1-md and 0.1-md case, and it is clear that water recovery reaches a plateau varying from 25-30% of the injected water by 50 days. Total injection and production of water is higher by roughly a factor of 2 in the 1-md case than in the 0.1-md case. This shows that injected and recovered volumes of water are similar; however, productivity is impacted more than injection. This is reasonable, as during injection, there are no segregation effects present in the fracture as the only phase flowing is water, while during production segregation effects are present as both phases are flowing in the fracture.

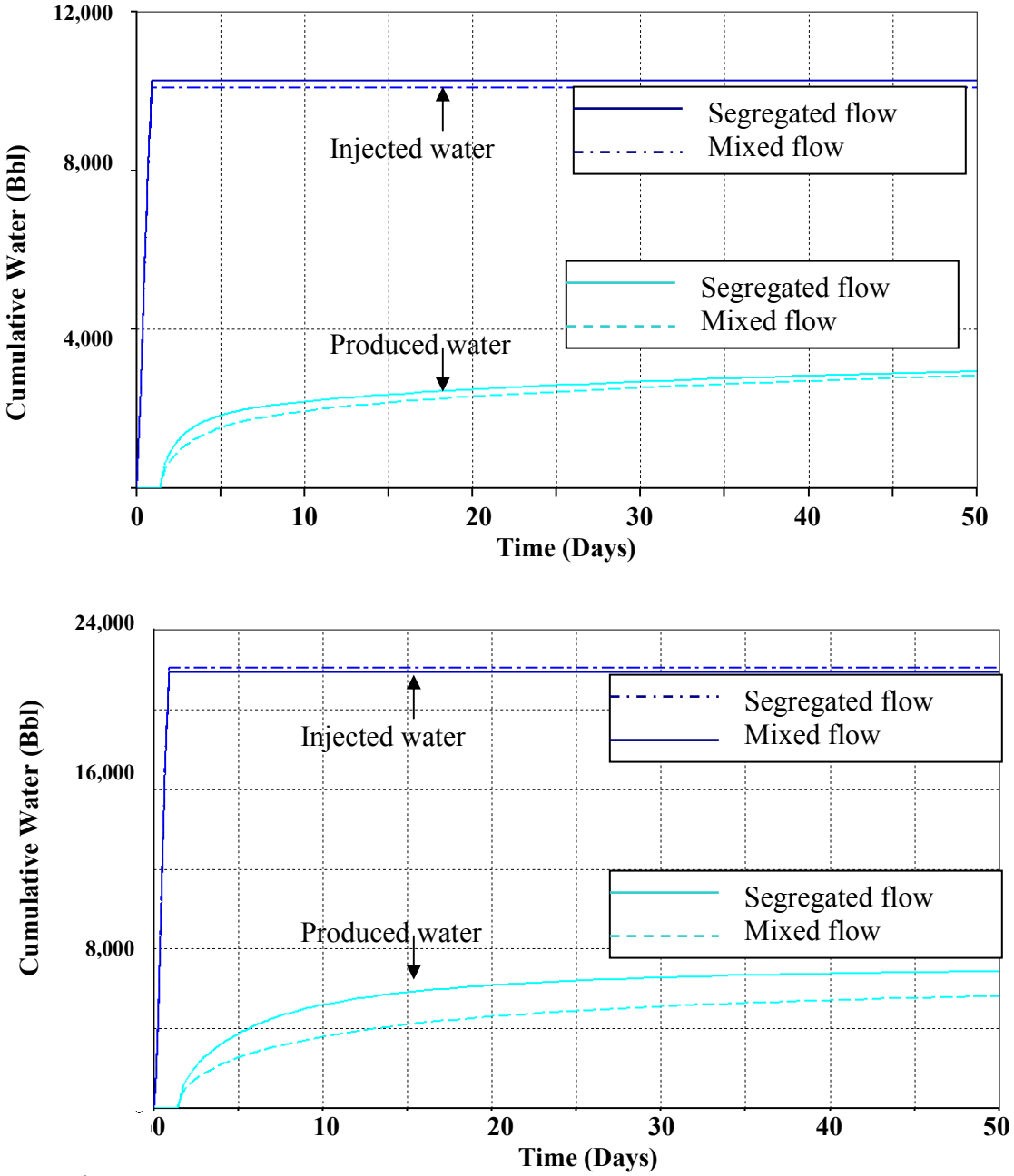

Fig. 3.28 Case 2: Injected vs. produced water for the first 50 days of production for mixed-flow and segregated-flow models, for $k = 0.1$ md (top) and $k = 1$ md (bottom).

Case 3:

Case 3 is a cleanup situation where there is also mobile water from a reservoir quality zone and it is slightly different from Cases 1 and 2 in that it has 2 reservoir quality layers, which are separated by a non-productive layer. The top layer is an aquifer with only 5% gas saturation and is connected to the top 1/3 of the hydraulic fracture. The gas permeability is zero as the gas saturation is below the residual gas saturation of 8.2%. The gas saturation is 5% and not zero and is reasonable for a case where some gas has leaked up into the aquifer from the lower reservoir. The lower layer is a gas zone at 70% gas saturation that is connected to the bottom 1/3 of fracture. A situation was modeled to see extent and impact of segregation in this adverse situation. I do not look at the difference between mixed flow and segregated flow in Case 3. Rather, this situation was done to see the impact of perforation locations on production in this situation, and to determine if the performance of the reservoir can be optimized by avoiding water production. Gas and water production will be compared between the mixed-flow models and segregated-flow models.

In Case 3 in the base case the original C_{fD} is 3.1 ($w_f k_f$ = 600 md·ft, L_f = 650ft, $k_{res,g}(S_{wi})$ = 0.3 md). Case 3 is completed in various locations, and the reservoir and fracture properties are the same as Cases 1 and 2 with the exception of the following:

- Initial water saturations:
    - Top reservoir (h = 25 ft), S_w = 95% (aquifer)
    - Lower reservoir (h = 25 ft), S_w = 30% (gas zone)
- Perforation location in fracture:

- "Base": fracture and perforations are only in the gas zone; aquifer does not produce
- "P1": entire fracture height is perforated
- "P2": perforations along lower half of the gas zone (1/6 of fracture height is perforated, Fig. 3.35)
- "P3": perforations along entire gas zone (lower 1/3 of fracture height is perforated, Fig. 3.35)
- "P4": perforations along aquifer zone (upper 1/3 of fracture height is perforated, Fig. 3.35)
- "P5": perforations along lower half of the aquifer zone (1/6 of fracture height is perforated, Fig. 3.35)

Water injection (Table 2.9) for Case 3 "Base" is similar to Case 1 and 2, and results in 8,840 BBl of cumulative water injected over 0.8 days (**Fig. 3.29**). Water/gas ratio during production in Case 3 "Base" is much lower than the other perforation scenarios, as the aquifer does not flow. The produced water in "Base" is from the injected stimulation water. All other perforation scenarios are approximately at the same WGR of 65 Bbl/MMscf (for $t > 40$ days).

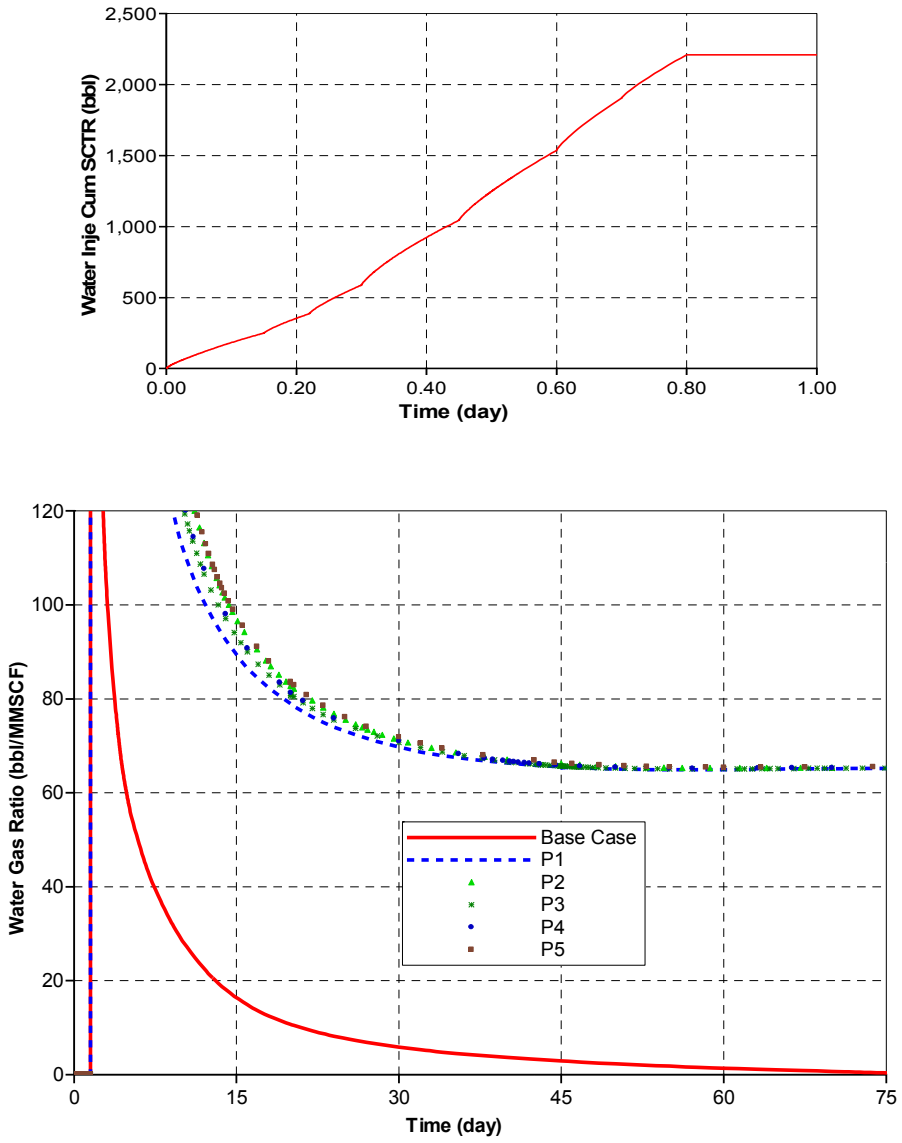

Fig. 3.29 Case 3: Cumulative water injected vs. time (for all scenarios) for all perforation scenarios for t = 0 – 1.0 days (injection stops at 0.8 days) (top) and water/gas ratio vs. time for t = 0-75 days (bottom).

In all perforation scenarios P1-P5 water cones towards the perforations, and segregation exists in the fracture even though water influx occurs at the top of the fracture and gas influx occurs at the bottom (**Fig. 3.30)**. Gas is still able to rise to the upper perforations (P4 and P5), even though the only way for the gas to reach these perforations is through the hydraulic fracture. Segregation is apparent even though the gas influx is from the lowest 1/3 of the fracture from the gas zone. Gas rises to the top of the fracture and flows to the wellbore along the high conductivity pathway to gas, regardless of the location of the perforation. This does not adversely affect production rates, as the amount of gas in the fracture (which directly is related to conductivity) is approximately the same in all scenarios and the water/gas ratio does not change for the different perforation scenarios (Fig. 3.29).

In the "Base" perforation scenario, the aquifer zone is not included, and the hydraulic fracture is limited to the reservoir zone. The "Base" scenario shows higher gas rate than the "P1" scenario by 10-15% at all times greater than 20 days. The highest multiphase gas rate is when the entire fracture height is perforated (P1). Gas production rates (**Fig. 3.31**) are 10% higher in the "P1" scenario, as in this scenario the perforations were in the entire vertical interval and there is no convergent flow towards the perforations. Cumulative gas production (after 50 days) is higher in the Base Case than the P1 scenario by 5 % (Fig. 3.31). The P1 scenario shows only 5% higher cumulative gas production than the P3 and P4 scenarios (1/3 of the fracture height is perforated). The lowest rates are when only 1/6 of fracture height is perforated (P2 and P5). From this I

conclude that the length of the perforated interval is more important than the location of the perforated interval, as segregation occurs in the fracture, and water cones into the perforations which does not affect productivity significantly.

Case 4:

Next I show in Case 4 a similar scenario as Case 3, however the water is entering from all gas zones, and 4 gas zones are used, with the only connectivity between the reservoirs being in the hydraulic fracture. In Case 4 there are 4 reservoir-quality zones connected to a hydraulic fracture. Each of the zones has mobile water, such that they provide gas and water flow into the fracture (Fig. 2.25). The zones communicate with each other via the hydraulic fracture only, as there are impermeable zones separating each of the 4 gas zones.

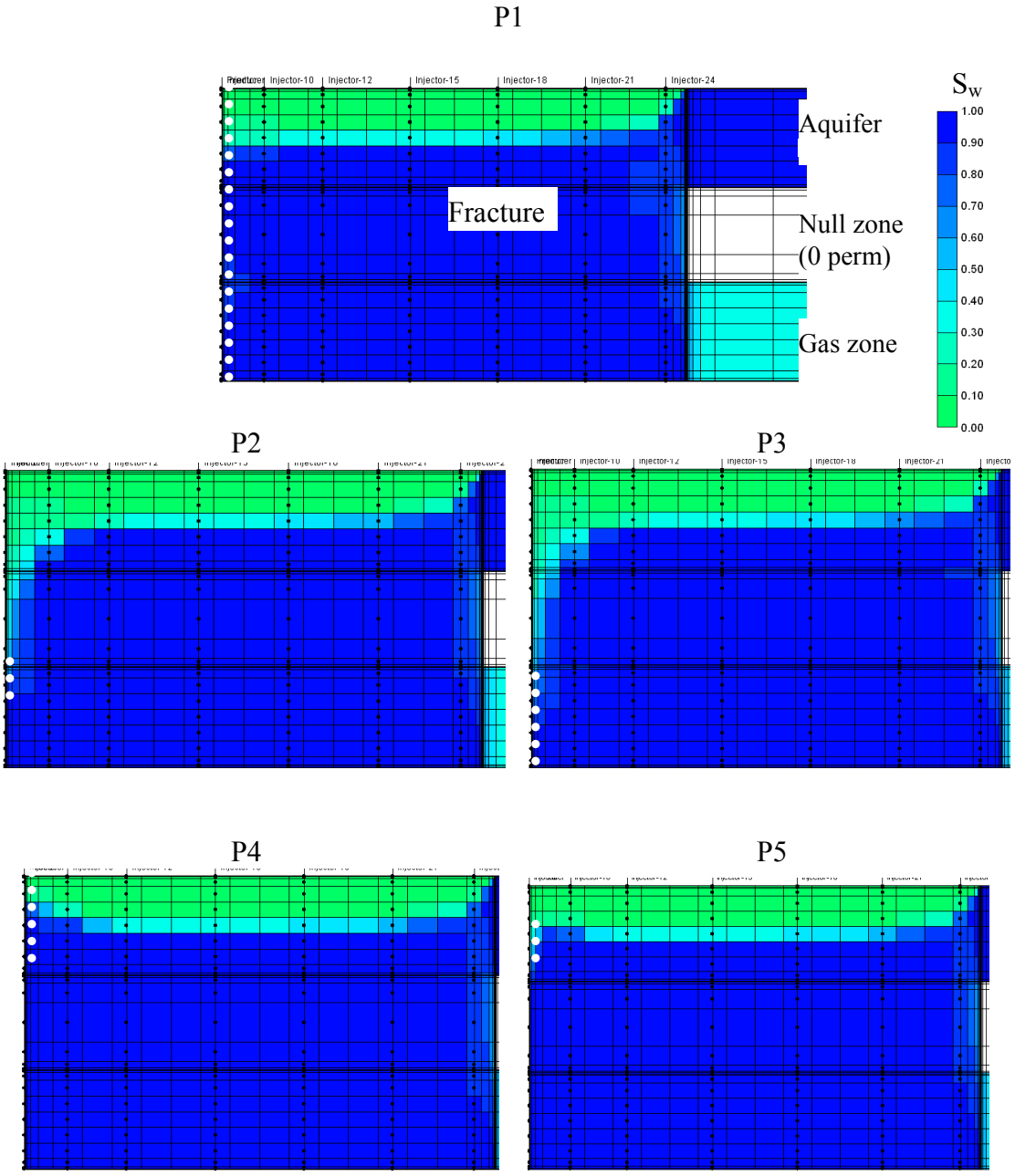

Fig. 3.30 Case 3: Water saturations in the fracture plane during production (t = 75 D). Perforations are shown as white circles and are on the left side of the saturation maps. Segregation is apparent even though the gas influx is from the lowest 1/3 of the fracture from the gas zone. Gas rises to the top of the fracture and flows to the wellbore along the high conductivity pathway to gas, regardless of the location of the perforation.

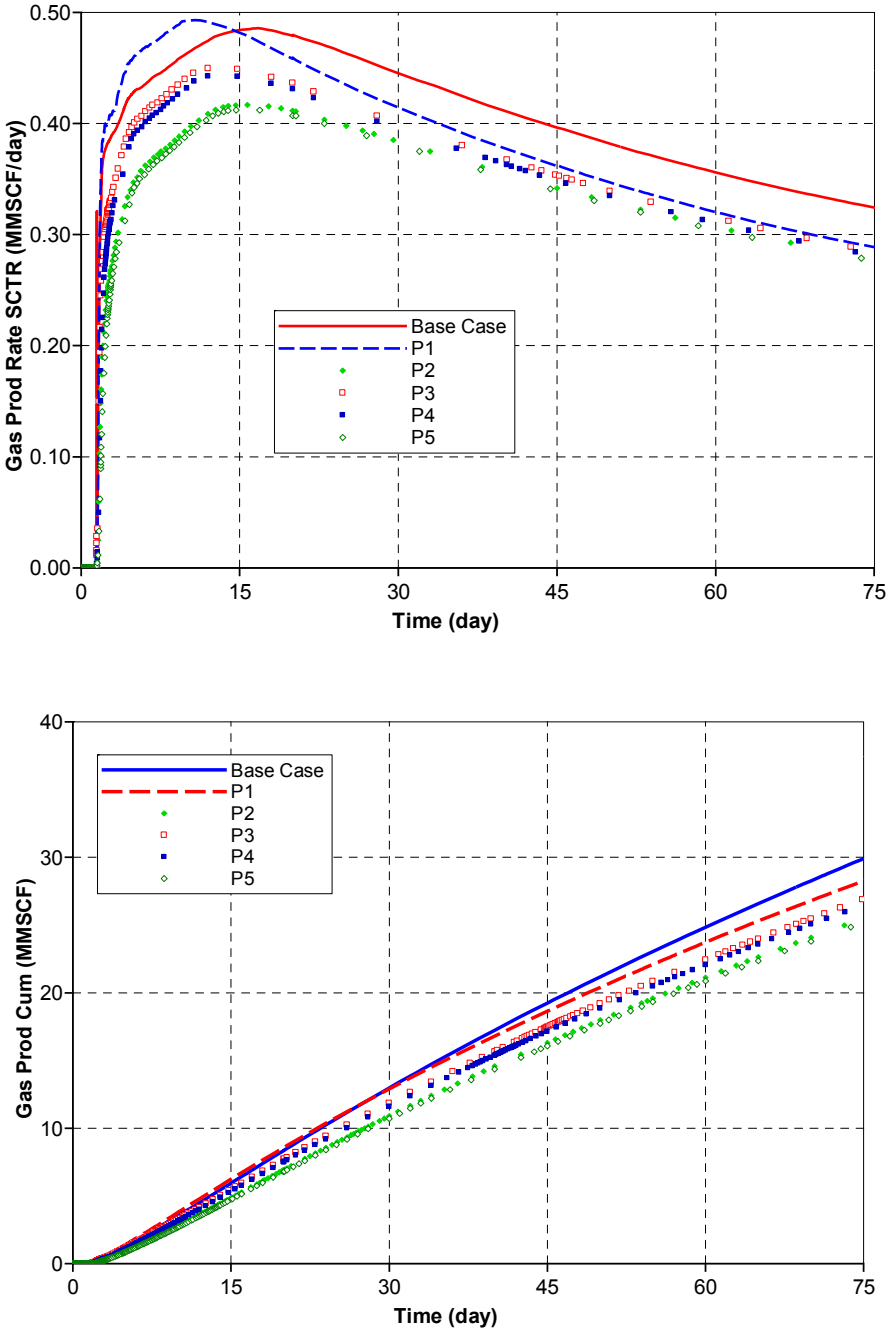

Fig. 3.31 Case 3: Gas rates for models P1-P5 (top) and Cumulative gas production (bottom). The base case shows higher gas rate by 10-15% at all times greater than 20 days.

In Case 4 in the base case the original C_{fD} is varied from 1.2 to 120. Fracture and reservoir parameters relevant to the C_{fD} calculation are:

- h_f = 100 or 400 ft
- In each of the 4 reservoir zones:
  i. $h = h_f / 7$ = 14.3 or 57.1 ft
  ii. S_{wi} = 66%
  iii. $k_{rg}(S_{wi}) = 0.052$, $k_{rw}(S_{wi}) = 0.08$
- w_f = 0.04 ft
- k_{res} = 0.3md
- $k_{res,eff}$ = 0.0156 md
- L_f = 640 ft
- k_f = 300; 3,000; 30,000 md
  i. original C_{fD} = 1.2; 12; 120

Case 4 is completed in various locations and for the following scenarios:

- "Base": perforations are in zone 1 and zone 4 only; no water is produced or flows (relative permeability to water is zero).
- Multiphase flow, with perforations in
  i. Z1 + Z2 (zone 1 and 2) or
  ii. Z1 + Z4 (zone 1 and 4)

In the base case, gas is the only mobile phase and the reservoir has the same initial gas in place and effective gas permeability as the other cases; however, the permeability to water is zero. In the other cases, as time increases, the amount of water in the fracture and the producing water/gas ratio both increase. Simulations are run until steady-state water saturations are changing little in the fracture. The simulation time to achieve this is from 80 to 300 days for the cases with C_{fD} = 10 to 100, and the resulting water/gas ratio is 16 to 17 Bbl/MMscf at the producer. For the C_{fD} = 1.2 case the saturations take

1,200 days to equilibrate, and the resulting water/gas ratio at the producer is 15 Bbl/MMscf. This is not quite as high as the water/gas ratio observed for the higher conductivities. I did not expect cases with different conductivities to reach exactly the same water/gas ratio, as the water/gas ratio depends on the effective permeability ratio of gas to water in the fracture, which will vary as the gas rate and gas resistance factor in the fracture vary. Since cases with different conductivities have different gas rates, the resulting water/gas ratio should also be different. This contrasts with the uniform flux where water/gas ratio was constrained, and not a result of the effective permeability ratio. Water/gas ratio is plotted for all the cases (with Z1+Z4 perforations) for time of 50 to 300 days (**Fig. 3.32**).

The lower reservoir zone is the main zone of interest in Case 4, since, when water fills up the fracture, this is the zone most likely to be affected. Segregation occurs whereby water sinks to the bottom of the fracture blocking off zones 3 and 4, even when only the top two zones produce (Z1+Z2). When the perforations are in only the top 2 layers, gas from the lowest zone can only be produced if gas enters into the fracture at the highly water-saturated region at the bottom of the fracture, and from there flows up into the perforations. By comparing the Z1+Z4 scenario with the Z1+Z2 scenario, the effect of perforations is isolated from the effect of multiphase flow (multiphase flow occurs for both the Z1+Z2 and Z1+Z4 cases, but not in the base case). I found negligible difference between the different perforation scenarios, whereby the gas is able to go into the high water saturation area at the bottom of the fracture with no difficulty.

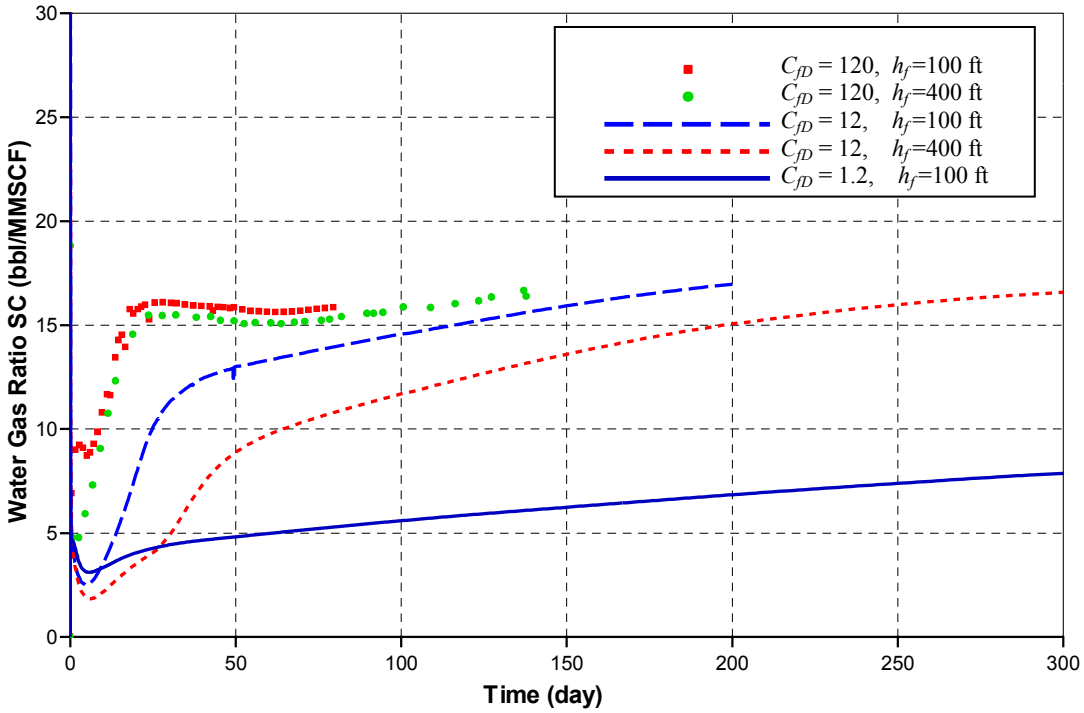

Fig. 3.32 Case 4: Water/gas ratio vs. time for the C_{fD} = 1.2 to 120 and h_f = 100 to 400 ft cases with Z1+Z4 perforations. As time increases, the water/gas ratio approaches 15 to 17.

To illustrate the entry of gas and water into the fracture in each zone, gas velocities in the j-direction in the j = 2 plane (adjacent to the fracture) were analyzed and are shown at t = 200 days for the C_{fD}=12, h_f=100 ft case (and the Z1+Z4 scenario) (**Fig. 3.33**). I show that gas is entering the fracture from the bottom zone, even though the lower part of the fracture is highly saturated with water. The gas influx velocity for the lowest reservoir zone is essentially the same as for the upper zones which are adjacent to regions in the fracture with lower water saturation. Thus, gas is not blocked from

entering the fracture even when high water saturation exists in the fracture where the gas is entering.

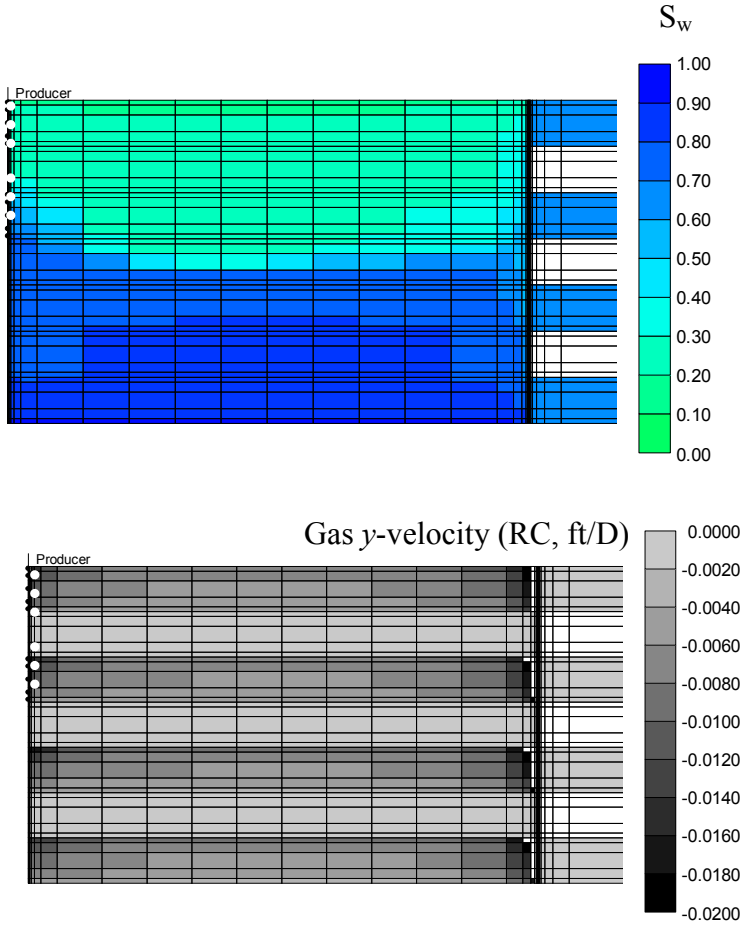

Fig. 3.33 Water saturation in the fracture (top) and superficial gas velocity (in reservoir conditions, ft/D) in the y-direction (into the fracture) is shown for the C_{fD} = 12, h_f = 100 ft case (bottom) and Z1+Z2 scenario at t = 200 days. Even though the lower areas of the fracture have high water saturation, gas enters the fracture with the same velocity in all gas zones.

Saturation maps are shown in **Fig. 3.34** for h_f = 100 ft and C_{fD} = 1.2 (at 1,200 days), C_{fD} = 12 (at 200 days), and C_{fD} = 120 (at 80 days). The same plots are shown in **Fig. 3.35**

for h_f = 400 ft. One of the main effects observed is that water and gas cone into the perforations. This coning occurs further into the reservoir in the higher fracture height. Also, at the C_{fD} = 120 and h_f = 400 ft, perforations impact the saturations more than in the other cases. When the perforations are in the upper and lower zones (Z1+Z4), the degree of segregation is much higher so that the water is only blocking the lowest zone (zone 4). I found that saturations stabilize by late times, as segregation develops. I also found that more segregation exists in scenarios with lower fracture height (higher fracture length to height ratio). This was also seen in uniform flux models and is caused by having a longer distance for segregation to develop. The amount of segregation increases at higher conductivity, which also was seen in uniform flux models, as the pressure gradient in the *x*-direction is lower. Also I found (as in Case 3) that perforations affect the coning near the perforations, and far away from the wellbore the saturations look similar for different perforation locations.

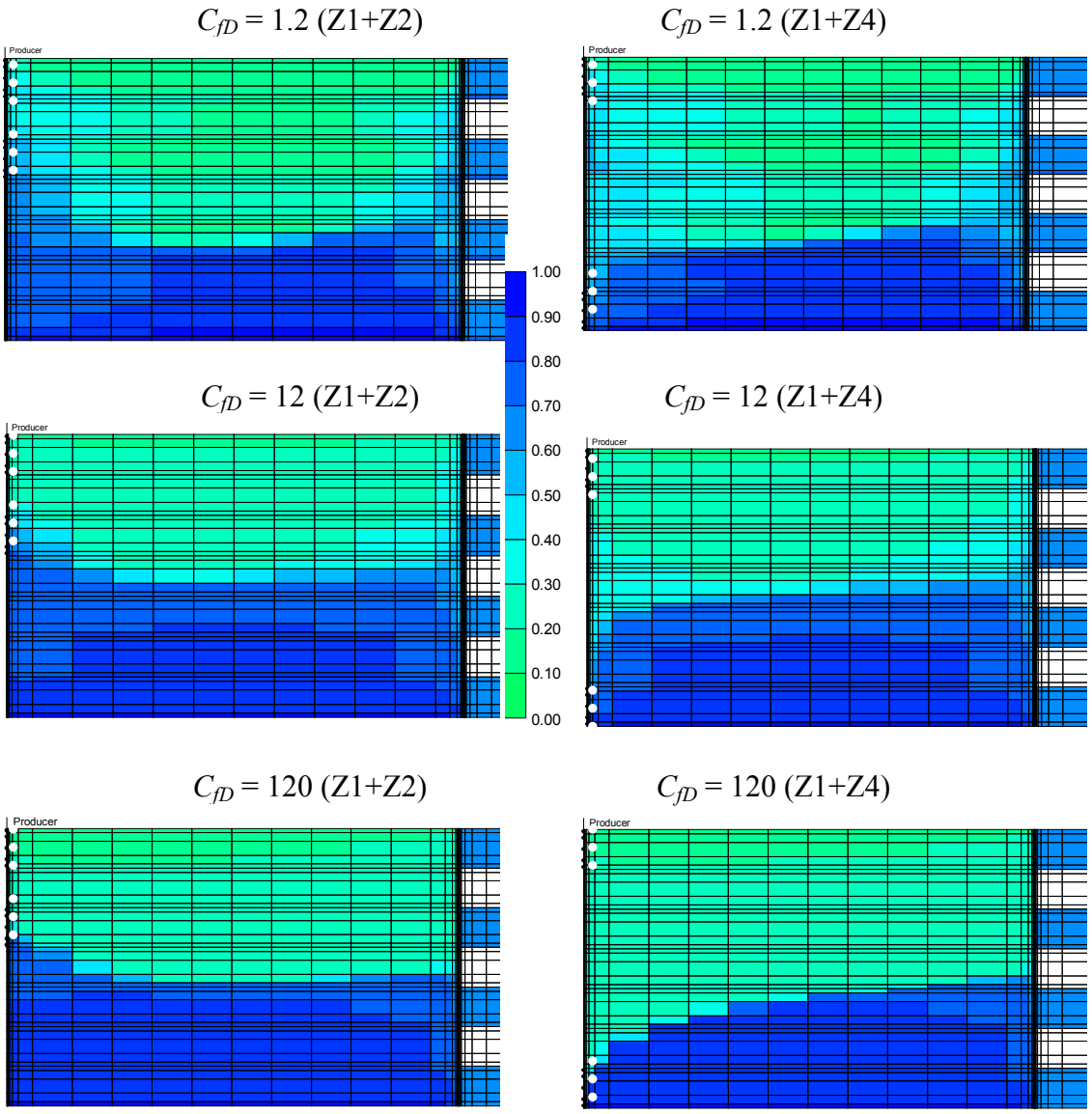

Fig. 3.34 Water saturation maps for h_f = 100 ft, C_{fD} = 1.2 (top), C_{fD} = 12 (middle) and C_{fD} = 120 (bottom). Plots on the left side are for Z1+Z2 perforations while on the right side plots are for Z1+Z4 perforations.

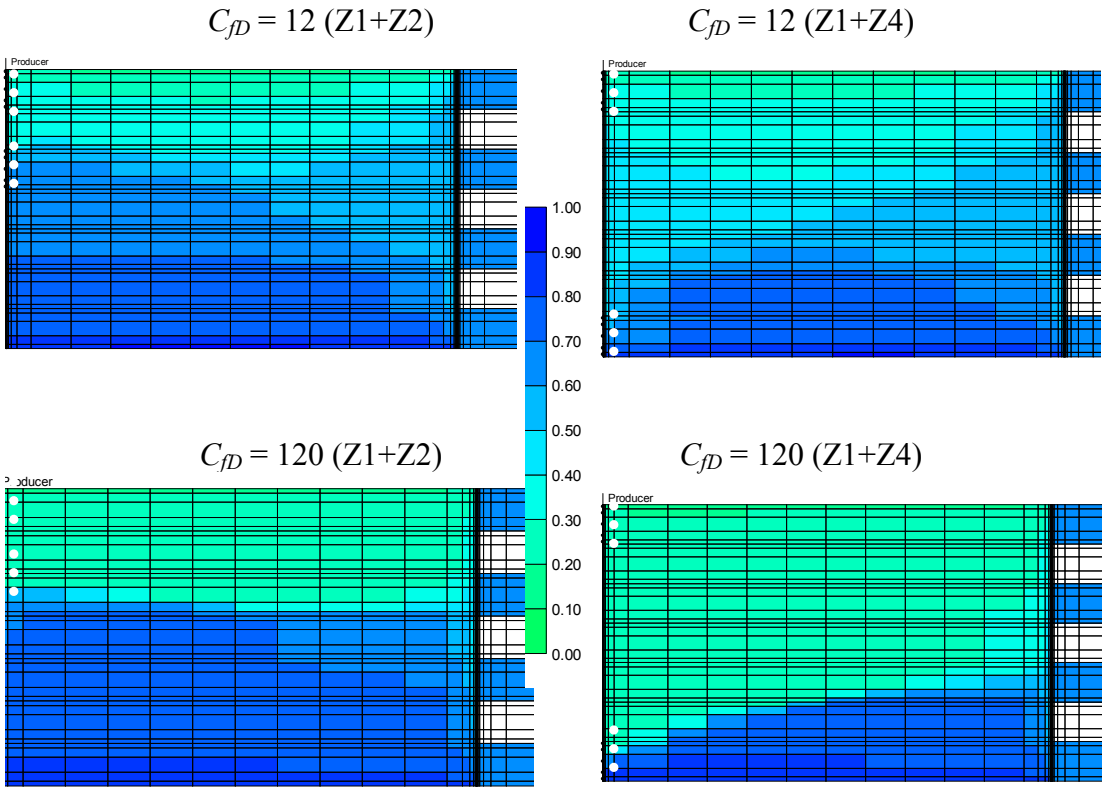

Fig. 3.35 Water saturation maps for h_f = 400 ft, C_{fD} = 12 (top) and C_{fD} = 120 (bottom). Plots on the left side are for Z1+Z2 perforations while on the right side plots are for Z1+Z4 perforations.

Gas production rates were compared for 3 scenarios: the base case (single-phase gas flow only), the Z1+Z2 scenario (top two zones are perforated) and the Z1+Z4 scenario (upper and lower zones are perforated). As the perforations are in the lowest zone in the Z1+Z4 case (where there is high water saturation adjacent to this zone in the fracture), I found (as expected) that the rates are higher for this perforation scenario (as compared to Z1+Z2). The base case always shows the highest rates, and perforations are in zones 1 and 4 (Z1+Z4). For the models with h_f = 100 ft and C_{fD} = 1.2 (**Fig. 3.36**), the Z1+Z2 case has a 15% lower gas rate than the base case. Comparing the Z1+Z2 to the Z1+Z4 case, the former is lower than the latter by only 3%. Thus, I have isolated the effect of perforations from the effect of multiphase flow by cross-comparing the 3 cases. The 15% in production rates going from the base case to the Z1+Z2 case is due mostly to multiphase non-Darcy conductivity reduction, as perforations minimally impacted production rates.

For the models with h_f = 100 ft and C_{fD} = 12 (**Fig. 3.37**), production rates are about 19% lower than the base case for the Z1+Z2 model, but only 2% of this difference is due to perforations. For the models with h_f = 100 ft and C_{fD} = 120 (**Fig. 3.38**), gas production rates are 24% lower than the base case (single-phase, Z1+Z4) at times 20-80 days for the Z1+Z2 model, but only 1% of this difference is due to perforations. For the thicker reservoirs with h_f = 400 ft and C_{fD} = 12 (**Fig. 3.39**), production rates are about 26% lower than the base case at times 20-80 days for the Z1+Z2 model, while 5% of this difference is due to perforations. For h_f =400 ft and C_{fD}=120 (**Fig. 3.40**), production rates are 10%

lower than the base case for the Z1+Z2 perforations at times 20-80 days, while only 3% of this difference is due to perforations. All cases show no more than 5% of the difference in production (at all times) from the base case to the Z1+Z2 case is due to perforation location (and the rest of the difference in productivity from the base case to the Z1+Z2 case is due to multiphase effects in the fracture). This 5% loss in productivity is due to perforation location (Z1+Z2 vs. Z1+Z4), as the gas and water must cone upwards into the Z1+Z2 perforations. Thus, perforation location does not have a large impact on gas rates, even when segregation exists and causes water to form in the fracture adjacent to a gas zone. As seen earlier in the gas entry velocity map in Fig. 3.33, gas is able to enter the fracture even if a highly-water saturated zone exists in the fracture adjacent to a gas zone.

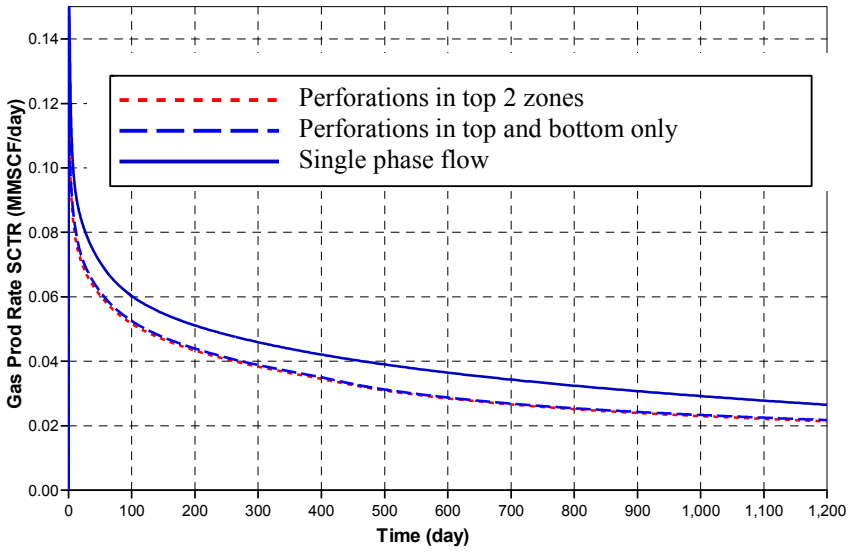

Fig. 3.36 Gas rates for different perforation scenarios and C_{fD} = 1.2, h_f =100 ft. Base case shows higher production rates by 15% but perforations only account for 3% of this. Most of the difference in production from the base case is caused by multiphase non-Darcy reduction in fracture permeability.

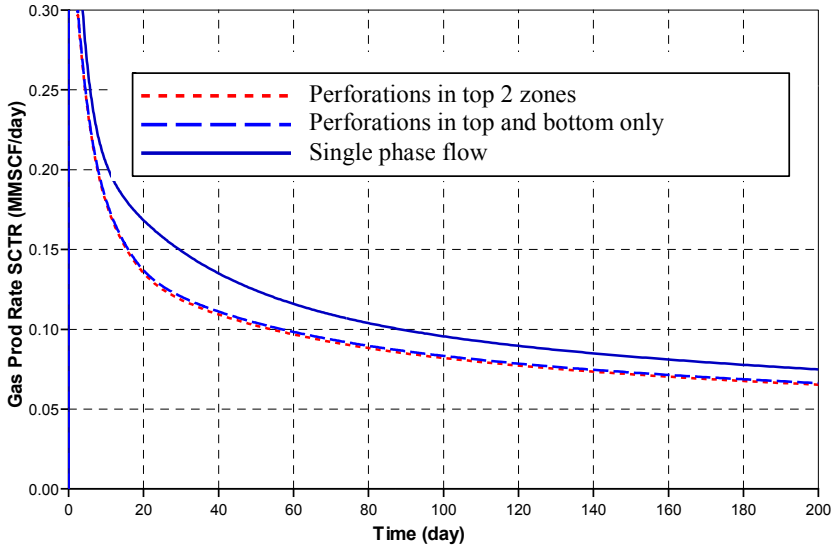

Fig. 3.37 Gas rates for different perforation scenarios and C_{fD} =12, h_f =100 ft. Production is 19% lower in multiphase flow but perforations account for only 2% of this difference.

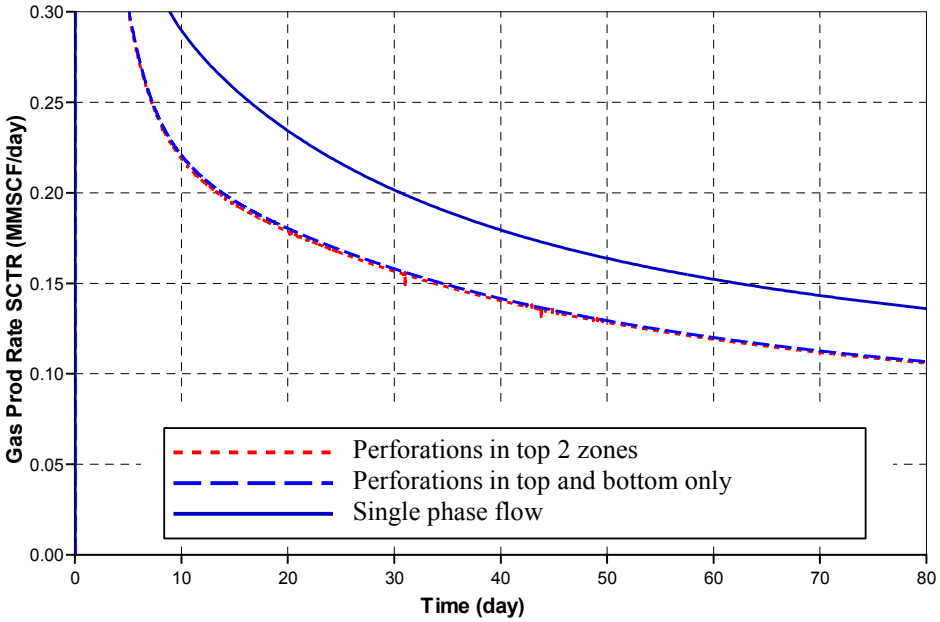

Fig. 3.38 Gas rates for different perforation scenarios and C_{fD} =120, h_f =100 ft. Production is 24% lower in multiphase flow but perforations are only 1% of this difference.

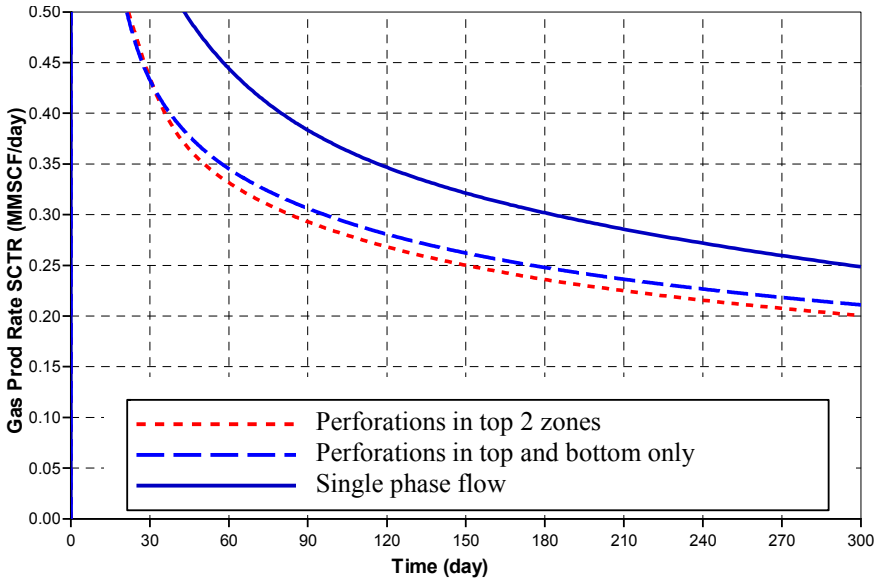

Fig. 3.39 Gas rates for different perforation scenarios and C_{fD} =12, h_f =400 ft. Production rates are 26% lower due to multiphase flow but perforations only account for 5% of this difference.

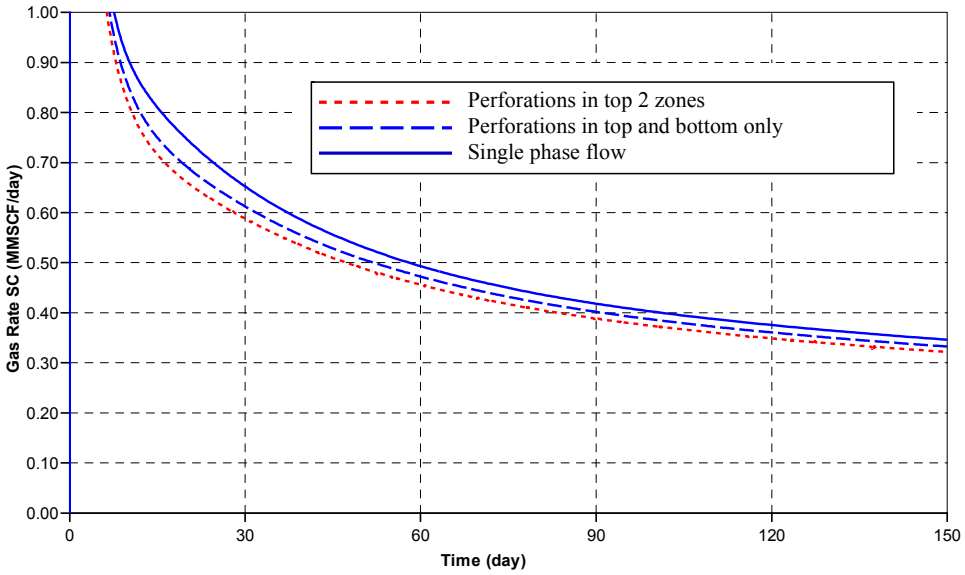

Fig. 3.40 Gas rates for different perforation scenarios and C_{fD}=120, h_f=400 ft. Z1+Z2 is 10% lower than base case, only 3% of this is due to perforations.

4. CONCLUSIONS

I found that hydraulically fractured wells with both gas and water flowing in the fracture show a difference in fracture conductivity due to segregation effects when non-Darcy flow with Geertsma's correlation is used.

- Segregation develops in the fracture over time (and develops even when the reservoir is in pseudo-steady state flow) so that the water saturation profile in the fracture will stabilize after long enough time has passed. The length of time depends on the effective dimensionless conductivity. Even if the fracture initially contains mostly water, or initially contains mostly gas, the ending profile is the same.
- The main controlling parameters on the impact of segregation in the hydraulic fracture are the non-linearity of the relative permeabilities, the degree of non-Darcy flow, the non-linearity of the non-Darcy correlation used with respect to water saturation, and the amount of segregation.
- Segregation effects do not cause a significant difference in effective conductivity or dimensionless productivity when both linear relative permeabilities and Darcy flow is modeled, even if phase segregation is present.
- I found that using non-linear relative permeabilities caused gravity segregation to have an effect on fracture conductivity. This is due to the non-linear dependence of relative permeability with respect to saturation. When the vertical average of gas saturation is the same, if a zone with high gas saturation exists in the fracture in

the segregated case, the effective fracture permeability will be higher than in mixed flow because of this non-linear dependence.

- I found that modeling non-Darcy flow with Geertsma's correlation caused an impact on effective fracture conductivity due to segregation effects. This is also due to the non-linear dependence of the beta factor with respect to water saturation.
- However, I found that non-linear relative permeabilities has a larger effect than non-Darcy flow for the range of parameters modeled, but this could change if the non-Darcy correlation has a higher exponent for water saturation or for different influx functions.
- If non-Darcy flow and non-linear relative permeabilities exist in the fracture, these effects need to be modeled. Non-Darcy effects in the reservoir are not important for the models investigated in this work, but could be more important for non-hydraulically fractured reservoirs with high flow rates near the wellbore.
- The amount of segregation increases under the following conditions: increase in fracture length-to-height ratio, or decrease in average pressure gradient in the fracture (due to increase in conductivity or decrease in gas rate). This is because; as the pressure gradient is lower or the fracture length-to-height ratio is higher the vertical pressure gradient is closer in magnitude to the horizontal pressure gradient.
- Gravity segregation impacts effective fracture conductivity when gas and liquid are being produced at water/gas ratios above 1 to 1.5 Bbl/MMscf if the pressure gradient in the x-direction is not very high and the fracture length-to-height ratio is high enough, and the mixed-flow effective dimensionless conductivity is below 10.

- When effective dimensionless conductivity is reduced in mixed-flow, the productivity will also be affected. This relationship is a logarithmic relationship for effective dimensionless conductivities between 0.1 and 10. For effective dimensionless conductivities outside of this range, the productivity is not affected as much for a given percent change in effective dimensionless conductivity.
- The effect of segregated flow on productivity during cleanup is very significant while water is present in the fracture (35% lower 50-day cumulative gas production for mixed flow as compared to segregated flow) for a fracture with original C_{fD} = 10.
    - Segregated flow effects during cleanup are important as long as the effective dimensionless conductivity in mixed flow is not very high ($C_{fD,\ eff}$<10) and the water/gas ratio is above 1.5 bbl/MMscf.
- If the fracture connects to an aquifer, the location of the perforations does not have a significant impact on water production. However, the perforated interval is more important and affects the productivities of both water and gas, but does not affect the water production independently from gas production.
- If a well with multiple stacked sands connected to a hydraulic fracture, gas is able to enter the fracture even if a highly-water saturated zone exists in the fracture adjacent to a gas zone. The gas can still enter the fracture, and rise up towards the gas zone. From the top of the gas zone, the gas easily flows horizontally and/or cones downward into the perforations.

REFERENCES

Barree, R.D., Cox, S.A., Gilbert, J.V., et al. 2003. Closing the Gap: Fracture Half-Length From Design, Buildup, and Production Analysis. Paper SPE 84491-PA presented at the SPE Annual Technical Conference and Exhibition, Denver, Colorado, 5-8 October. DOI: 10.2118/84491-PA.

Barree, R.D., Conway, M.W. 2007. Multiphase Non-Darcy Flow in Proppant Packs. Paper SPE 109561-MS presented at the SPE Annual Technical Conference and Exhibition, Anaheim, California, 11-14 November. DOI: 10.2118/109561-MS.

Bidner, M.S., Savioli, G.B. 2003. On the Mechanisms of Mobilization of Residual Oil Left After Waterflooding. Paper SPE 81019-MS presented at the SPE Latin American and Caribbean Petroleum Engineering Conference, Port-of-Spain, Trinidad, West Indies, 27-30 April. DOI: 10.2118/81019-MS.

Camilleri, D., Engelsen, S., Lake, L.W., Lin, E.C., Ohno, T., Pope, G.A., Sephernoori, K. 1987. Description of an Improved Compositional Micellar/Polymer Simulator. *Soc. Pet. Eng. Res. Eng.* **2** (4) 427-432.

De la Porte, J., Kossack, C.A. 2005. The Effect of Fracture Relative Permeabilities and Capillary Pressures on the Numerical Simulation of Naturally Fractured Reservoirs. Paper SPE 95241-MS presented at the SPE Annual Technical Conference and Exhibition, Dallas, Texas, USA, 9-12 October. DOI: 10.2118/95241-MS.

Economides, M., Oligney, R., Valko, P. 2002. *Unified Fracture Design: Bridging the Gap Between Theory and Practice*, Alvin, Texas. Orsa Press.

Flowers, J.R., Hupp, M.T., Ryan, J.D. 2003. The Results of Increased Fracture Conductivity on Well Performance in a Mature East Texas Gas Field. Paper SPE 84307 presented at the SPE Annual Technical Conference and Exhibition, Denver, Colorado, 5-8 October. DOI: 10.2118/84307-MS.

Forchheimer, P. 1901. "Wasserbewegung durch Boden," *Zeits. V. deutsch. Ing.* 45, 1782-1788.

Frederick, D.C., Graves, R.M. 1994. New Correlations to Predict Non-Darcy Flow Coefficients at Immobile and Mobile Water Saturation. Paper SPE 28451-MS presented at the SPE Annual Technical Conference and Exhibition, New Orleans, Louisiana, 25-28 September. DOI: 10.2118/28451-MS.

Foulser, R.W.S., Goodyear, S.G., Sims, R.J. 1992. Two- and Three-Phase Relative Permeability Studies at High-Capillary Numbers. Paper SPE 24152-MS presented at

the SPE/DOE Enhanced Oil Recovery Symposium, Tulsa, Oklahoma, 22-24 April. DOI: 10.2118/24152-MS.

Geertsma, J., 1974. Estimating the Coefficient of Inertial Resistance in Fluid Flow Through Porous Media. *SPE Journal*. **14** (5). 445-450.

Lolon, E.P., McVay, D. A., Schubarth, S. K. 2003. Effect of Fracture Conductivity on Effective Fracture Length. Paper SPE 84311 presented at the SPE Annual Technical Conference and Exhibition, Denver, Colorado, 5-8 October. DOI: 10.2118/84311-MS.

Mendoza, C. A. 1992. Capillary Pressure and Relative Transmissibility Relationships Describing Two-Phase Flow Through Rough-Walled Fractures in Geological Materials. Ph.D. dissertation. U. of Waterloo, Canada.

Montgomery, K.T. 1990 (a). Effects of Fracture Fluid Invasion on Cleanup Behavior and Pressure Buildup Analysis. Paper SPE 20643-MS presented at the SPE Annual Technical Conference and Exhibition, Houston, Texas, 23-26 September. DOI: 10.2118/20643-MS.

Montgomery, K.T. 1990 (b). Factors That Affect Fracture Fluid Cleanup and Pressure Buildup Test Results in Tight Gas Reservoirs. MS thesis. Texas A&M U., College Station, Texas.

Olson, K.H., S., Milton-Tayler, D., Olsen, E. 2004. Multiphase Non-Darcy Pressure Drop in Hydraulic Fracturing. Paper SPE 90406-MS presented at the SPE Annual Technical Conference and Exhibition, Houston, Texas, 26-29 September. DOI: 10.2118/90406-MS.

Persoff, P., Prueas, K., Myer, L. 1991. Two-Phase Flow Visualization and Relative Permeability Measurements in Transparent Replicas of Rough-Walled Rock Fractures. *Proc. 16th Workshop on Geothermal Reserv. Eng.*, Stanford, California, 23-25 Jan.

Penny, G.S., Jin, L. 1995. The Development of Laboratory Correlations Showing the Impact of Multiphase Flow, Fluid, and Proppant Selection Upon Gas Well Productivity. Paper SPE 30494 presented at the SPE Annual Technical Conference and Exhibition, Dallas, Texas, 22-25 October. DOI: 10.2118/30494-MS.

Pruess, K., Tsang, Y. W. 1990. On Two-Phase Relative Permeability and Capillary Ressure of Rough-Walled Fracture. *Water Resour. Res.* **26**, 1915-1926.

Romm, E.S. 1972. *Fluid Flow in Fractured Rocks* (English translation). W. R. Blake (transl.), Phillips Petroleum Co., Bartlesville, Oklahoma.

Rossen, W. R., Kumar, A. T. A. 1992. Single- and Two-Phase Flow in Natural Fractures. Paper SPE 24915 presented at the SPE Annual Technical Conference and Exhibition, Washington, D.C., 4-7 October. DOI: 10.2118/24915-MS.

Rossen, W. R., Kumar, A. T. A. 1994. Effect of Fracture Relative Permeabilities on Performance of Naturally Fractured Reservoirs. Paper SPE 28700 presented at the SPE International Petroleum Conference and Exhibition of Mexico, Veracruz, Mexico, 10-13 October. DOI: 10.2118/28700-MS.

Rossen, W.R., van Duijn, C.J., Nguyen, Q.P. 2006. Injection Strategies To Overcome Gravity Segregation in Simultaneous Gas Liquid Injection into Homogenous Reservoirs. Paper SPE 99794 presented at the SPE/DOE Symposium on Improved Oil Recovery, Tulsa, Oklahoma, 22-26 April. DOI: 10.2118/99794-MS.

Schubarth, S.K., Chabaud, R.A., Penny, G.S. 1995. Moxa Arch Frontier Development Success Through Increased Fracture Conductivity - Part 2. Paper SPE 30717 presented at the SPE Annual Technical Conference and Exhibition, Dallas, Texas, 22-25 October. DOI: 10.2118/30717-MS.

Schubarth, S.K., Yeager, R.R., Murphy, D.W. 1998. Advanced Fracturing and Reservoir Description Techniques Improves Economics in Utah, Green River Formation Oil Project. Paper SPE 39777 presented at the SPE Permian Basin Oil and Gas Recovery Conference, Midland, Texas, 23-26 March. DOI: 10.2118/39777-MS.

Schubarth, S.K., Milton-Tayler, D. 2004. Investigating How Proppant Packs Change Under Stress. Paper SPE 90562-MS presented at the SPE Annual Technical Conference and Exhibition, Houston, Texas, 26-29 September. DOI: 10.2118/90562-MS

Shi, J.X., Rossen, W.R., 1998. Simulation of Gravity Override in Foam Processes in Porous Media. Reservoir Evaluation and Engineering. **1**. 148-154.

Sullivan, R.B., Rushing, J.A., Bachman, R.C., et al. 2006. Evaluation of Nonlinear Fracture Relative Permeabilities and Their Impact on Water-Frac Performance in Tight Gas Sands. Paper SPE 98329 presented at the International Symposium and Exhibition on Formation Damage Control, Lafayette, Louisiana, 15-17 February. DOI: 10.2118/98329-MS.

Stone, H.L. 1982. Vertical Conformance in an Alternating Water-Miscible Gas Flood. Paper SPE 11130 presented at the SPE Annual Technical Conference and Exhibition, New Orleans, Louisiana, 26-29 September. DOI: 10.2118/11130-MS.

Tannich, J.D. 1975. Liquid Removal from Hydraulically Fractured Gas Wells. MS thesis. Texas A&M U., College Station, Texas.

Tidwell, V., Parker, M. 1996. Laboratory Imaging of Stimulation Fluid Displacement from Hydraulic Fractures. Paper SPE 36491 presented at the SPE Annual Technical Conference and Exhibition, Denver, Colorado, 6-9 October. DOI: 10.2118/36491-MS.

Vincent, M.C., Pearson, C.M., Kullman, J. 1999. Non-Darcy and Multiphase Flow in Propped Fractures: Case Studies Illustrate the Dramatic Effect on Well Productivity. Paper SPE 54630 presented at the SPE Western Regional Meeting, Anchorage, Alaska, 26-28 May. DOI: 10.2118/54630-MS.

APPENDIX

NOMENCLATURE

Y = water/gas ratio[Bbl/MMscf]
q_g = gas flow rate [MMscf/D]
u_g = gas flux; Darcy velocity; superficial velocity [ft/D]
B_g = gas formation volume factor [rb/scf]
E_g = gas expansion factor; Darcy velocity [scf/rb]
μ_g = gas viscosity [cp]
ρ_g = gas density [lbm/ft^3]

ρ_w = water density (at reference pressure) [lbm/ft^3]
B_w = water formation volume factor [rb/stb]
c_w = water compressibility [1 / psi]
μ_w = water viscosity [cp]
$P_{ref,w}$ = reference pressure for water properties [psi]

J_D = dimensionless well productivity
C_{fD} = original dimensionless fracture conductivity (singe-phase dimensionless fracture conductivity)
$C_{fD,eff}$ = effective dimensionless fracture conductivity (multiphase dimensionless fracture conductivity)

k, k_f = reservoir permeability, fracture permeability [md]
k_{abs}, k_{eff} = absolute permeability, effective permeability [md]
$k_{eff,f}$, $k_{eff,res}$ = effective fracture permeability, effective reservoir permeability [md]
$\left(k / k_{ref}\right)_{stress}$ = reduction factor for permeability due to stress (less than or equal to 1)
GRF = gas resistance factor for permeability due to non-Darcy flow (greater or equal to 1)
wk_f = fracture conductivity [md•ft]
x = position along the hydraulic fracture direction [ft]
x_D= dimensionless distance along fracture
x_f= fracture length [ft]
h, h_f = reservoir height, fracture height [ft]
N_w = Corey exponent to water
N_g= Corey exponent to gas
$k_{rg}(S_{wir})$ = permeability to gas at residual water
$k_{rw}(S_{gir})$ = permeability to water at residual gas
S_{wir}= Corey exponent to water
S_{gir}= Corey exponent to water

VITA

Name:	Mark Dickins
Address:	Petroleum Engineering Dept.. c/o Dr. Duane McVay Texas A&M University College Station, TX 77843-3116
Email Address:	mark.dickins@pe.tamu.edu
Education:	B.S., Physics, The University of Texas at Austin, 2006 M.S., Petroleum Engineering, Texas A&M University, 2008